

Force and Torque Sensing with Galfenol Alloys

THESIS

Presented in Partial Fulfillment of the Requirements for the Degree Master of Science in
the Graduate School of The Ohio State University

By

Arjun Mahadevan, B.E.

Graduate Program in Mechanical Engineering

The Ohio State University

2009

Master's Examination Committee:

Dr. Marcelo J. Dapino, Advisor

Dr. Stephen E. Bechtel

© Copyright by
Arjun Mahadevan
2009

ABSTRACT

Galfenol is a class of smart material that combines moderate magnetostriction (up to 400 ppm) and excellent mechanical strength. In this work two $\langle 100 \rangle$ oriented highly textured polycrystalline Galfenol alloys with different Gallium (Ga) content have been characterized. The two alloys have been studied under tensile and compressive loads. Magnetization versus field measurements are presented for the two alloys at different bias stresses ranging from -63.71 MPa to 63.71 MPa. The magnetization versus applied stress measurements are presented for the two alloys at different bias fields. The stress-dependent magnetic susceptibility change of these alloys has been studied; the susceptibility of the higher concentration Ga alloy is more sensitive to stress in the domain rotation region of the magnetization process and operates over a larger stress range, whereas the low Ga concentration sample is more sensitive in the domain wall motion region. The stress-dependent susceptibility change of these alloys can be used to develop a force sensor or a torque sensor. A force sensor which utilizes the principle of stress-dependent susceptibility is demonstrated. The stress range for a force sensor using the two alloys is determined. The same principle can be used to measure the torque in a non-contact way by bonding rolled Galfenol steel on a shaft. The principle is demonstrated by measuring the change in susceptibility that occurs when a rolled Galfenol patch bonded on a non-magnetic substrate is stressed.

ACKNOWLEDGMENTS

I would have not made it this far if not for the superior efforts and dedication of several individuals. Firstly I would like to thank The Ohio State University, Graduate School and Department of Mechanical Engineering for providing me an opportunity to do my Graduate studies at this prestigious institution and funding my first year of research through a University Fellowship. I express my gratitude to my advisor, Professor Marcelo Dapino for his support and guidance through the past two years and most importantly his patience in making me a better professional. I would like to acknowledge Phillip Evans and Suryarghya Chakrabarti for their insightful technical discussions, which have greatly helped me complete my thesis. I express my thanks to Professor Stephen Bechtel for serving on my exam committee. My thanks to American Axle and Manufacturing, and Moog Inc for their support with the project. Thanks to Eric Summers for providing me with rolled Galfenol samples and insights into rolled Galfenol steel.

I express my thanks to my colleagues at the Smart Materials and Structures laboratory. I appreciate all the help, advice and support you have given me. I feel happy to have worked with all of you and all the best in your future endeavors. Thanks to Neil Gardner and Gary Gardner, I appreciate your advice and help in the machine shop. I would like to thank Ross Baldwin at the Materials Science Department for his

help in scheduling tests and helping me use the MTS test frame. Thanks to Jeremy Seidt and Ravi Yarnalkar for your time and help with the Instron tests.

To my friends Aarthi, Guru, Shunmugam, Shravan, Surya, Vignesh, Vijay, and Angel. You have given me irreplaceable experiences that have made my graduate life very memorable. To my sister, brother, aunts and cousins thank you for your love, support and encouragement. Finally to my parents, your love, sacrifice, support and encouragement has brought me to what I am today. I have no words to Thank You.

VITA

Septembe 9, 1984Born - Salem, Tamil Nadu, India

May 2002Montfort A. I. Hr. Sec. School

May 2007B.E. Mechanical Engineering (Sand-
wich), PSG College of Technology
(Anna University)

2007 - 2008University Fellow, The Ohio State Uni-
versity

2008 - presentGraduate Research Associate,
The Ohio State University

FIELDS OF STUDY

Major Field: Mechanical Engineering

Studies in Smart Materials and Structures:

TABLE OF CONTENTS

	Page
Abstract	ii
Acknowledgments	iii
Vita	v
List of Tables	ix
List of Figures	x
Chapters:	
1. Introduction	1
1.1 Thesis Overview	1
1.2 Galfenol	2
1.3 Force Sensing	3
1.4 Torque Sensing	4
2. Quasi-static Characterization of Textured Polycrystalline 18.4 at.% Ga and 20.9 at.% Ga Galfenol Alloys	5
2.1 Inverse (Actuation) Effect	5
2.1.1 Sample Preparation	6
2.1.2 Magnetic Transducer	6
2.1.3 Magnetization versus Applied Field and Magnetostriction versus Applied Field Measurements	11
2.1.4 Results and Discussion Inverse Effect	11
2.2 Direct (Sensing) Effect	20
2.2.1 Sample Preparation	20

2.2.2	Magnetic Transducer	20
2.2.3	Magnetization versus Stress and Strain versus Stress Measurements	20
2.2.4	Results and Discussion Direct Effect	22
2.3	Stress Dependent Susceptibility	28
2.3.1	Susceptibility Change of 18.4 at.% Ga Alloy at Constant Stress	28
2.3.2	Susceptibility Change of 20.9 at.% Ga Alloy at Constant Stress	30
2.3.3	Comparison of the Differential Susceptibility	30
3.	Force Sensing Using Textured Polycrystalline Galfenol Alloys	34
3.1	Force Sensor Principle	34
3.2	Force Sensor Measurements	37
3.2.1	Measurements	37
3.2.2	Full Wave Phase Sensitive Demodulation	38
3.2.3	Demodulated Stress Dependent Susceptibility	44
3.3	COMSOL Simulation of Force Sensor	47
3.3.1	Linear Piezomagnetic Equations	47
3.3.2	Governing Equations and Weak Forms	48
3.3.3	Results and Discussion	53
4.	Torque Sensing Using Textured Polycrystalline Rolled Galfenol	62
4.1	Contactless Sensing Principle	62
4.2	Hot Forming of Rolled Galfenol Steel	64
4.2.1	Hot Forming and Bonding of Rolled Galfenol Steel	65
4.2.2	Strain Matching	69
4.3	Contactless Measurements	72
4.4	Discussion and Future Work	73
5.	Summary and Conclusions	77
Appendices:		
A.	Torque Sensing using Polycrystalline Rolled Galfenol Steel and an Integrating Fluxgate Magnetometer	81
A.1	Integrating Fluxgate Magnetometer	81
A.1.1	An Analytical Model for an Integrating Fluxgate Magnetometer	84
A.1.2	Characterization and Testing of an Integrating Fluxgate Magnetometer	86

A.2	Contactless Torque Sensing	86
A.2.1	Contactless Torque Sensing Measurement Setup	88
A.2.2	Results and Discussion	91
	Bibliography	95

LIST OF TABLES

Table	Page
3.1 Value of constants for steel used in the finite element simulation. . .	53
3.2 Value of constants for Galfenol used in the finite element simulation.	54

LIST OF FIGURES

Figure	Page
2.1 $\text{Fe}_{81.6}\text{Ga}_{18.4}$ test sample with threaded ends and strain gage bonded at the center.	7
2.2 Magnetic transducer made of laminated steel plates. The arrows indicate the flux path when the coils are excited with the Galfenol sample at the center.	8
2.3 Magnetic transducer assembly with the Galfenol rod, stainless steel end caps and pickup coil.	8
2.4 Quasi-static 3-D COMSOL simulation: slice plot of the Y-component of flux in the transducer with the Galfenol sample for an applied current density of 1000 kA/m^2	9
2.5 Quasi-static 3-D COMSOL simulation: slice plot of the Y-component micro-strain in the Galfenol sample for an applied current density of 1000 kA/m^2	10
2.6 Test setup for actuation and sensing characterization.	12
2.7 Test sample mounted on the hydraulic grips for applying tensile and compressive loads.	12
2.8 Magnetization curves for $\text{Fe}_{81.6}\text{Ga}_{18.4}$ at constant stress	14
2.9 Magnetostriction curves for $\text{Fe}_{81.6}\text{Ga}_{18.4}$ at constant stress	15
2.10 Magnetization curves for $\text{Fe}_{79.1}\text{Ga}_{20.9}$ at constant stress	16
2.11 Magnetostriction curves for $\text{Fe}_{79.1}\text{Ga}_{20.9}$ at constant stress	17

2.12	Feedback control used to maintain constant magnetic field ($k_p=0.35$, $k_i=0.55$).	21
2.13	Magnetization curves for $\text{Fe}_{81.6}\text{Ga}_{18.4}$. Top: Constant current to the coils. Bottom: Constant magnetic field (0, 20, 30, 40, 50, 60, 70, 80, 90, 100, 110, 120, 130, 140, 180 Oersted).	23
2.14	Strain-Stress curves for $\text{Fe}_{81.6}\text{Ga}_{18.4}$. Top: Constant current to the coils. Bottom: Constant magnetic field (0, 20, 30, 40, 50, 60, 70, 80, 90, 100, 110, 120, 130, 140, 180 Oersted).	24
2.15	Magnetization curves for $\text{Fe}_{79.1}\text{Ga}_{20.9}$. Top: Constant current to the coils. Bottom: Constant magnetic field (0, 10, 20, 30, 40, 50, 60, 70, 80, 90, 100, 120, 130, 140, 180 Oersted).	26
2.16	Strain-Stress curves for $\text{Fe}_{79.1}\text{Ga}_{20.9}$. Top: Constant current to the coils. Bottom: Constant magnetic field (0, 10, 20, 30, 40, 50, 60, 70, 80, 90, 100, 120, 130, 140, 180 Oersted).	27
2.17	Differential susceptibility change as function of applied field for $\text{Fe}_{81.6}\text{Ga}_{18.4}$ at constant stress (63.71, 56.63, 49.56, 42.47, 35.4, 28.31, 21.23, 14.15, 7.07, 0, -7.07, -14.15, -21.23, -28.31, -35.4, -42.47, -49.56, -56.63 and -63.71 MPa).	28
2.18	Differential susceptibility change as function of applied field for $\text{Fe}_{79.1}\text{Ga}_{20.9}$ at constant stress (63.71, 56.63, 49.56, 42.47, 35.4, 28.31, 21.23, 14.15, 7.07, 0, -7.07, -14.15, -21.23, -28.31, -35.4, -42.47, -49.56, and -56.63 MPa).	31
2.19	Stress dependent susceptibility of $\text{Fe}_{81.6}\text{Ga}_{18.4}$ and $\text{Fe}_{79.1}\text{Ga}_{20.9}$ at zero applied field.	32
3.1	Schematic of a Galfenol force sensor.	35
3.2	Modulated measurement of magnetization and magnetic field for $\text{Fe}_{81.6}\text{Ga}_{18.4}$ Galfenol alloy for a sinusoidal stress cycle (63.71 MPa to -63.71 MPa at 0.04Hz) and an AC drive current of (338 mA at 5 Hz).	39

3.3	Modulated measurement of magnetization and magnetic field for $\text{Fe}_{79.1}\text{Ga}_{20.9}$ Galfenol alloy for a sinusoidal stress cycle (63.71 MPa to -63.71 MPa at 0.04Hz) and an AC drive current of (338 mA at 5 Hz).	40
3.4	Carrier wave and signal before modulation.	41
3.5	Modulated carrier wave and signal.	42
3.6	Demodulated carrier wave and signal.	42
3.7	FFT of signal, carrier wave, modulated signal and demodulated signal.	43
3.8	Lowpass filtered demodulated signal.	43
3.9	Demodulated stress-dependent magnetization of $\text{Fe}_{81.6}\text{Ga}_{18.4}$ and $\text{Fe}_{79.1}\text{Ga}_{20.9}$ Galfenol alloys.	45
3.10	Demodulated stress-dependent susceptibility of $\text{Fe}_{81.6}\text{Ga}_{18.4}$ and $\text{Fe}_{79.1}\text{Ga}_{20.9}$ Galfenol alloys.	46
3.11	COMSOL model mechanical boundary conditions.	55
3.12	COMSOL model boundary conditions and direction current density in the coils.	56
3.13	COMSOL Model - Slice plot of flux density B_Y (Tesla).	57
3.14	COMSOL Model - Slice plot of Strain S_{YY} (microstrain).	58
3.15	Modulated change in flux density measured as voltage across pick up coil for a cyclic stress of -10 MPa to 10 MPa.	59
3.16	Modulated applied field for a cyclic stress -10 MPa to 10 MPa.	60
3.17	Demodulated susceptibility for a cyclic stress -10 MPa to 10 MPa.	61
4.1	Magnetic circuit schematic.	63
4.2	Schematic of Galfenol patch bonded at 45° on the shaft.	63

4.3	Highly textured polycrystalline $\text{Fe}_{81.6}\text{Ga}_{18.4}$ rolled Galfenol patch with $\langle 100 \rangle$ orientation along the length.	64
4.4	Magnetostriction of highly textured polycrystalline rolled Galfenol steel (18.4 at.% Ga + 1002 low carbon steel).	66
4.5	Hot forming dies.	67
4.6	Hot forming dies with the polycrystalline rolled Galfenol sandwiched between the dies.	68
4.7	Hot formed polycrystalline $\text{Fe}_{81.6}\text{Ga}_{18.4}$ split ring.	69
4.8	Polycrystalline rolled $\text{Fe}_{81.6}\text{Ga}_{18.4}$ hot formed to suit a 2 in diameter shaft.	70
4.9	Polycrystalline rolled $\text{Fe}_{81.6}\text{Ga}_{18.4}$ hot formed and bonded on a 2 in diameter shaft.	70
4.10	Strain matching between the bonded Galfenol ring and steel shaft. .	71
4.11	Measurement system with polycrystalline rolled $\text{Fe}_{81.6}\text{Ga}_{18.4}$ bonded to aluminum substrate.	72
4.12	Stress input to the aluminum sample with the bonded Galfenol steel patch.	74
4.13	Modulated voltage measurement from pick-up coil for a sinusoidal compressive stress input to the Galfenol Steel patch bonded on aluminum substrate.	74
4.14	Demodulated voltage measurement from pick-up coil as function of strain measured on the Galfenol steel patch.	75
A.1	Laboratory fluxgate magnetometer for a 1 inch diameter shaft . . .	82
A.2	Integrating fluxgate magnetometer schematic.	83
A.3	Schematic of fluxgate magnetometer	85

A.4	Second harmonic output voltage from the feedback coil at increasing sinusoidal excitation voltage at a frequency of 3 KHz, for a sinusoidal external field (H_x) of ± 30 kA/m at 0.04 Hz.	87
A.5	Second harmonic output voltage from the feedback coil at increasing number of turns in the feedback coil, 10 V sinusoidal excitation voltage at a frequency of 3 KHz, for a sinusoidal external field (H_x) of ± 30 kA/m at 0.04 Hz.	87
A.6	Second harmonic output voltage from the feedback coil at different excitation waveform, 10 V_{pp} voltage at a frequency of 3 KHz, for a sinusoidal external field (H_x) of ± 30 kA/m at 0.04 Hz.	88
A.7	Spline shaft with the hot formed polycrystalline rolled Galfenol ring bonded to the shaft using M bond 200.	89
A.8	Torque arm used to torque the spline shaft with the bonded Galfenol.	89
A.9	Second harmonic output of the integrating fluxgate magnetometer.	90
A.10	Fluxgate output at different magnitudes of torque starting from a bias torque of 3300 lbs-in.	91
A.11	Fluxgate output as a function of input torque.	92
A.12	Fluxgate output as a function of shear strain on the rolled Galfenol ring.	92
A.13	Fluxgate output as at different torque cycle frequency.	93
A.14	Fluxgate output as at different torque cycle frequency.	94

CHAPTER 1

INTRODUCTION

1.1 Thesis Overview

Magnetostrictive materials are a class of metallic alloys which deform in response to magnetic fields. The deformation is a function of magnetoelastic coupling, crystalline anisotropy and magnetic moment orientation. Joule magnetostriction which is most commonly used, refers to the strain produced in the direction of applied field [6]. This is called inverse effect which is used in the design of actuators. The magnetoelastic coupling in the material is bidirectional. The reversible effect where the magnetic state of the material changes in response to stress is called the Villari or direct effect. This effect provides the fundamental principle for magnetostrictive force and torque sensors [6]. Galfenol ($\text{Fe}_{(100-x)}\text{Ga}_x$) is a recent class of smart material which combines steel-like strength and moderate magnetostriction (up to 400 ppm) [3]. Earlier magnetostrictive materials like Terfenol-D exhibit very large magnetostriction (~ 1600 ppm), but are brittle and must be operated in compression only. Galfenol can be subjected to tension, bending and shock loads, moreover it can be machined, rolled, extruded, welded and hot-formed. These properties enable the unprecedented development of sensors, actuators and active structures with 3-D

functionality and load-bearing capabilities. The thesis discusses the characterization of two highly textured polycrystalline Galfenol alloys with varying at.%Ga and the use of these alloys as a sensing elements in force and torque sensors.

1.2 Galfenol

Several researchers have the magnetomechanical properties of single crystal FeGa alloys with varying Ga content. Clark et al. [3] have studied the magnetostriction for Ga concentrations of 0 – 35 at.% Ga. It was found that peaks occur at 19 at.% Ga and 27 at.% Ga and a drop in magnetostriction was observed at 24.7 at.% Ga [3]. Jayasimha et al. [1] have compared the sensing and actuation behavior of single crystal iron-gallium alloys with 19 at.% Ga, 24.7 at.% Ga and 29 at.% Ga. They compared an energy based model with experimental magnetization, magnetostriction curves and used the model to plot d_{33}^H and μ_r^H at different stress levels (0 to 80 MPa) [1]. It was reported by Rafique et al. [19] that K_1 and K_2 both drop gradually up to 18 at.% Ga and that there is a sharp drop in the anisotropy constants at 20 at.% Ga. Wun-Fogle et al. [22] used a magnetization rotation model to calculate the magnetomechanical properties (coupling constant, piezo-magnetic constant and permeability) of $\text{Fe}_{(100-x)}\text{Ga}_x$ [$x = 0.125, 0.18, \text{ and } 0.22$]. This study showed that stress annealing had minimal effect on a 22 at.% Ga sample whereas the stress annealing significantly altered the magneto-mechanical properties of an 18 at.% Ga sample and created transduction well into the tensile region [22]. Clark et al. [4] have found that $\text{Fe}_{100-x}\text{Ga}_x$ Galfenol alloys, $20 < x < 30$ have a stress dependent magnetostriction. Previous work on the characterization of polycrystalline Galfenol has been restricted to 18.4 at.% Ga composition [2]. Moreover, the full set of properties of the alloys in

tension has not been reported. In Chapter 2, actuation and sensing characteristics of 18.4 at.% Ga and 20.9 at.% Ga research grade, highly textured, $\langle 100 \rangle$ oriented polycrystalline Galfenol alloys in tension and compression are discussed. It has been observed that these alloys have a stress dependent susceptibility change which makes these alloys attractive for force and torque sensing.

1.3 Force Sensing

Conventional force sensors and load cells are typically based on strain gages or piezoelectric materials. Strain gages require precise bonding and elaborate signal processing. They have finite fatigue life and no overload protection [13]. Piezoelectric sensors are not readily suitable for harsh environments and cannot measure dc forces. The force sensing principle using Galfenol alloys is aimed at creating a simple robust force sensor that can easily be embedded in dynamic structures. Some applications that would benefit are electrohydraulic actuators, magnetic actuators and CNC machine tools that require continuous monitoring of force but have space constraints. Because Galfenol is a structural material, Galfenol sensors can bear large loads and can thus be placed in the load path. These embedded parts can behave as structural members as well as active sensors in harsh environments. Moreover, sensors based on magnetostrictive materials can be used in dynamic and static conditions unlike piezo based devices which can only be used in dynamic loading conditions. In Chapter 3 the principle of a force sensor utilizing the stress-dependent susceptibility change of Galfenol alloys is discussed.

1.4 Torque Sensing

Measurement of torque is useful in diverse range of automotive and industrial fields. It is one of the two fundamental physical quantities required to analyze rotating drive mechanisms. The other physical quantity is the speed of rotation. For example, the torque being transmitted by a driveshaft can provide information about the performance of the power train and the chassis of a vehicle. It is also useful in quantifying and analyzing transmission efficiencies. Previously, torque measurement was accomplished using contact type sensors directly attached to the shaft. Strain gage based torque sensors are popular, where one or more strain gauges are directly attached to the outer peripheral surface of the shaft and the shear strain measured is calibrated as the torque. However, contact-type sensors are relatively unstable and of limited reliability due to the direct contact with the rotating shaft. In addition, they are very expensive and are thus commercially impractical for use on a commercial vehicle [11]. In the analysis of existing torque sensing technologies, it has been concluded that in the automotive field a torque sensing system requiring neither components attached to, nor functionally in contact with the shaft would be desirable. Magnetoelastic torque sensors appear to meet these requirements [11]. In Chapter 4 the formability and the stress dependent susceptibility of Galfenol alloys is used to develop a contactless torque sensor.

CHAPTER 2

QUASI-STATIC CHARACTERIZATION OF TEXTURED POLYCRYSTALLINE 18.4 AT.% GA AND 20.9 AT.% GA GALFENOL ALLOYS

In this section the actuation and sensing characteristics of two research grade, highly textured, $\langle 100 \rangle$ oriented polycrystalline Galfenol alloys with 18.4 at.% Ga and 20.9 at.% Ga composition are discussed. Previous work on the characterization of polycrystalline Galfenol has been restricted to 18.4 at.% Ga composition [2]. The full set properties of the alloys in tension has not been reported; in this study, the two alloys are tested in tension and compression. The 20.9 at.% Ga alloy is used due to its low magnetocrystalline anisotropy and linear regions of stress-dependent magnetization [9]. The direct properties of the alloys aid in determining a suitable range of operation for sensing applications. It has been observed that these alloys have a stress-dependent susceptibility change which makes them attractive for force sensing.

2.1 Inverse (Actuation) Effect

The inverse effect based on magnetization versus field (M-H) and magnetostriction versus field (λ -H) measurements for the 18.4 at.% Ga and 20.9 at.% Ga Galfenol alloys are discussed in this section. The tests consists of applying a cyclic magnetic

field at a low frequency (~ 0.1 Hz), while measuring the change in magnetization ($M-H$) and magnetostriction ($\lambda-H$). This is repeated at constant tensile and compressive bias stress levels. A closed magnetic circuit with a flux return path is used to apply the magnetic field. A loading system with suitable fixtures is used to apply tensile and compressive loads on the sample. Sample preparation, description of the magnetic transducer and the measurement system are discussed in detail in the following subsections. Followed by that are results and discussion.

2.1.1 Sample Preparation

The alloys characterized for this study were purchased from Etrema Products. The $\text{Fe}_{81.6}\text{Ga}_{18.4}$ sample has a diameter of 0.25 inches and a length of 2.9 inches. The material was cut by wire EDM from the center of a 1.0 inch diameter rod by 2.9 inch length rod grown by the FSZM method. The $\text{Fe}_{79.1}\text{Ga}_{20.9}$ sample used for the test was 0.25 inch diameter by 2.9 inch long cut by wire EDM from a 0.25 inch diameter rod which had a length of 4.0 inches, also grown by the FSZM method. The ends of the test samples were threaded ($1/4 \times 28$ inch) using standard HSS tools and standard thread cutting procedures (Figure 2.1). The speeds and feeds used for machining were similar to that of cast iron. The threading was done to adapt to stainless steel end caps that would facilitate tensile and compressive loading of the samples using MTS 647 Hydraulic Wedge grips. An OMEGA (SGD-3/350-LY11) linear axial strain gage was bonded at the center of the test samples to measure the surface strain.

2.1.2 Magnetic Transducer

A magnetic circuit with two excitation coils and a flux return path was constructed using laminated steel plates as shown in Figure 2.2. The laminated steel plates

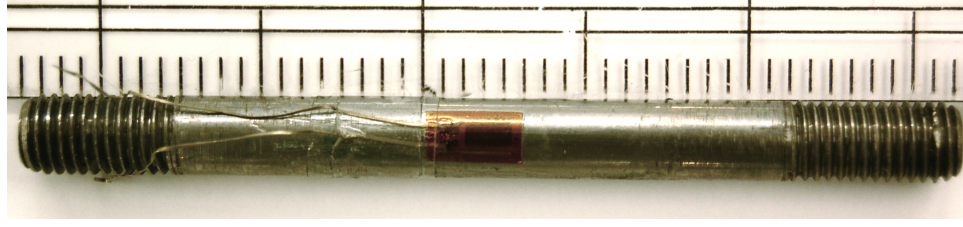


Figure 2.1: $\text{Fe}_{81.6}\text{Ga}_{18.4}$ test sample with threaded ends and strain gage bonded at the center of the rod.

reduce eddy currents in the circuit. The transducer can produce a magnetic field of $\sim 30\text{kA/m}$, measured at the mid-span of the Galfenol test sample along its length. This is intense enough to saturate both alloys in the stress range of interest. The two coils have windings in opposite direction and excited in parallel, such that they generate flux flowing in opposite directions as shown in Figure 2.2. Figure 2.3 shows the entire transducer assembly with the Galfenol sample, end caps, and pick-up coil. A 1:1 scale 3-D model of the transducer was simulated in COMSOL to study the flux distribution and strain developed in the Galfenol rod. A relative permeability value of 329 was used for the Galfenol material. Figure 2.4 shows the axial flux density (BY) when a current density of 1000 kA/m^2 is applied to the coils. Figure 2.5 shows the axial strain (Y-component) developed in the rod when a current density of 1000 kA/m^2 is applied to the coils. It is seen from the simulations that the flux density is concentrated and uniform in the sample and the strain due to the magnetoelastic coupling occurs in the region where the flux density is most concentrated.

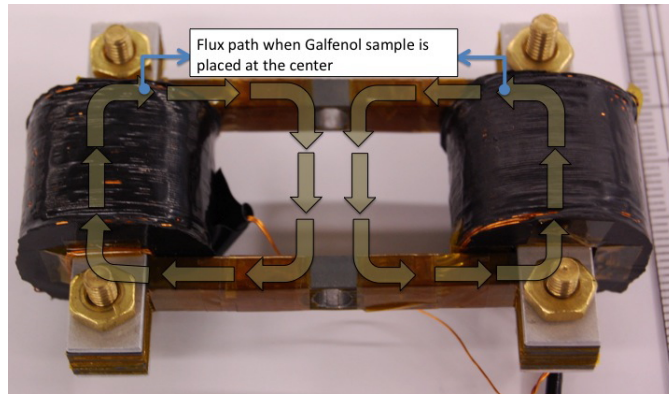


Figure 2.2: Magnetic transducer made of laminated steel plates. The arrows indicate the flux path when the coils are excited with the Galfenol sample at the center.

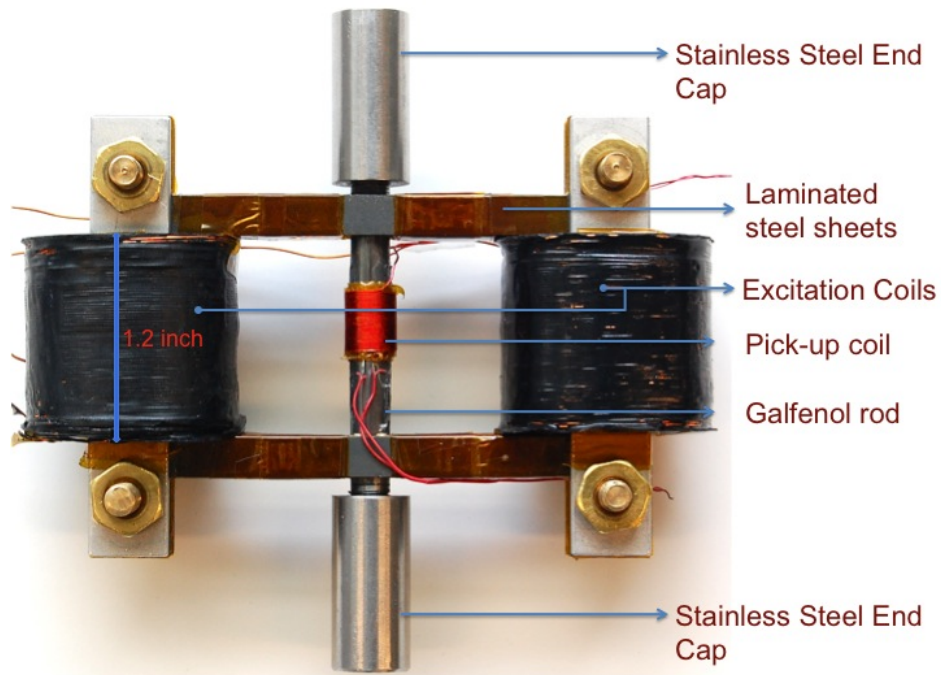


Figure 2.3: Magnetic transducer assembly with the Galfenol rod, stainless steel end caps and pickup coil.

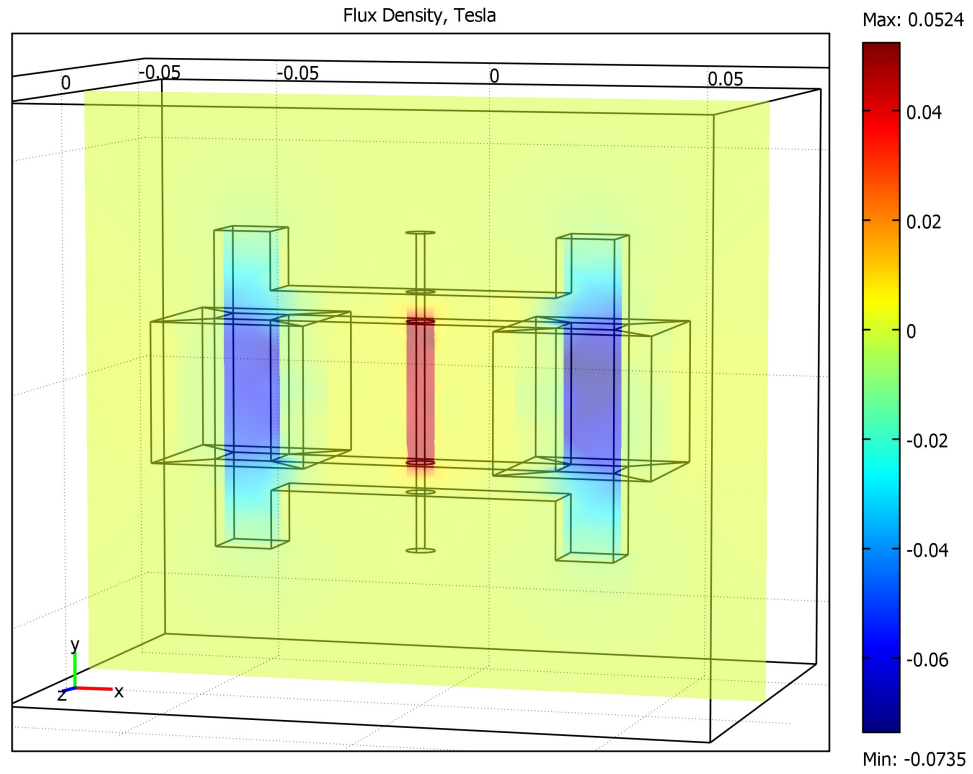


Figure 2.4: Quasi-static 3-D COMSOL simulation: slice plot of the Y-component of flux in the transducer with the Galfenol sample for an applied current density of 1000 kA/m².

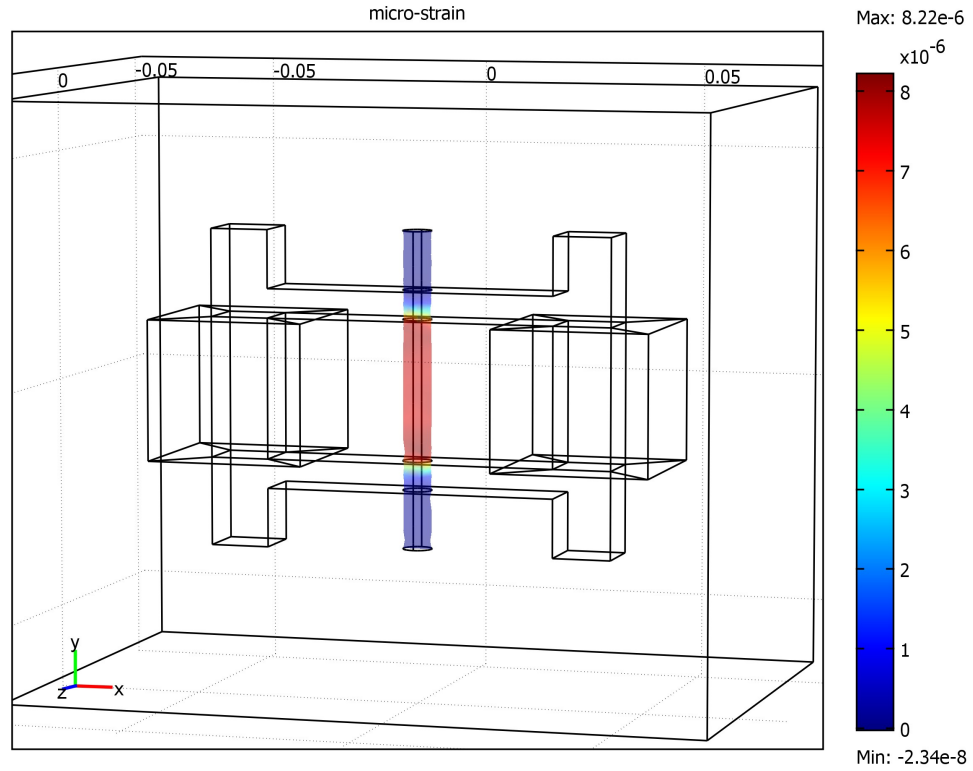


Figure 2.5: Quasi-static 3-D COMSOL simulation: slice plot of the Y-component micro-strain in the Galfenol sample for an applied current density of 1000 kA/m^2 .

2.1.3 Magnetization versus Applied Field and Magnetostriction versus Applied Field Measurements

An elastomer test frame (MTS 831.1) was used to apply the constant bias stress from -63.71 MPa to 63.71 MPa prior to magnetic field application. The test setup is shown in Figure 2.6. A close-up view of the test sample mounted on the hydraulic grips with the Hall probe and pick up coil is shown in Figure 2.7. A sinusoidal magnetic field of 25kA/m at 0.1 Hz was applied using the transducer described in the previous section. The flux density was measured using a Walker Scientific MF 5D Fluxmeter and a pick-up coil midway along the length of the test sample (Figure 2.7). The magnetic field was measured using a Hall probe and Walker Scientific MG-4D Gaussmeter (Figure 2.7). The Hall probe was positioned using a micro-positioning fixture within 1 mm from the sample surface immediately after the pick-up coil at the mid length of the rod to get an accurate measure of the field in the sample. The magnetization is calculated by subtracting the applied field from the flux density measurement. The strain in the sample was measured using an OMEGA (SGD-3/350-LY11) axial strain gage and a Vishay 2310 B signal conditioner. The Quattro-Signal Calc data acquisition system manufactured by Data Physics Corporation was used to acquire all the measurements. For all tests the sampling frequency was 102.45 Hz for a total time span of 20.0 seconds.

2.1.4 Results and Discussion Inverse Effect

The magnetization curves for the $\text{Fe}_{81.6}\text{Ga}_{18.4}$ Galfenol alloy at constant stress values are shown in Figure 2.8. The M-H curves show a steep rise in magnetization

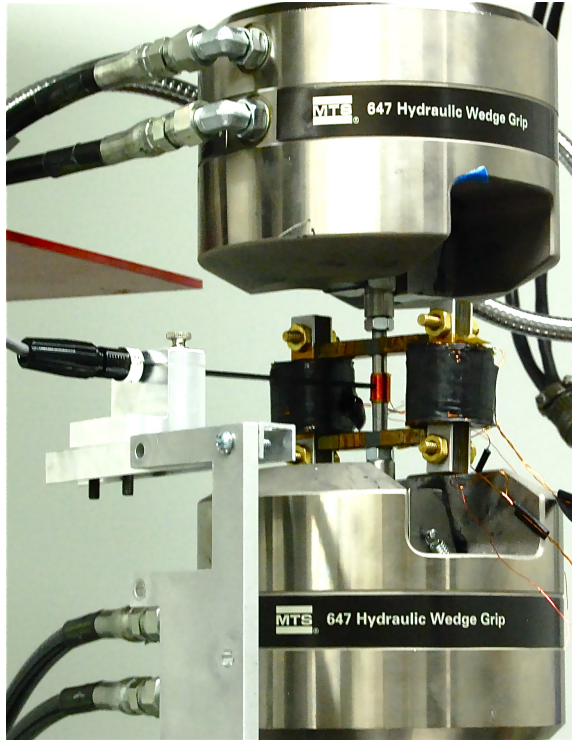


Figure 2.6: Test setup for actuation and sensing characterization.

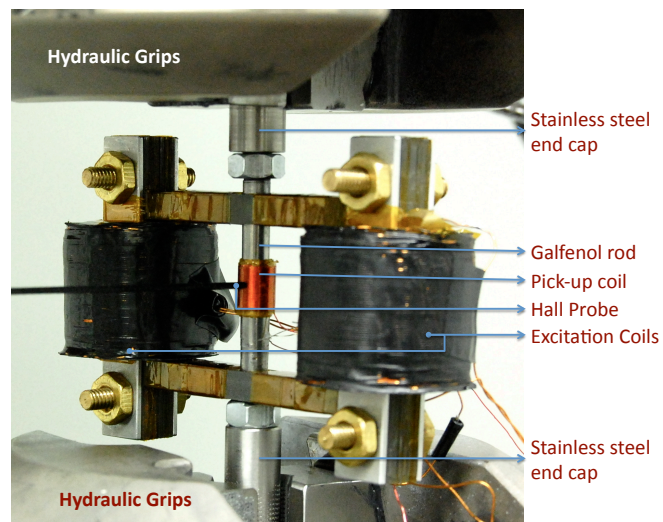


Figure 2.7: Test sample mounted on the hydraulic grips for applying tensile and compressive loads.

under constant tensile stress and a distinct kinking behavior under constant compressive stress. The magnetization change under constant compressive stress can be divided into three regions. Region 1 is characterized by small changes in magnetization at low applied fields, region 2 is characterized by a steep rise in magnetization for small changes in applied field and in region 3 saturation occurs where there is no change in magnetization with increase in applied field. When the compressive stress is increased, the range of region 1 extends and larger magnetic fields are required to saturate the material. The magnetostriction curves are shown in Figure 2.9. The saturation magnetostriction λ_s , decreases with increasing tensile stress and drops to zero at 21.23 MPa and higher tensile stress levels. The saturation magnetostriction increases with increasing compressive stress up to -49.56 MPa and there is a slight drop in the saturation magnetostriction at -56.63 MPa and -63.71 MPa. This slight drop in λ_s at higher compressive stress levels has been observed earlier by previous researchers [2]. The exact reason for this behavior is still not known.

The magnetization curves for the Fe_{79.1}Ga_{20.9} Galfenol alloy at constant stress values are shown in Figure 2.10. The behavior of 20.9 at.% Ga alloy is similar to the lower Ga content alloy under tensile loading, but under compressive loading the behavior is slightly different. The distinct kinking observed in the lower Ga content alloy is absent and the magnetization curves are more smooth and rounded. Though the kinking is absent there are two regions of different slopes observed with increasing compressive stress. The magnetostriction curves at constant stress values are shown in Figure 2.11. λ_s decreases with increasing tensile stress and drops to zero at 35.4 MPa and higher tensile stress levels. λ_s increases with increasing compressive stress up to -49.56 MPa and there is a slight drop in λ_s at -56.63 MPa and -63.71 MPa. λ_s

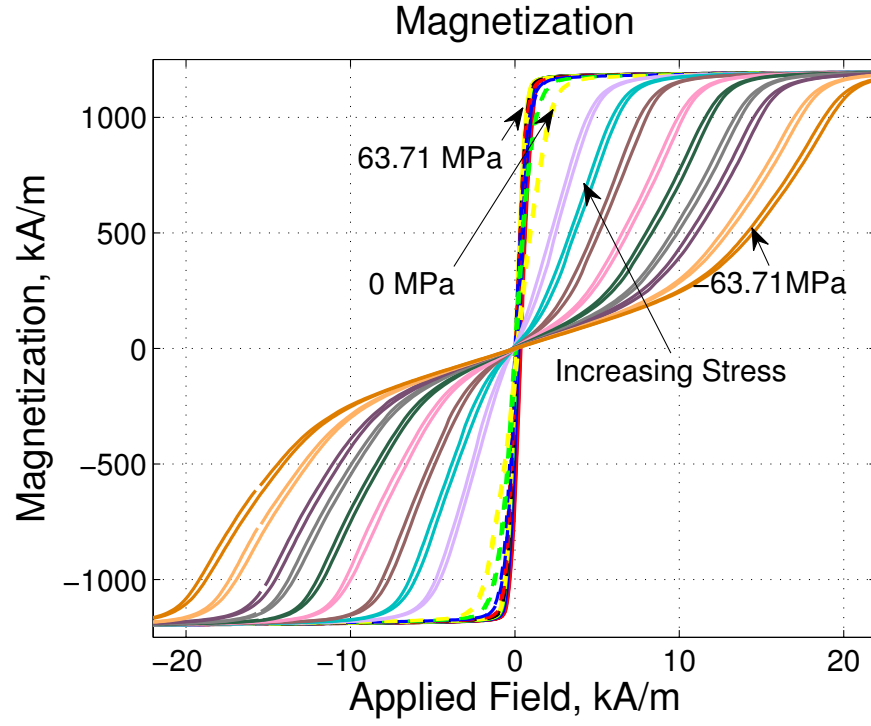


Figure 2.8: Magnetization curves for Fe_{81.6}Ga_{18.4} at constant stress (63.71, 56.63, 49.56, 42.47, 35.4, 28.31, 21.23, 14.15, 7.07, 0, -7.07, -14.15, -21.23, -28.31, -35.4, -42.47, -49.56, -56.63 and -63.71 MPa).

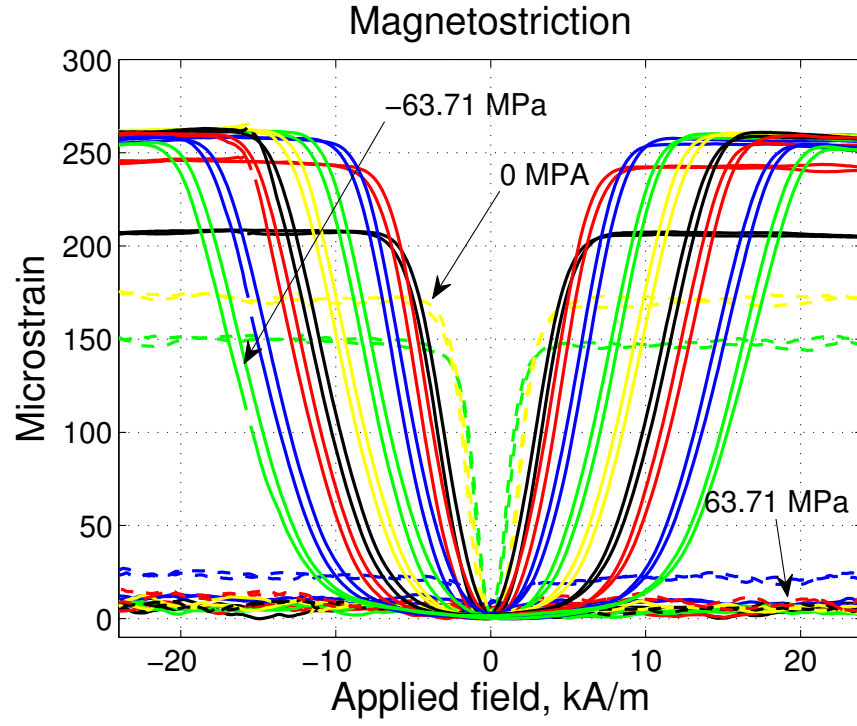


Figure 2.9: Magnetostriction curves for $\text{Fe}_{81.6}\text{Ga}_{18.4}$ at constant stress (63.71, 56.63, 49.56, 42.47, 35.4, 28.31, 21.23, 14.15, 7.07, 0, -7.07, -14.15, -21.23, -28.31, -35.4, -42.47, -49.56, -56.63 and -63.71 MPa).

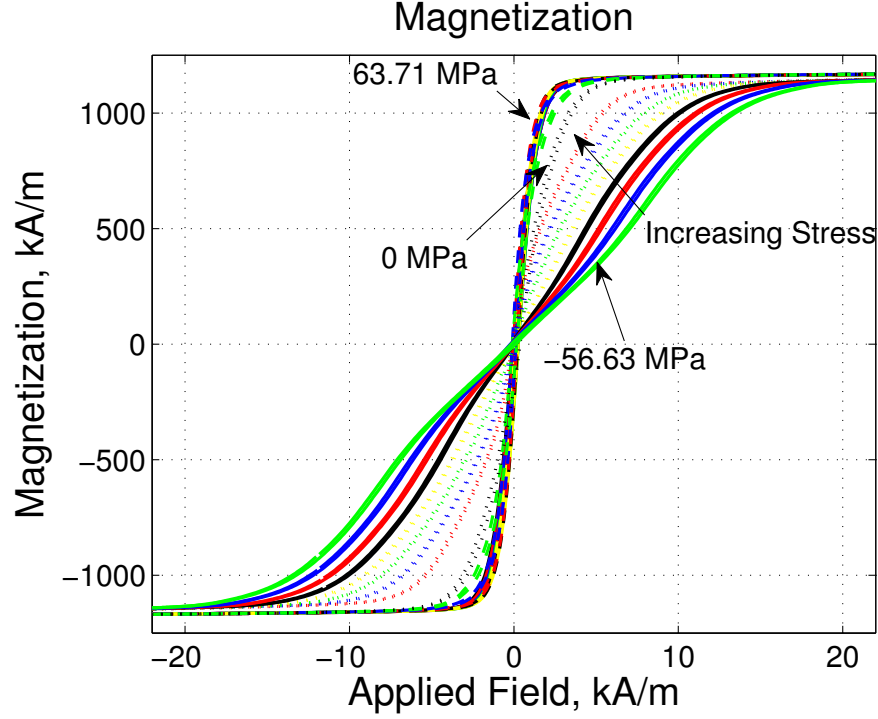


Figure 2.10: Magnetization curves for Fe_{79.1}Ga_{20.9} at constant stress (63.71, 56.63, 49.56, 42.47, 35.4, 28.31, 21.23, 14.15, 7.07, 0, -7.07, -14.15, -21.23, -28.31, -35.4, -42.47, -49.56, and -56.63 MPa).

is lower for the 20.9 at.% Ga alloy ($\lambda_s=200\text{ppm}$ at -49.56 MPa prestress) compared to the 18.4 at% Ga alloy ($\lambda_s=265\text{ppm}$ at -49.56 MPa prestress).

The fact that ferromagnetic materials are composed of regions of uniform magnetization below the Curie temperature is used to explain the magnetization and magnetostriction behavior. These regions of uniform magnetization are called domains, the magnetic domains have preferred orientations which depend on anisotropy, magnetic field and stress. In the absence of magnetic field and stress Galfenol has six equilibrium orientations in the [100] directions. An external applied field causes the domain orientations to rotate towards the direction of the field and compressive stress

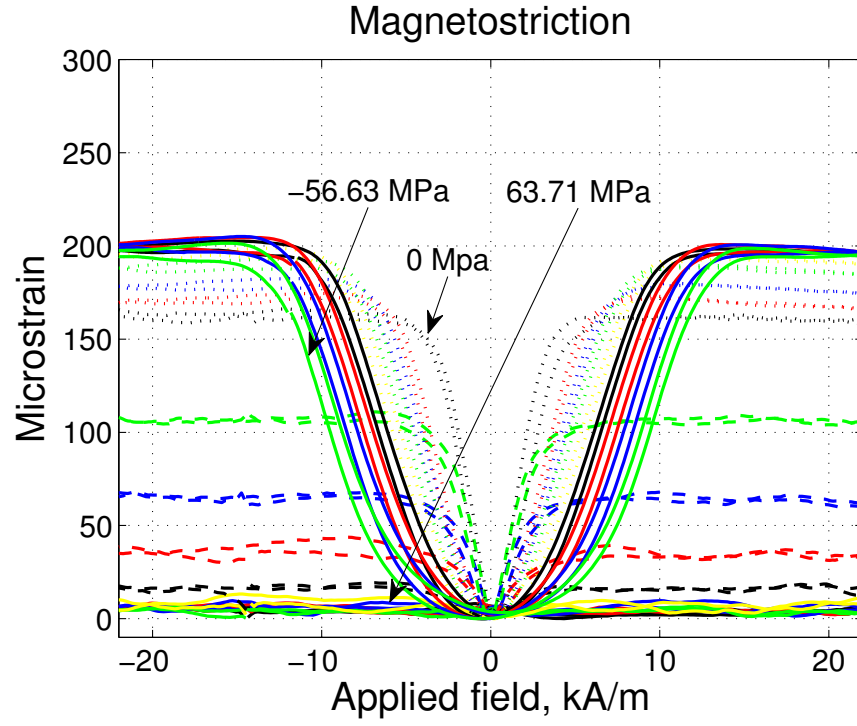


Figure 2.11: Magnetostriction curves for $\text{Fe}_{79.1}\text{Ga}_{20.9}$ at constant stress (63.71, 56.63, 49.56, 42.47, 35.4, 28.31, 21.23, 14.15, 7.07, 0, -7.07, -14.15, -21.23, -28.31, -35.4, -42.47, -49.56, and -56.63 MPa).

cause the domain orientations to rotate perpendicular to the direction of the stress. At zero applied field, the compressive stress lowers the energy of the four basal planes $[010]$, $[0\bar{1}0]$, $[001]$ and $[00\bar{1}]$; with sufficient compressive stress across the area of the magnetostrictive material, $\langle 100 \rangle$ oriented domains in the rod are forced to align along the basal planes perpendicular to the axis of the rod. In the low magnetic field region (Region 1) the change in the magnetization is dominated by the stress dependent rotation of domains. The energy due to applied magnetic field goes into overcoming the stress anisotropy and domains start to rotate from the basal plane towards the direction of the applied field. In this region there is a small rise in magnetostriction. A critical field is reached when the domains start flipping, and the size of favorably oriented domains increase at the expense of other higher energy domains by domain wall motion, which is region 2 where there is a steep increase in the magnetization and magnetostriction. The volume of the material is constant and the increase in axial strain causes a reduction in diameter. For a positive magnetostrictive material the axial strain is always positive (increase in length) irrespective of the direction of the applied axial field. Once all the domains align in the direction of the magnetic field by domain rotation, domain flipping and domain wall motion, the material saturates (Region 3) and there is little change in the magnetization and magnetostriction with increasing magnetic field. Since all the domains do not rotate and flip simultaneously there is a gradual switch from domain rotation to domain flipping to domain wall motion. While a certain volume fraction of the domains rotate there is a certain volume fraction that starts flipping and another that increase in size by domain wall motion, hence the smooth transitions in the magnetization and magnetostriction curves rather than sharp transitions. Region 2 for the magnetization curves at -7.07

MPa and -14.15 MPa is small as the compressive stress is not sufficient to align all the domains along the basal planes, thus the domain flipping and domain wall motion are dominant. An interesting behavior is the small reduction in the magnetostriction at higher compressive stress levels (-56.63 MPa and -63.71 MPa).

A steep increase in the magnetization is observed at zero applied stress and when a constant tensile stress is applied. This is due to the flipping of the $\langle 100 \rangle$ oriented domains to align in the direction of the magnetic field, the tensile stress aligns all the domains in the $\langle 100 \rangle$ and the applied field goes into flipping them all to the direction of the applied field. Under tension λ_s decreases with increasing tensile stress and after a tensile stress level there is no magnetostriction in the material. Under tension the domains align in the direction of the tensile stress which is the $\langle 100 \rangle$ direction. Since the applied field is also in the $\langle 100 \rangle$ direction there is no further increase in magnetostriction in the same direction due to the applied field. There is no magnetostriction in the material beyond 21.23 MPa and the material behaves as an ordinary ferromagnetic material. The applied field has no effect on the 18.4 at.% Ga alloy beyond 21.23 MPa.

In the case of the higher Ga content alloys the crystal anisotropy is low [19]. Hence, the change in magnetization is dominated by stress anisotropy rather than magnetocrystalline anisotropy at all applied fields until saturation. The steep rise in magnetization at intermediate fields (kinking behavior) is not observed in 20.9 at.% Ga sample as the domain flipping seen in overcoming crystal anisotropy in this alloy is almost absent. The energy due to applied magnetic field goes into overcoming the stress anisotropy and domains rotate from the basal plane towards the direction of the applied field. The stress dependent change in magnetization of this alloy and the

linear regions in the magnetization curves make this alloy a suitable candidate for stress dependent sensing applications. The saturation magnetostriction of this alloy is low compared to 18.4 at.% Ga alloy, which is in line with the observation of Clark et al [3]. The magnetostriction starts to drop after 19 at.% Ga up to 24.7 at.% Ga [3].

2.2 Direct (Sensing) Effect

Magnetization versus stress ($M-\sigma$) and strain versus stress ($\epsilon-\sigma$) measurements for the 18.4 at.% Ga and 20.9 at.% Ga Galfenol alloys are discussed. Studying the direct effect involves application of cyclic stress at a low frequency (0.04 Hz in this case), while measuring the change in magnetization ($M-\sigma$) and strain ($\epsilon-\sigma$). This measurement is repeated at different bias fields.

2.2.1 Sample Preparation

Research grade highly textured $\langle 100 \rangle$ oriented polycrystalline $\text{Fe}_{81.6}\text{Ga}_{18.4}$ and $\text{Fe}_{79.1}\text{Ga}_{20.9}$ samples that were used to study the inverse effect are used to study the direct effect.

2.2.2 Magnetic Transducer

The same magnetic transducer shown in Figure 2.3 that was used to study the inverse effect is used to study the direct effect of these alloys.

2.2.3 Magnetization versus Stress and Strain versus Stress Measurements

An INSTRON 1321 test frame was used to apply the cyclic stress between -63.71 MPa to 63.71 MPa at a frequency of 0.04Hz. The tests were conducted in the setup shown in Figure 2.7. The magnetization and strain in response to a cyclic stress were

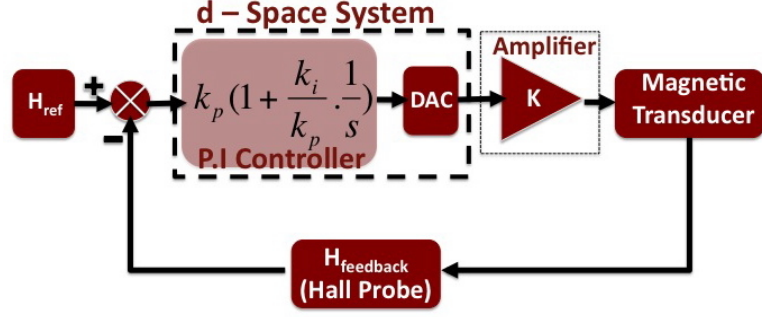


Figure 2.12: Feedback control used to maintain constant magnetic field ($k_p=0.35$, $k_i=0.55$).

measured at constant DC bias field levels. The $M-\sigma$ and $\epsilon-\sigma$ curves were measured in two ways: (i) Maintaining constant current to the magnetic transducer and (ii) Maintaining constant magnetic field in the Galfenol sample by using a closed loop feedback control. In the second case a PI controller as shown in Figure 2.12 was used to maintain the magnetic field constant by varying the current to the magnetic transducer based on the feedback signal. The magnetic field was measured using a Hall probe and Walker Scientific MG-4D Gaussmeter (Figure 2.7). The Hall probe was positioned using a micro-positioning fixture within 1 mm from the sample surface immediately after the pick-up coil at the mid length of the sample to get an accurate measure of the field in the sample. The magnetization was calculated by subtracting the applied field from the flux density measurement. The strain in the sample was measured using an OMEGA (SGD-3/350-LY11) axial strain gage and a Vishay 2310 B signal conditioner which had an in-built strain bridge. The MTS Station Manager data acquisition system was used to acquire all the measurements. The sampling frequency was 100 Hz for a total time span of 50.0 seconds.

2.2.4 Results and Discussion Direct Effect

The magnetostrictive sample which is a part of the magnetic circuit can alter the reluctance of the circuit. The susceptibility of Gallenol alloy changes as a function of applied stress. The change in susceptibility of the sample as a function of stress cause a change in the reluctance of the magnetic circuit. When the drive current to the coils is constant the actual field seen by the sample changes as the stress varies between 63.71 MPa to -63.71 MPa. In order to maintain a constant magnetic field in the sample during the stress cycle a PI controller was used to compensate the current based on feedback from the Hall probe and Gaussmeter. The schematic of the feedback loop is shown in Figure 2.12.

Figure 2.13 shows the M - σ curves when the drive current is constant and when the magnetic field is constant using a feedback loop. The magnetization change is more sensitive to changes in stress when the magnetic field is constant which make the M - σ curves look steeper when compared to the constant drive current measurements. Figure 2.14 shows the ϵ - σ curves when the drive current is constant and when the magnetic field is constant using a feedback loop. The non-linear strain change as a function of stress is more evident when the magnetic field is held constant using the control loop. Figure 2.15 shows the M - σ curves when the drive current is constant and when the magnetic field is constant using a feedback loop. Figure 2.16 shows the ϵ - σ curves when the drive current is constant and when the magnetic field is constant using a feedback loop. In discussing the sensing behavior all references to the M - σ and ϵ - σ curves will be made to the constant magnetic field measurements.

The magnetic field is applied along the $\langle 100 \rangle$ direction which cause the domains to align along $\langle 100 \rangle$. During the compressive stress cycle the domains try to rotate

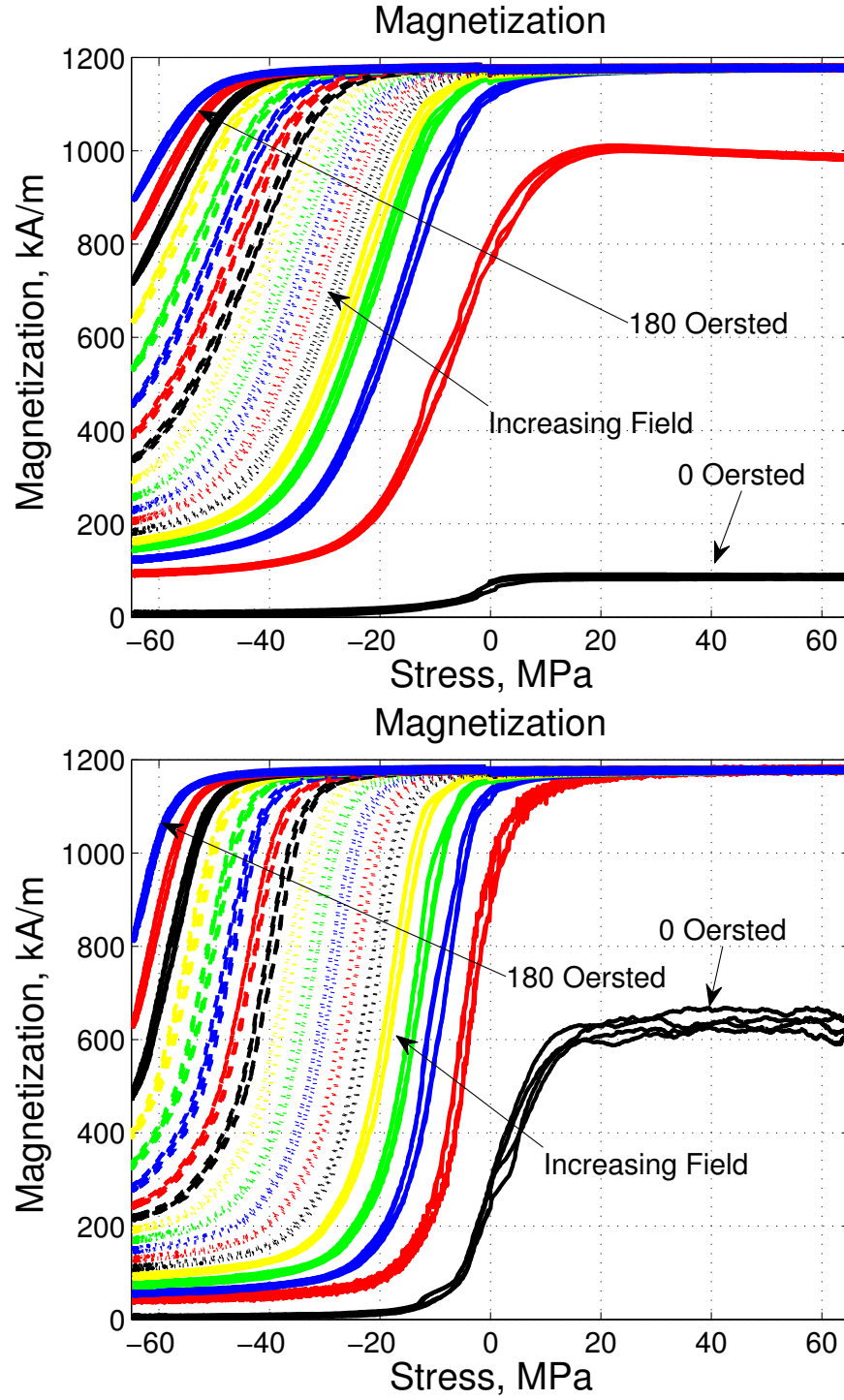


Figure 2.13: Magnetization curves for $\text{Fe}_{81.6}\text{Ga}_{18.4}$. Top: Constant current to the coils. Bottom: Constant magnetic field (0, 20, 30, 40, 50, 60, 70, 80, 90, 100, 110, 120, 130, 140, 180 Oersted).

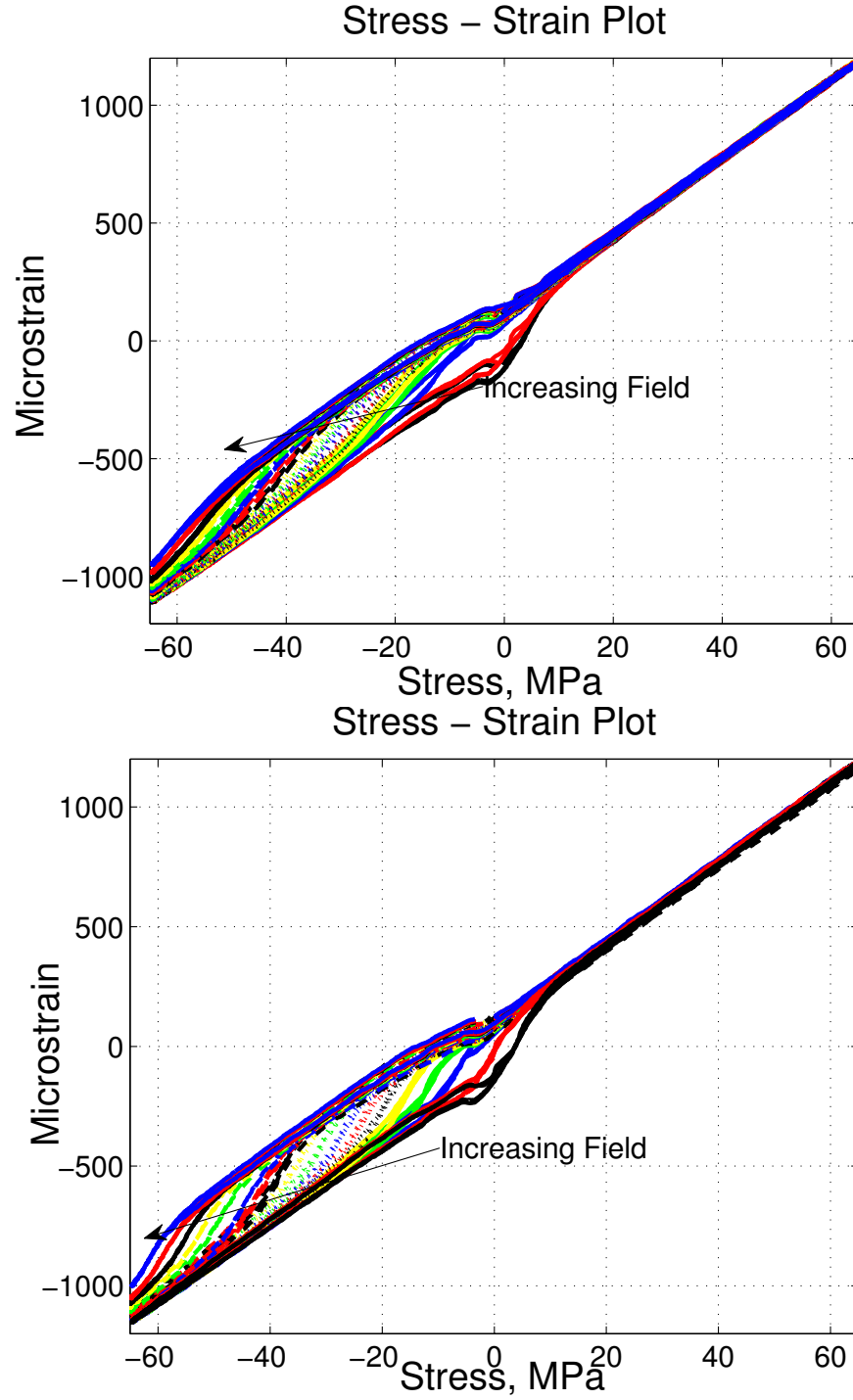


Figure 2.14: Strain-Stress curves for $\text{Fe}_{81.6}\text{Ga}_{18.4}$. Top: Constant current to the coils. Bottom: Constant magnetic field (0, 20, 30, 40, 50, 60, 70, 80, 90, 100, 110, 120, 130, 140, 180 Oersted).

perpendicular to the direction of the applied stress and magnetic field. The compressive stress reduces the energy of the four basal planes ($[010]$, $[0\bar{1}0]$, $[001]$ and $[00\bar{1}]$). The domains rotate and flip towards the basal plane overcoming the applied field and anisotropy energy. This is seen as the steep increase in magnetization as a function of stress. When all the domains align along the four basal planes under sufficient compressive stress the material saturates and there is no change in magnetization with increasing stress. At small applied fields the stress required to overcome the applied field and anisotropy is small. Hence a steep change in magnetization as a function of stress occurs at lower values of stress. With increasing bias fields large stresses are required to overcome the energy due to applied field. Under tensile stress there is no change in the magnetization at all field levels. The applied field and tensile stress make $\langle 100 \rangle$ direction to be the easy axis. All the domains are aligned in the $\langle 100 \rangle$ direction and the material behaves like an ordinary ferro-magnetic material. The stress-strain relation is also linear in the tensile region as the material saturates with all the domains aligned in along $\langle 100 \rangle$.

Comparison of the 18.4 at.% Ga alloy 20.9 at.% Ga alloys indicates that the higher Ga content alloy has smoother and more rounded curves. The 18.4 at.% Ga alloy is more sensitive as a large change in magnetization is observed for a given increase in stress. The change in magnetization as a function of stress is more gradual for the 20.9 at.% Ga alloy. The magnetization changes are extended over a larger stress range. The operating stress range of the 20.9 at.% alloy is larger than the 18.4 at.% alloy. The increase in stress range is due to the lower anisotropy and stress-dependent magnetization change of the higher Ga content alloy. The steep change in

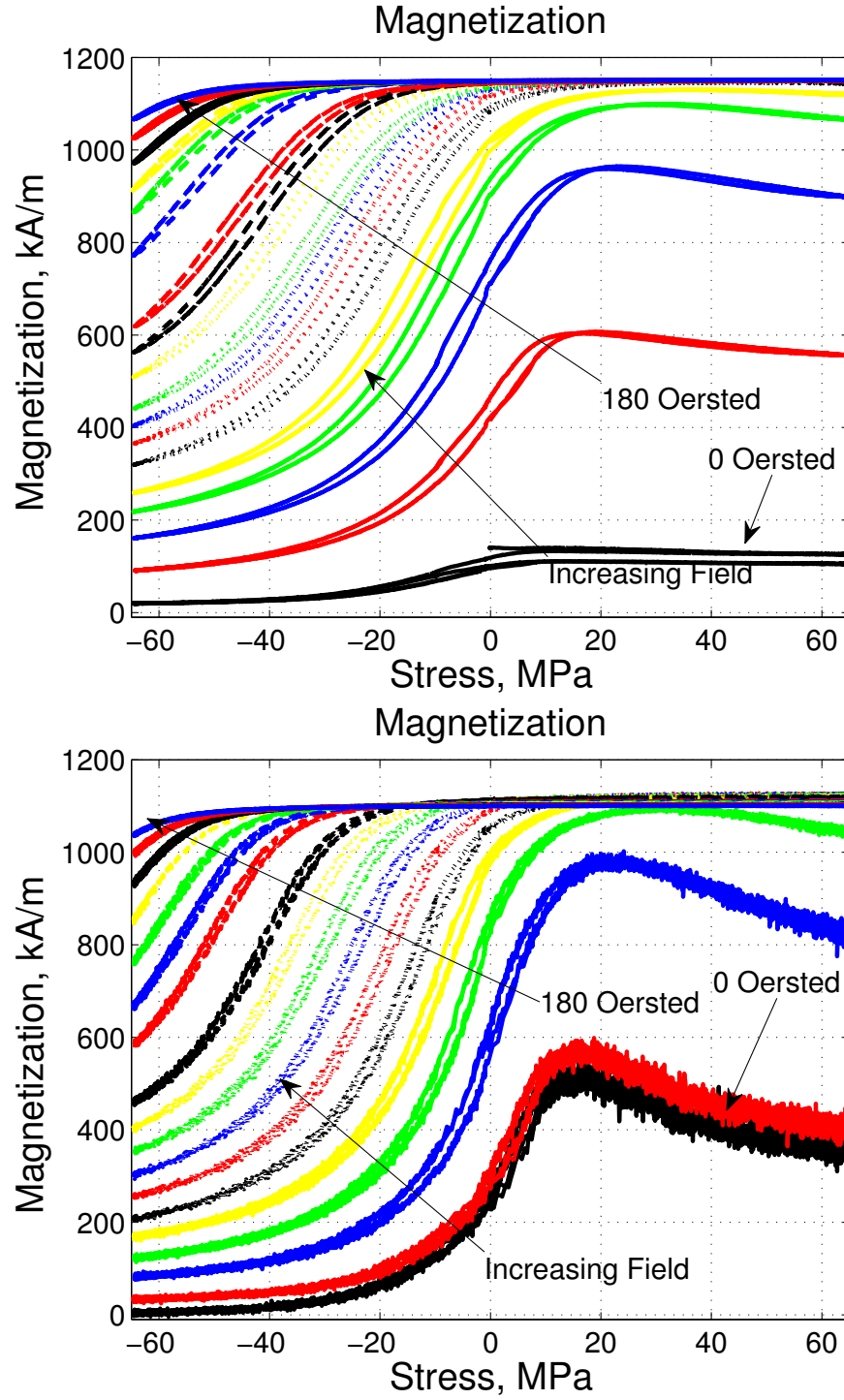


Figure 2.15: Magnetization curves for $\text{Fe}_{79.1}\text{Ga}_{20.9}$. Top: Constant current to the coils. Bottom: Constant magnetic field (0, 10, 20, 30, 40, 50, 60, 70, 80, 90, 100, 120, 130, 140, 180 Oersted).

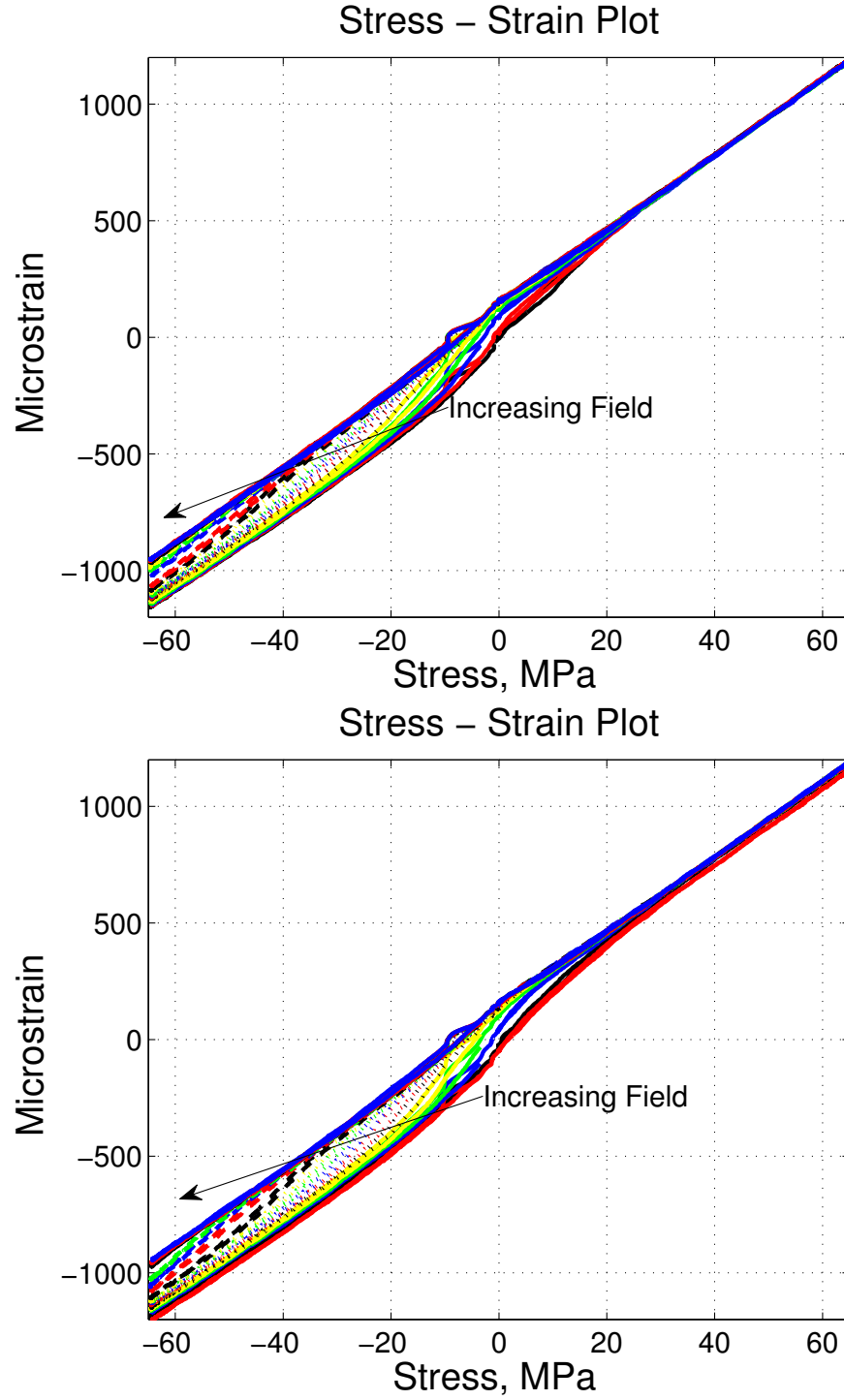


Figure 2.16: Strain-Stress curves for $\text{Fe}_{79.1}\text{Ga}_{20.9}$. Top: Constant current to the coils. Bottom: Constant magnetic field (0, 10, 20, 30, 40, 50, 60, 70, 80, 90, 100, 120, 130, 140, 180 Oersted).

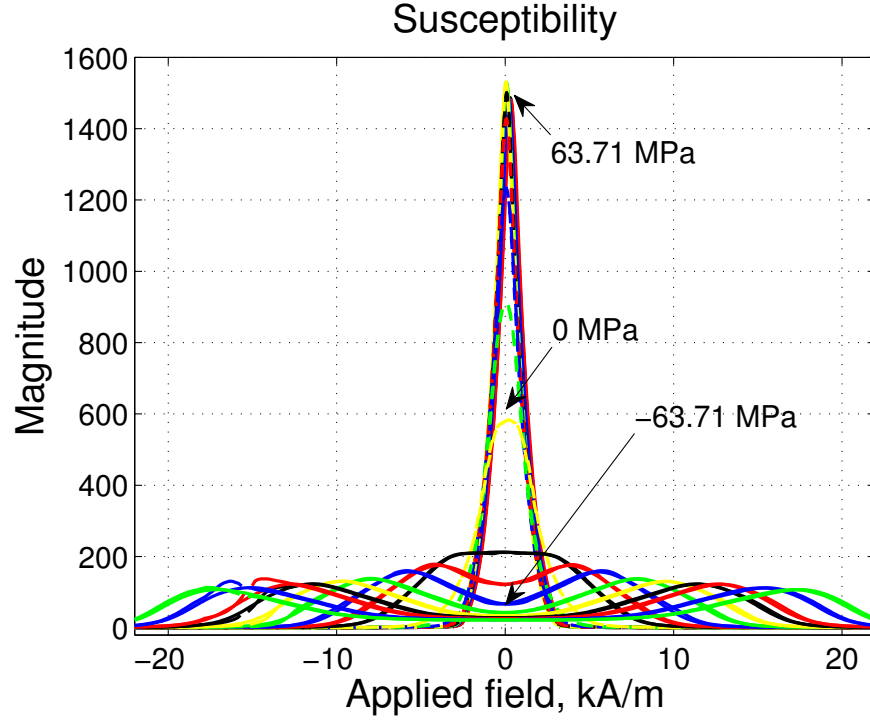


Figure 2.17: Differential susceptibility change as function of applied field for $\text{Fe}_{81.6}\text{Ga}_{18.4}$ at constant stress (63.71, 56.63, 49.56, 42.47, 35.4, 28.31, 21.23, 14.15, 7.07, 0, -7.07, -14.15, -21.23, -28.31, -35.4, -42.47, -49.56, -56.63 and -63.71 MPa).

magnetization, when the crystal anisotropy is overcome, is absent in the 20.9 at.% Ga alloy.

2.3 Stress Dependent Susceptibility

2.3.1 Susceptibility Change of 18.4 at.% Ga Alloy at Constant Stress

The differential susceptibility is defined as the change in the magnetization for a step change in the applied field, and is obtained by differentiation from the $M - H$ measurements. Figure 2.17 shows the susceptibility change as a function of applied field at constant stress values for 18.4 at.% Ga alloy. A single peak occurs at zero

applied field when no stress is applied and at constant tensile stress. When a constant compressive stress is applied the kinking behavior observed in the magnetization measurements for this sample manifests as two peaks, one at positive field value and one at the negative field value. The valley at low applied fields is the region of stress-dependent domain rotation. The susceptibility at zero applied field decreases with increasing compressive stress. The cubic magnetocrystalline anisotropy for Ga alloys decreases with increasing Ga content. It has been shown in previous literature that K_1 and K_2 both drop gradually and there is a sharp drop at 20 at.% Ga [19]. The higher magnetocrystalline anisotropy of the 18 at.% Ga alloy is responsible for the kinking behavior shown in the magnetization curves, the magnetocrystalline anisotropy needs to be overcome before the domains start flipping to align in the direction of the field [1]. The material has $\langle 100 \rangle$ orientation and when the tensile stress is applied along $\langle 100 \rangle$ direction it further lowers the energy along this direction. In this condition, at zero stress or in tension, the domains aligned along one of the $[100]$ directions immediately overcome the anisotropy energy and flip to the $\langle 100 \rangle$ direction along which field is applied. Additionally, the peak value of susceptibility at zero applied field increases with increasing tensile stress up to +35MPa and then starts to decrease. When a constant compressive stress is applied, the domain rotation region observed in the magnetization curves is seen as the valley in the susceptibility curves. Followed by the valley at low applied fields are two peaks; one at a positive field and one at a negative field. In this region, the magnetocrystalline anisotropy is overcome and the domains flip into the direction of the applied field. This is followed by saturation and the susceptibility change starts to decay.

2.3.2 Susceptibility Change of 20.9 at.% Ga Alloy at Constant Stress

Figure 2.18 shows the susceptibility change as a function of applied field at constant stress values for the 20.9 at.% Ga alloy. The susceptibility curves at constant tensile stress are similar to the lower Ga content alloy, but the magnitude of the peak susceptibility at zero applied field for the same stress is much lower. Under constant compressive stress there is only one peak at zero applied field until -35MPa, and as the compressive stress increases from -35 MPa to -56 MPa the two peaks at intermediate fields and a valley in the low field region are observed. The peaks have a larger radius of curvature and are less sharp compared to the susceptibility curves of the 18.4 at.% Ga sample. Both of the above described effects are due to its low crystal anisotropy.

2.3.3 Comparison of the Differential Susceptibility

The susceptibility change as a function of stress is maximum at zero applied field for both samples, as shown in Figure 2.19. The lower Ga content alloy has a larger magnitude of susceptibility at all tensile stress values. The susceptibility of the lower Ga content alloy has greater sensitivity to stress in the domain rotation region ($\pm 5\text{kA/m}$ applied field) at stresses ranging from -20 MPa to +20 MPa, but starts to decay below -20 MPa. The susceptibility of the higher Ga content alloy is sensitive to a larger stress range from -56.63 MPa to 20 MPa in the domain rotation region and the stress-dependent susceptibility change is more gradual than it is for the lower Ga content alloy. The susceptibility change decays below -56.63 MPa and there is little change in the susceptibility with further increase in compression. The measurements

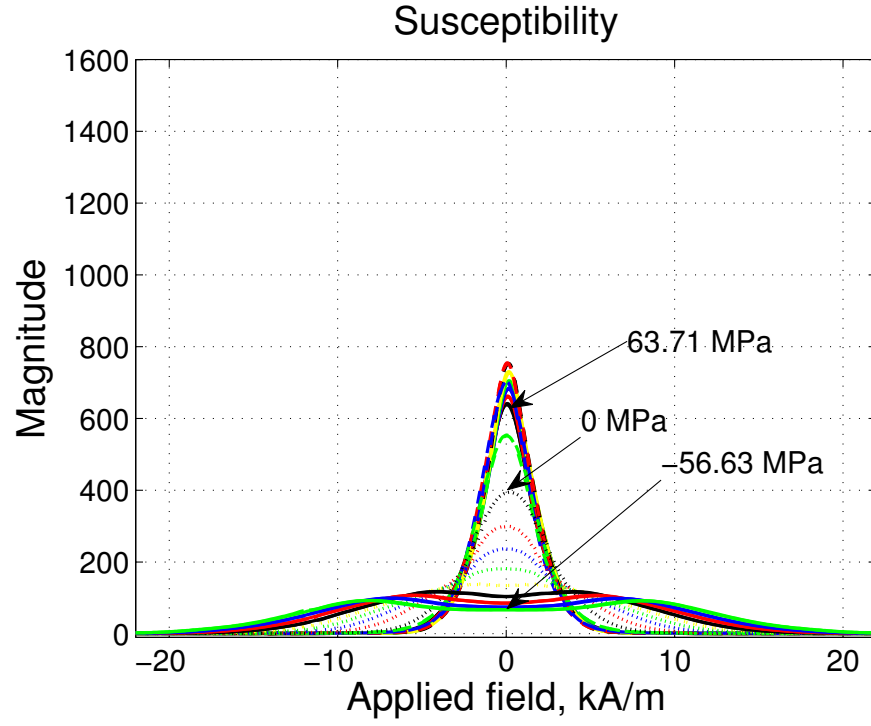


Figure 2.18: Differential susceptibility change as function of applied field for $\text{Fe}_{79.1}\text{Ga}_{20.9}$ at constant stress (63.71, 56.63, 49.56, 42.47, 35.4, 28.31, 21.23, 14.15, 7.07, 0, -7.07, -14.15, -21.23, -28.31, -35.4, -42.47, -49.56, and -56.63 MPa).

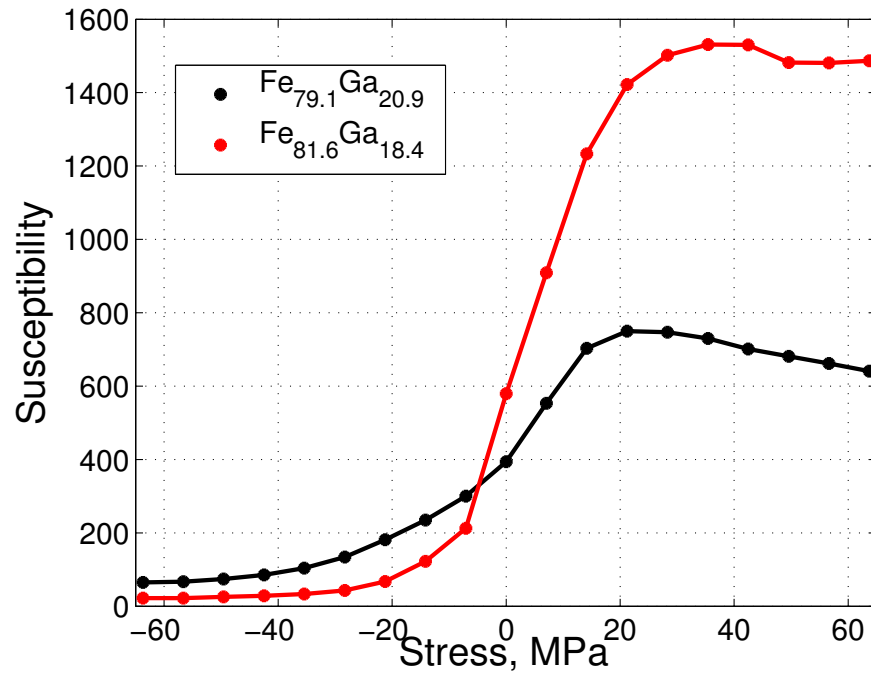


Figure 2.19: Stress dependent susceptibility of $\text{Fe}_{81.6}\text{Ga}_{18.4}$ and $\text{Fe}_{79.1}\text{Ga}_{20.9}$ at zero applied field.

presented above for the two Ga alloys can serve as a database for these two materials. These measurements can be used to design a force sensor or a torque sensor working on the principle of stress-dependent susceptibility.

CHAPTER 3

FORCE SENSING USING TEXTURED POLYCRYSTALLINE Galfenol ALLOYS

In the current chapter, the principle of a force sensor utilizing the stress-dependent susceptibility change of Galfenol alloys is discussed. Proof of concept experiments are done using 18.4 at.% Ga and 20.9 at.% Ga Galfenol alloys. These experiments also determine the usable range for quasi-static operation of the two alloys for force sensing. The sensor principle is also simulated in COMSOL. The sensor principle is based on amplitude modulation which would create a robust sensor that would not be contaminated by external noise when used in harsh environments. The sensor has good sensitivity and low energy is required to excite the system.

3.1 Force Sensor Principle

Kleinke and Uras [13] proposed a magnetoelastic force sensor using a transformer made from a magnetostrictive material with an excitation coil in one arm and a detection coil in the other. An amplitude modulated signal results and the stress or force is related to the amplitude ratio between the drive and pickup coil. A similar principle is used to develop a Galfenol force sensor. When force is applied to a Galfenol sample placed in a closed magnetic circuit with a flux return path, the stress causes

a change in its permeability, which in turn changes the reluctances of the magnetic circuit. This change in reluctance is detected by a pick-up coil wound on the sample (Figure 3.1). When the magnetic circuit is excited by an AC magnetic field at a frequency sufficiently higher than the stress frequency, the reluctance change in the circuit is detected as a modulated voltage across the pick-up coil. The pick-up voltage can be demodulated to extract the permeability change which in turn can be related to the force.

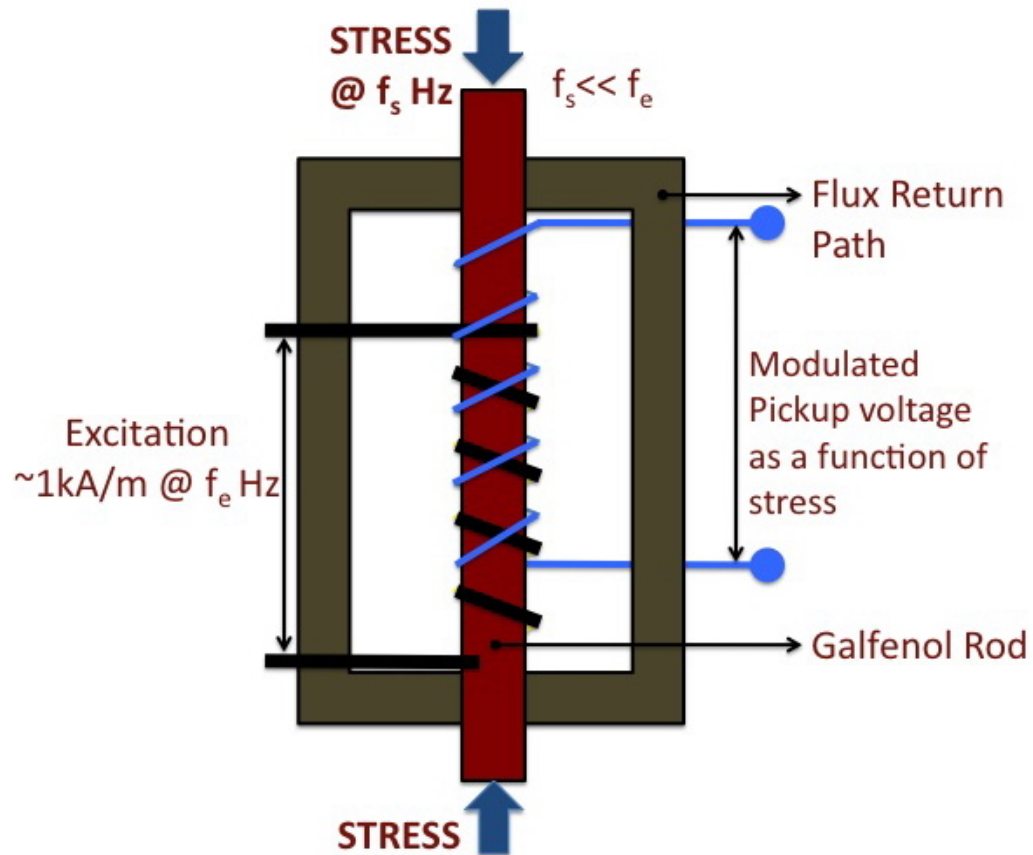


Figure 3.1: Schematic of a Galfenol force sensor.

Evans and Dapino [9] have modeled the stress-dependent susceptibility of single crystal Galfenol of 20.9 at.% Ga and 18.4 at.% Ga in the domain rotation region. In the domain rotation region the stress-dependent susceptibility is given by

$$\chi(T) = \frac{\mu_0 M_s^2}{2K_4 - 3\lambda_{100}T} \quad (3.1)$$

where $\chi(T)$ is the stress-dependent susceptibility, μ_0 is the permeability of free space, M_s is the saturation magnetization, K_4 is the anisotropy constant, λ_{100} is the saturation magnetostriction, and T is the stress. The voltage in the pickup coil is given by

$$V = -N \frac{d\phi}{dt}, \quad (3.2)$$

where N is the number of turns in the pickup coil. The flux flowing in a closed magnetic circuit can be written as,

$$B = \frac{\phi}{A} = \mu_0 \mu_r H_e, \quad (3.3)$$

where A is the area of the core, μ_0 is the permeability of free space, μ_r is the relative permeability of the material which can be written as $(1+\chi)$ and H_e is the applied field. For Galfenol $\chi=\chi(T)$, Equation 3.3 can be rewritten as,

$$\frac{1}{A\mu_0} \phi = [1 + \chi(T)] H_e \approx \chi(T) H_e, \quad (3.4)$$

The flux due to the field can be neglected as $\chi(T) \gg 1$,

$$V = -\mu_0 N A \left[\chi(T) \frac{dH_e}{dt} + \frac{d\chi(T)}{dt} \frac{dT}{dt} H_e \right]. \quad (3.5)$$

When the excitation field frequency f_e is sufficiently larger than the force frequency f_s the second term in (3.5) can be neglected. The amplitude of the voltage detected

in the feedback coil (\bar{V}_d) is given by (3.6). The output voltage (\bar{V}_d) measured by the pickup coil is an amplitude modulated signal of H_e and $\chi(T)$,

$$\bar{V}_d = -\mu_0 N A \omega_e \chi(T) \bar{H}_e. \quad (3.6)$$

The susceptibility change as a function of stress is not linear, but follows an inverse relation. It was also noted in the quasi-static measurements (Figure 2.19) in the previous chapter that the susceptibility change at zero applied field follows an inverse relationship with stress. However, there is a range of stress values where the susceptibility change is linear. By operating the sensor in the appropriate stress range, a linear output can be obtained. Experiments have been conducted using the magnetic transducer described in Chapter 2 to measure the stress-dependent susceptibility of 18.4 at.% Ga and 20.9 at.% Ga polycrystalline Galfenol alloys. By this, the suitable operating range of these alloys for a force sensor working on the principle of stress-dependent susceptibility is determined.

3.2 Force Sensor Measurements

The force sensor principle is verified using the magnetic transducer described in Figure 2.3. The two alloys that were characterized are tested and a suitable linear operating range is determined.

3.2.1 Measurements

An INSTRON 1321 test frame was used to apply a cyclic stress between -63.71 MPa to 63.71 MPa at a frequency of 0.04 Hz for two cycles. The measurement system discussed in the previous chapter was used for the test. The two coils were excited by an AC drive current of 338 mA at a frequency of 5 Hz. The magnetic field was

measured using a Hall probe and Walker Scientific MG-4D Gaussmeter(Figure 2.7). The Hall probe was positioned using a micro-positioning fixture within 1mm from the surface of Galfenol sample. The magnetization is calculated by subtracting the applied field from the flux density measurement. The strain in the sample was measured using an OMEGA (SGD-3/350-LY11) axial strain gage and a Vishay 2310 B signal conditioner which had an in-built strain bridge. The MTS Station Manager data acquisition system was used to acquire all the measurements. The sampling frequency was 100 Hz for a total time span of 50.0 seconds.

The two Galfenol alloys $\text{Fe}_{81.6}\text{Ga}_{18.4}$ and $\text{Fe}_{79.1}\text{Ga}_{20.9}$ were tested. Figure 3.2 shows the modulated magnetization and magnetic field measurements of $\text{Fe}_{81.6}\text{Ga}_{18.4}$. Figure 3.3 shows the modulated magnetization and magnetic field measurements of $\text{Fe}_{79.1}\text{Ga}_{20.9}$. The stress is sinusoidal, varies between -63.71 MPa and 63.71 MPa for two cycles. The permeability of the material is maximum at zero stress, does not change in tension, and reduces with increasing compressive stress. This explains the shape of the modulated magnetization measurements shown in Figure 3.2 and Figure 3.3. The magnetization is minimum at -63.71 MPa (@18.75 and 43.75 seconds) and maximum at zero MPa. The magnetization does not change in the tensile stress region. The magnetic field reduces with increasing permeability, hence we see that the field is minimum at zero applied stress and maximum in the compressive stress region.

3.2.2 Full Wave Phase Sensitive Demodulation

The modulated flux density and magnetic field are demodulated off line in Matlab/Simulink. A full wave phase sensitive demodulation scheme is used. To explain

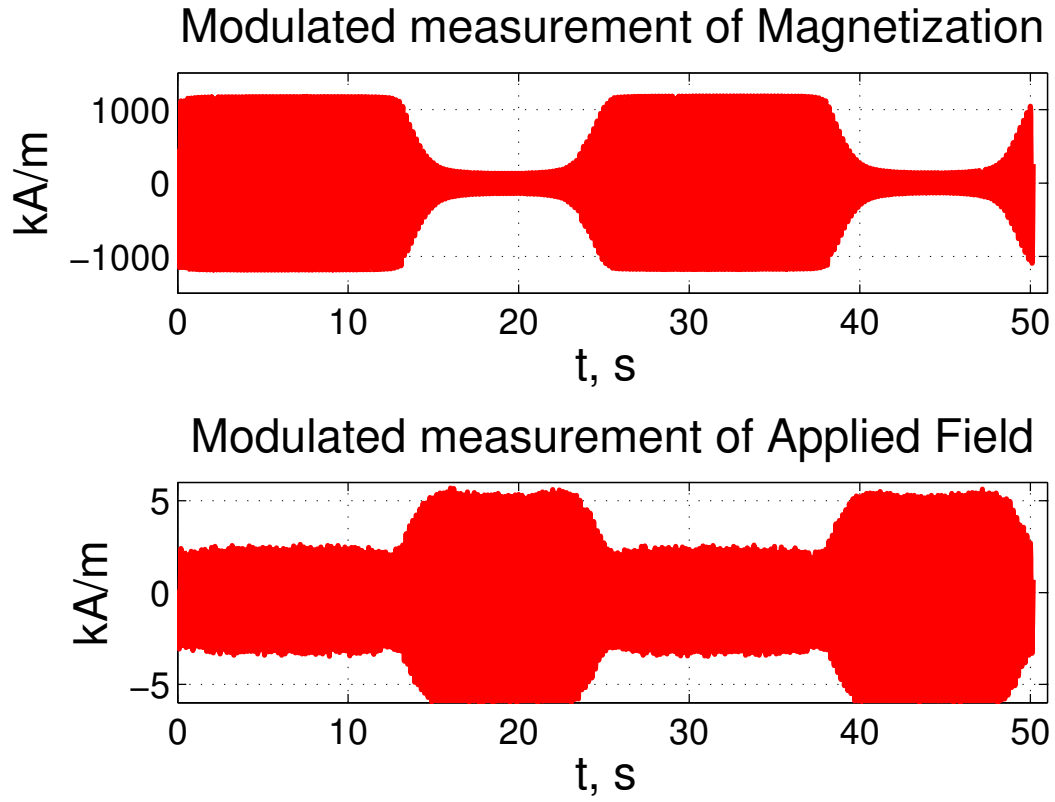


Figure 3.2: Modulated measurement of magnetization and magnetic field for $\text{Fe}_{81.6}\text{Ga}_{18.4}$ Galfenol alloy for a sinusoidal stress cycle (63.71 MPa to -63.71 MPa at 0.04Hz) and an AC drive current of (338 mA at 5 Hz).

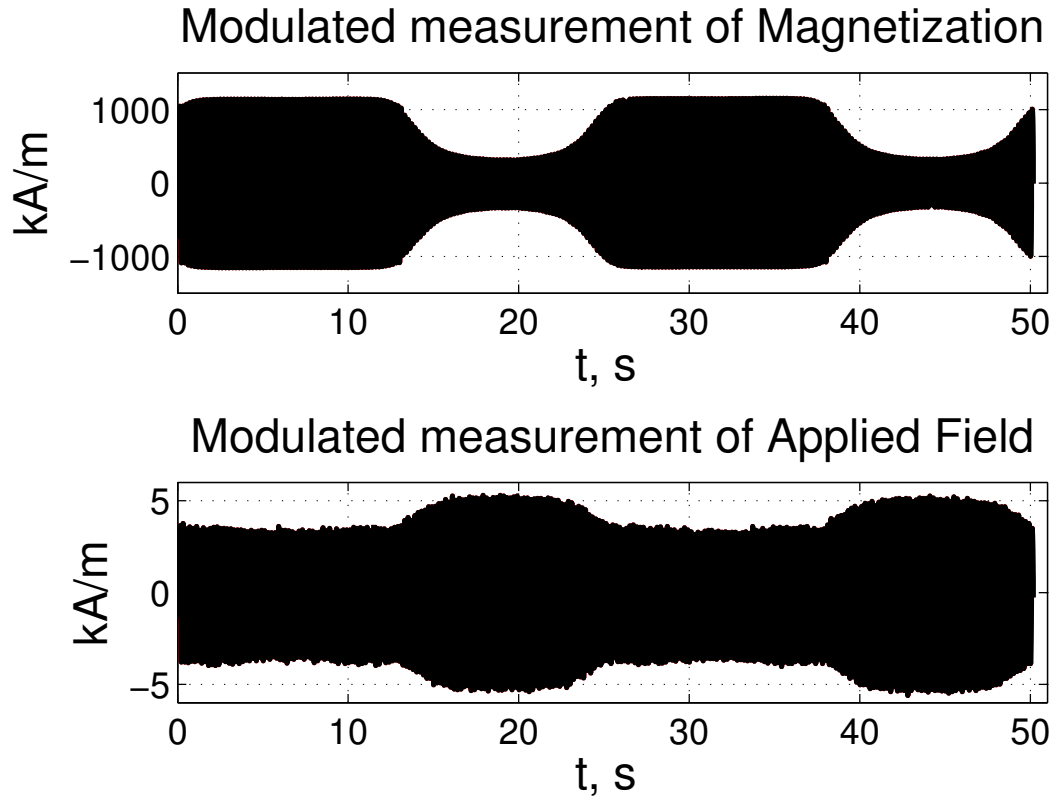


Figure 3.3: Modulated measurement of magnetization and magnetic field for $Fe_{79.1}Ga_{20.9}$ Galfenol alloy for a sinusoidal stress cycle (63.71 MPa to -63.71 MPa at 0.04Hz) and an AC drive current of (338 mA at 5 Hz).

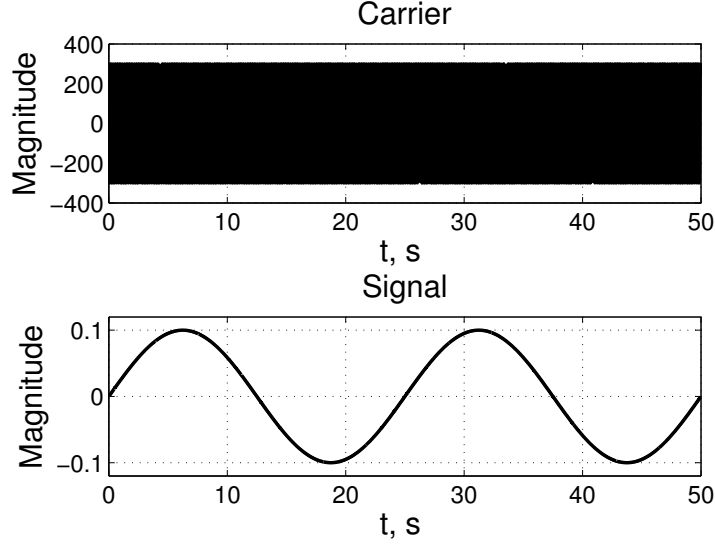


Figure 3.4: Carrier wave and signal before modulation.

the modulation/demodulation scheme two sinusoidal signals of frequency f_c and f_s are considered. The carrier wave is

$$A_{CarrierWave} = X_c \sin(2\pi f_c t), \quad (V) \quad (3.7)$$

whereas the signal is

$$A_{Signal} = X_s \sin(2\pi f_s t), \quad (V). \quad (3.8)$$

The product of the two signals results in the modulated signal. In our case the flux density change due to the applied current and the flux density change due to applied stress are modulated. The frequency of the signal is 0.04 Hz and the frequency of the carrier wave is 5 Hz. The carrier wave frequency must be much higher than the signal frequency. The modulated wave has two frequencies $(f_c - f_s)$ and $(f_c + f_s)$,

$$A_{modulated} = X_s X_c \sin(2\pi f_s t) \sin(2\pi f_c t), \quad (V^2) \quad (3.9)$$

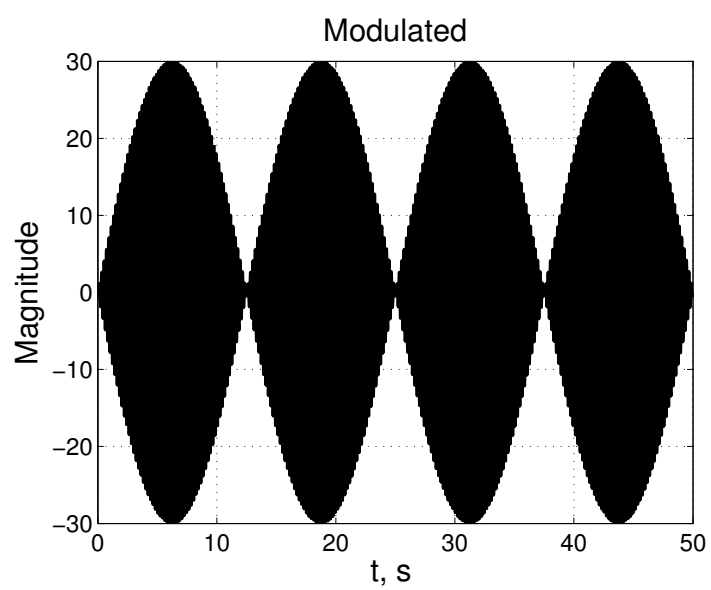


Figure 3.5: Modulated carrier wave and signal.

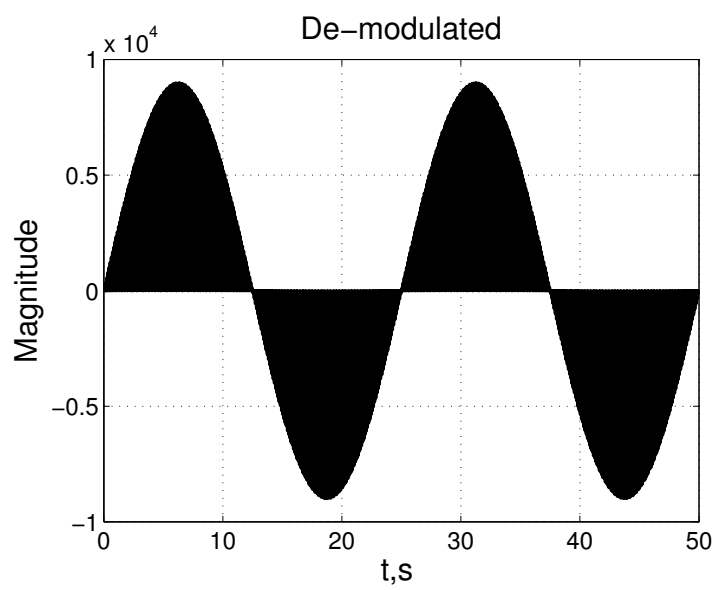


Figure 3.6: Demodulated carrier wave and signal.

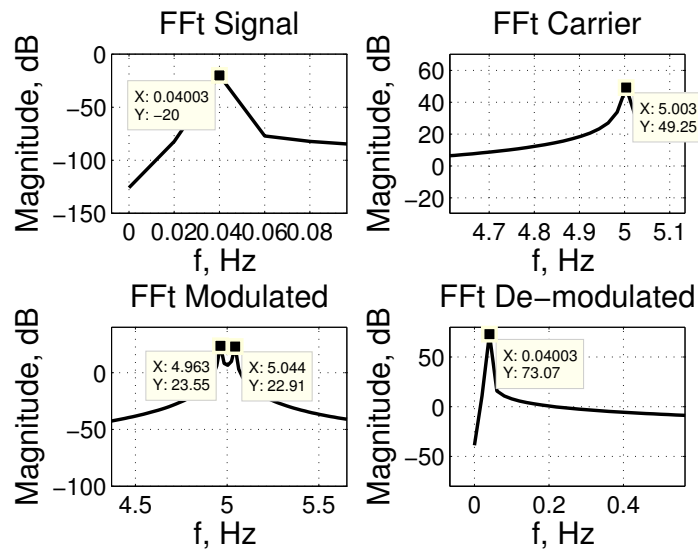


Figure 3.7: FFT of signal, carrier wave, modulated signal and demodulated signal.

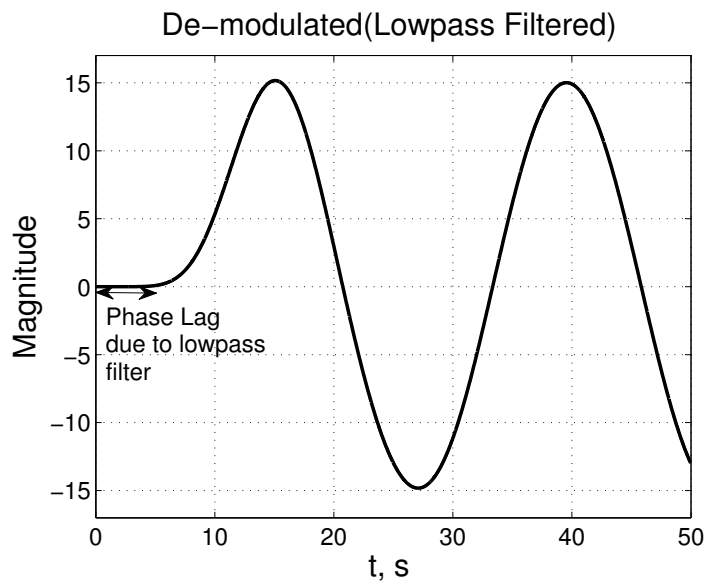


Figure 3.8: Lowpass filtered demodulated signal.

The modulated signal is shown in Figure 3.5. For a full wave phase sensitive demodulation we multiply the modulated signal

$$A_{modulated} = \frac{X_c X_s}{2} [\cos(2\pi(f_c - f_s)t) - \cos(2\pi(f_c + f_s)t)] \quad (V^2) \quad (3.10)$$

by (3.8) which gives

$$A_{Demodulated} = \frac{X_c^2 X_s}{4|X_c|^2} [\sin(2\pi(f_s)t) - \sin(2\pi(2f_c - f_s)t)] \quad (V). \quad (3.11)$$

The demodulated signal is shown in Figure 3.6 has frequency content f_s and $2f_c - f_s$. The FFT of the signal, carrier wave, modulated signal and demodulated signal are shown in Figure 3.7. The demodulated signal can be low pass filtered to remove the $2f_c - f_s$ frequency component to get the original signal (Figure 3.8). An 8th order lowpass Butterworth filter with a cut-off frequency of 0.5 Hz was used to get the demodulated output.

The above described modulation scheme was used to demodulate the flux density and magnetic field. The carrier signal for the flux density and magnetic field was obtained by exciting the coils with the same drive current at 5Hz frequency and measuring the flux density and magnetic field with no stress cycle. A phase lag is introduced by the filter, this is taken into account while plotting the stress versus the demodulated signals.

3.2.3 Demodulated Stress Dependent Susceptibility

The demodulated magnetization curves for Fe_{81.6}Ga_{18.4} and Fe_{79.1}Ga_{20.9} are shown in Figure 3.9. The magnetization change of the 18.4 at.% Ga alloy is linear and steep between -25 MPa and 10 MPa; saturation occurs outside of this range. The magnetization change of the 20.9 at.% Ga alloy is gradual between -63.71 MPa and

0 MPa; it is larger than the 18.4 at.% Ga sample between -20 MPa and -63.71 MPa. This trend can be compared to the actuation characteristics of the two alloys shown in Figure 2.13 and Figure 2.15. The demodulated stress-dependent susceptibility ($\chi(T)$) for the two alloys are shown in Figure 3.10. The trend of $\chi(T)$ compares well with that of the quasi-static measurements at zero applied field discussed in the previous chapter (Figure 2.19). The 18.4 at.% Ga alloy has a large susceptibility change between -10 MPa and 10 MPa. The 20.9 at.% Ga alloy has a more gradual change over a larger stress bandwidth. The $\text{Fe}_{81.6}\text{Ga}_{18.4}$ has a large susceptibility

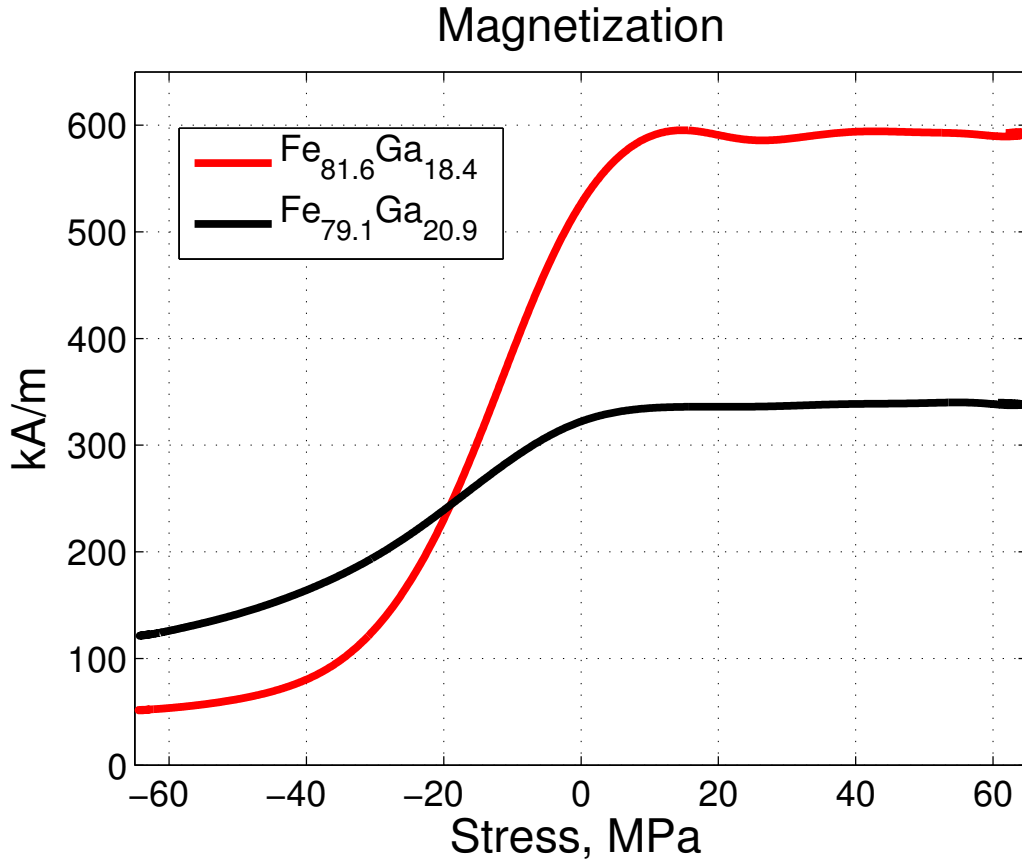


Figure 3.9: Demodulated stress-dependent magnetization of $\text{Fe}_{81.6}\text{Ga}_{18.4}$ and $\text{Fe}_{79.1}\text{Ga}_{20.9}$ Galfenol alloys.

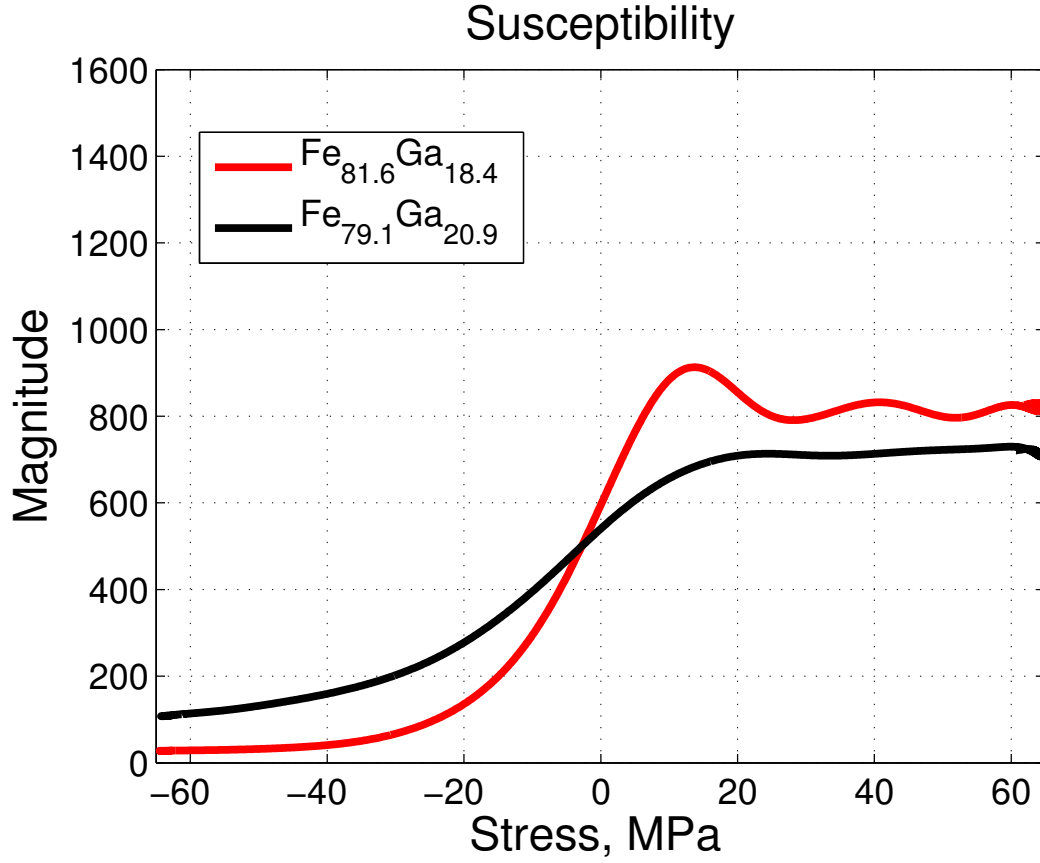


Figure 3.10: Demodulated stress-dependent susceptibility of $\text{Fe}_{81.6}\text{Ga}_{18.4}$ and $\text{Fe}_{79.1}\text{Ga}_{20.9}$ Galfenol alloys.

change between -10 MPa and 10 MPa, this alloy can be used in the low stress region with high sensitivity. The $\text{Fe}_{79.1}\text{Ga}_{20.9}$ alloy has two linear regions of susceptibility change, one between -20 MPa and 10 MPa and another between -63.71 MPa and -30 MPa. Both alloys can be used for a force sensor working on the principle of stress-dependent susceptibility, the low Ga content alloy can be used in the low stress regime with large sensitivity and the higher Ga content alloy can be used over a larger range of stress

3.3 COMSOL Simulation of Force Sensor

A 1:1 scale model of the magnetic transducer along with the Galfenol rod was developed in COMSOL. Linear piezomagnetic equations were used to model the Galfenol behavior. The weak form formulation to model magnetostrictive materials in COMSOL developed by Evans [10] was used to solve the problem.

3.3.1 Linear Piezomagnetic Equations

The linear piezomagnetic equations were used to build the material model for Galfenol which are given by (3.12)-(3.13). Parameter C is the modulus of elasticity tensor at constant field along the different crystallographic directions (3.14), S is the strain tensor(3.15), q is the linear coupling coefficients tensor(3.16), ν is the inverse of relative permeability. B is the flux density (3.17), T is the stress and H is the applied field.

$$[T] = [C][S] - [q]^T[B] \quad (3.12)$$

$$[H] = [\nu][B] - [q][S] \quad (3.13)$$

$$[C] = \begin{bmatrix} c_{11} & c_{12} & c_{13} & 0 & 0 & 0 \\ c_{12} & c_{22} & c_{12} & 0 & 0 & 0 \\ c_{13} & c_{12} & c_{33} & 0 & 0 & 0 \\ 0 & 0 & 0 & c_{44} & 0 & 0 \\ 0 & 0 & 0 & 0 & c_{44} & 0 \\ 0 & 0 & 0 & 0 & 0 & c_{44} \end{bmatrix} \quad (3.14)$$

$$[S] = \begin{bmatrix} S_{XX} \\ S_{YY} \\ S_{ZZ} \\ S_{XY} \\ S_{YZ} \\ S_{XZ} \end{bmatrix} \quad (3.15)$$

$$[q] = \begin{bmatrix} 0 & 0 & 0 & q_{14} & 0 & 0 \\ q_{21} & q_{22} & q_{23} & q_{24} & q_{25} & 0 \\ 0 & 0 & 0 & 0 & q_{35} & 0 \end{bmatrix} \quad (3.16)$$

$$[B] = \begin{bmatrix} B_X \\ B_Y \\ B_Z \end{bmatrix} \quad (3.17)$$

3.3.2 Governing Equations and Weak Forms

In this section the governing equations and a brief description of the weak form formulation by Evans [10] is discussed. Followed by the weak form equations the subdomain settings and boundary conditions used to solve the problem in COMSOL are discussed. For an electro-magneto-mechanical system, the objective is to determine the electric flux density, magnetic flux density and strain as well as their work conjugates electric field, magnetic field and stress as a function of the spatial coordinates x and time t . These are kinematically related with other quantities of interest such as voltage, vector magnetic potential and displacement. In the strong form, the spacial and temporal variations of the work conjugates are described by Maxwell's equations and Newton's second law. Electrical quantities are governed by two of Maxwell's equations, the Lenz-Faraday law

$$\nabla \times E = -\frac{\delta B}{\delta t}, \quad (3.18)$$

and Gauss' law for electric flux density

$$\nabla \cdot D = \rho_q. \quad (3.19)$$

Magnetic quantities are governed by Ampère's law

$$\nabla \times H = J + \frac{\delta D}{\delta t}, \quad (3.20)$$

and Gauss' law for magnetic flux density

$$\nabla \cdot B = 0. \quad (3.21)$$

Mechanical quantities are governed by

$$\rho_m \frac{\partial^2 u}{\partial t^2} + c \frac{\partial u}{\partial t} = \nabla \cdot T + f_B, \quad (3.22)$$

where E is the electric field, B is the magnetic flux density, H is the magnetic field, J is the current density which is the sum of the source current J_s and eddy currents J_e . The displacement current $\frac{\delta D}{\delta t}$ gives rise to electromagnetic radiation. This can be neglected at low frequency operation ($\ll 30$ MHz). Parameter ρ_m is the density, c is the damping coefficient, u is the displacement, and T is the stress.

The weak form of the above equations are derived by applying the method of weighted residuals. In the weak form formulation, the two governing equations to be solved are:

$$\epsilon_{i,j,k} \frac{\partial H_k}{\partial x_j} = (J_s)_i - \sigma \frac{\partial A_i}{\partial t}, \quad (3.23)$$

$$\rho_m \frac{\partial^2 u_i}{\partial t^2} + c \frac{\partial u_i}{\partial t} = \frac{\partial T_{ij}}{\partial x_j} + (f_B)_i. \quad (3.24)$$

where $\epsilon_{i,j,k}$ is the permutation tensor given by

$$\epsilon_{i,j,k} = \begin{cases} 1, & \text{clockwise sequence } (123, 231, 312), \\ -1, & \text{counter clockwise sequence } (321, 213, 132), \\ 0, & \text{any two indices equal.} \end{cases} \quad (3.25)$$

The flux density is related to the vector magnetic potential by $B = \nabla \times A$ and strain is related to the displacement by $S = \nabla u$. Thus using the linear piezomagnetic equation to build the material model for Galfenol, the two initial boundary value problems (3.23) and (3.24) can be formulated with flux density (B_X, B_Y, B_Z) , displacement (u_X, u_Y, u_Z) , source terms current density, and stress. The boundary conditions are

defined for vector potential and displacements. The derivation of the weak forms is given in [10]. The final matrix notation of the weak form is given by

$$\int_{V_B} H.(\nabla \times \delta A) dV_B + \int_{V_B} \sigma \frac{\delta A}{\delta t} . \delta A dV_B = \int_{\delta V_B} (H \times n). \delta A d\delta V_B + \int_{V_B} J_e . \delta A dV_B \quad (3.26)$$

$$\int_{V_u} T. \nabla . \delta u dV_u + \int_{V_u} \rho \frac{\delta^2 u}{\delta t^2} . \delta u dV_u + \int_{V_u} c \frac{\delta u}{\delta t} . \delta u dV_u = \int_{\delta V_u} T n . \delta u d\delta V_u + \int_{V_u} f_B \delta u dV_u \quad (3.27)$$

The volumes V_B and V_u are subdomains for which the flux density and mechanical displacements are defined. The weak form is the virtual work of the system δB and δS are defined by the following relationships, $\delta B = \nabla \times \delta A$ and $\delta S = \nabla \delta u$. Substituting δB and δS one gets

$$\int_{V_B} H.(\delta B) dV_B + \int_{V_B} \sigma \frac{\delta A}{\delta t} . \delta A dV_B = \int_{\delta V_B} (H \times n). \delta A d\delta V_B + \int_{V_B} J_e . \delta A dV_B, \quad (3.28)$$

$$\int_{V_u} T. \delta S dV_u + \int_{V_u} \rho \frac{\delta^2 u}{\delta t^2} . \delta u dV_u + \int_{V_u} c \frac{\delta u}{\delta t} . \delta u dV_u = \int_{\delta V_u} T n . \delta u d\delta V_u + \int_{V_u} f_B \delta u dV_u. \quad (3.29)$$

Additionally, the surface traction at the mechanical boundary is $t = Tn$ and the tangent field at the magnetic boundary is $H_T = H \times n$. The piezomagnetic equations can be re-written as (3.30) and (3.31), where δS is the weak form energy given by (3.32), and δB is the weak form energy given by (3.33). The magnetic field H_k is related to the flux density and strain of Galfenol by (3.38). For passive materials it is related to the flux density ($H = \frac{B}{\mu_r}$). The stress (T_{ij}) is related to flux density and strain by (3.37) for Galfenol and stress is simply related to strain ($\sigma = E\nu$) for passive materials. Substitution of (3.34) and (3.35) in (3.30) gives (3.37). Substitution of (3.15), (3.16), (3.17) and (3.33) in (3.31) gives (3.38). Expression (3.37) is used for the mechanical weak form formulation for Galfenol subdomain in COMSOL and

(3.38) is used for the magnetic weak form formulation for Galfenol subdomain in COMSOL. For other materials (steel flux path, copper coils and air) the weak form terms relating B-H and σ - ν are direct $[(H = \frac{B}{\mu_r}, (\sigma = E\nu)]$.

$$[T].\delta S = [C][S].\delta S - [q]^T[B].\delta S \quad (3.30)$$

$$[H].\delta B = [\nu][B].\delta B - [q][S].\delta B \quad (3.31)$$

$$[\delta S] = \begin{bmatrix} \delta S_{XX} \\ \delta S_{YY} \\ \delta S_{ZZ} \\ \delta S_{XY} \\ \delta S_{YZ} \\ \delta S_{XZ} \end{bmatrix} \quad (3.32)$$

$$[\delta B] = \begin{bmatrix} \delta B_X \\ \delta B_Y \\ \delta B_Z \end{bmatrix} \quad (3.33)$$

$$[C][S].\delta S = \begin{bmatrix} c_{11} & c_{12} & c_{13} & 0 & 0 & 0 \\ c_{12} & c_{22} & c_{12} & 0 & 0 & 0 \\ c_{13} & c_{12} & c_{33} & 0 & 0 & 0 \\ 0 & 0 & 0 & c_{44} & 0 & 0 \\ 0 & 0 & 0 & 0 & c_{44} & 0 \\ 0 & 0 & 0 & 0 & 0 & c_{44} \end{bmatrix} \begin{bmatrix} S_{XX} \\ S_{YY} \\ S_{ZZ} \\ S_{XY} \\ S_{YZ} \\ S_{XZ} \end{bmatrix} \cdot \begin{bmatrix} \delta S_{XX} \\ \delta S_{YY} \\ \delta S_{ZZ} \\ \delta S_{XY} \\ \delta S_{YZ} \\ \delta S_{XZ} \end{bmatrix} \quad (3.34)$$

$$[q]^T[B].\delta S = \begin{bmatrix} 0 & 0 & 0 & q_{14} & 0 & 0 \\ q_{21} & q_{22} & q_{23} & q_{24} & q_{25} & 0 \\ 0 & 0 & 0 & 0 & q_{35} & 0 \end{bmatrix}^T \begin{bmatrix} B_X \\ B_Y \\ B_Z \end{bmatrix} \cdot \begin{bmatrix} \delta S_{XX} \\ \delta S_{YY} \\ \delta S_{ZZ} \\ \delta S_{XY} \\ \delta S_{YZ} \\ \delta S_{XZ} \end{bmatrix} \quad (3.35)$$

$$\begin{bmatrix} T_{XX}.\delta S_{XX} \\ T_{YY}.\delta S_{YY} \\ T_{ZZ}.\delta S_{ZZ} \\ T_{XY}..\delta S_{XY} \\ T_{YZ}.\delta S_{YZ} \\ T_{XZ}.\delta S_{XZ} \end{bmatrix} = \begin{bmatrix} c_{11}S_{XX} + c_{12}S_{YY} + c_{13}S_{zz} \\ c_{12}S_{XX} + c_{22}S_{YY} + c_{12}S_{ZZ} \\ c_{13}S_{XX} + c_{12}S_{YY} + c_{33}S_{ZZ} \\ c_{44}S_{XY} \\ c_{44}S_{YZ} \end{bmatrix} \cdot \begin{bmatrix} \delta S_{XX} \\ \delta S_{YY} \\ \delta S_{ZZ} \\ \delta S_{XY} \\ \delta S_{YZ} \\ \delta S_{XZ} \end{bmatrix} \quad (3.36)$$

$$- \begin{bmatrix} q_{21}B_Y \\ q_{22}B_Y \\ q_{23}B_Y \\ q_{14}B_X + q_{24}B_Y \\ q_{25}B_y + q_{35}B_z \\ 0 \end{bmatrix} \cdot \begin{bmatrix} \delta S_{XX} \\ \delta S_{YY} \\ \delta S_{ZZ} \\ \delta S_{XY} \\ \delta S_{YZ} \\ \delta S_{XZ} \end{bmatrix}$$

$$\begin{bmatrix} T_{XX}.\delta S_{XX} \\ T_{YY}.\delta S_{YY} \\ T_{ZZ}.\delta S_{ZZ} \\ T_{XY}..\delta S_{XY} \\ T_{YZ}.\delta S_{YZ} \\ T_{XZ}.\delta S_{XZ} \end{bmatrix} = \begin{bmatrix} \delta S_{XX}(c_{11}S_{XX} + c_{12}S_{YY} + c_{13}S_{zz} - q_{21}B_Y) \\ \delta S_{YY}(c_{12}S_{XX} + c_{22}S_{YY} + c_{12}S_{ZZ} - q_{22}B_Y) \\ \delta S_{ZZ}(c_{13}S_{XX} + c_{12}S_{YY} + c_{33}S_{ZZ} - q_{23}B_Y) \\ \delta S_{XY}(c_{44}S_{XY} - q_{14}B_X - q_{24}B_Y) \\ \delta S_{YZ}(c_{44}S_{YZ} - q_{25}B_y - q_{35}B_z) \\ \delta S_{XZ}(c_{44}S_{XZ}) \end{bmatrix} \quad (3.37)$$

$$\begin{bmatrix} \left(\frac{B_X}{\mu_1}\right).\delta B_X - q_{14}S_{XY}.\delta B_X \\ \left(\frac{B_Y}{\mu_2}\right).\delta B_Y - (q_{21}S_{XX} + q_{22}S_{YY} + q_{23}S_{ZZ} + q_{24}S_{XY} + q_{25}S_{YZ}).\delta B_Y \\ \left(\frac{B_Z}{\mu_3}\right).\delta B_Z - q_{35}S_{YZ}.\delta B_Z \end{bmatrix} = \begin{bmatrix} H_X.\delta B_X \\ H_Y.\delta B_Y \\ H_Z.\delta B_Z \end{bmatrix} \quad (3.38)$$

In the finite element method, the solution domain is discretized into finite elements and the integration in the weak form (3.26) and (3.27) are performed over elements. The finite element formulation has two weak forms, a mechanical weak form in which only the Galfenol rod is active and a magnetic weak form in which the air space, steel flux path, copper coils, and the Galfenol rod are active. The value of constants used in the simulation are given in Table 3.1 and Table 3.2. These constants were obtained from single crystal 18.4 at.% Ga Galfenol alloy data by Evans et al. [9].

Description	Value	Units.
σ_s	59.61×10^5	1/(ohm.m)
ρ_s	7860	kg/m ³
E_s	211×10^9	Pa
c_{11_s}	$E_S(1 - \nu)/((1 + \nu)(1 - 2\nu))$	Pa
c_{12_s}	$E_S(\nu)/((1 + \nu)(1 - 2\nu))$	Pa
c_{44_s}	$E_S(\frac{1}{2} - \nu)/((1 + \nu)(1 - 2\nu))$	Pa
ν	0.3	no unit

Table 3.1: Value of constants for steel used in the finite element simulation.

The permeability of the Galfenol along the length of the rod is modeled as a linear function of stress. The permeability is given by $\mu_y = \mu_0(a + bT_{YY})$. The constants a and b are found by a linear curve fit of the slope of the M-H curves in the domain rotation region (± 5 kA/m), for 18.4 at.% Ga single crystal Galfenol alloy ($\simeq -22$ MPa pre-stress) [9]. The mechanical boundary conditions are shown by a schematic in Figure 3.11. The direction for current density in the coils are given by Figure 3.12.

3.3.3 Results and Discussion

The problem was solved for a total time of 40 seconds, linear solver was used to obtain the solutions. Figure 3.13 shows a slice plot of axial component flux density B_Y at t=8 s, Figure 3.14 shows a slice plot of the axial strain S_{YY} at t=8 s. Figure 3.15 shows the modulated flux density ($\frac{dB_Y}{dt} = \frac{1}{L} \int_{Galfenol\ Subdomain} (\frac{\delta^2 A_X}{\delta z \delta t} - \frac{\delta^2 A_Z}{\delta x \delta t})$).

Description	Value	Units.
σ_G	59.61×10^5	1/(ohm.m)
ρ_G	7870	kg/m ³
E_G	211×10^9	Pa
c_{11_G}	63.6×10^9	Pa
c_{12_G}	21.5×10^9	Pa
c_{13_G}	33.7×10^9	Pa
c_{22_G}	78.5×10^9	Pa
c_{33_G}	63.6×10^9	Pa
c_{44_G}	63.6×10^9	Pa
T_s	20×10^6	Pa
J_s	1×10^6	A/m ²
μ_0	$4\pi \times 10^{-7}$	N/A ²

Table 3.2: Value of constants for Galfenol used in the finite element simulation.

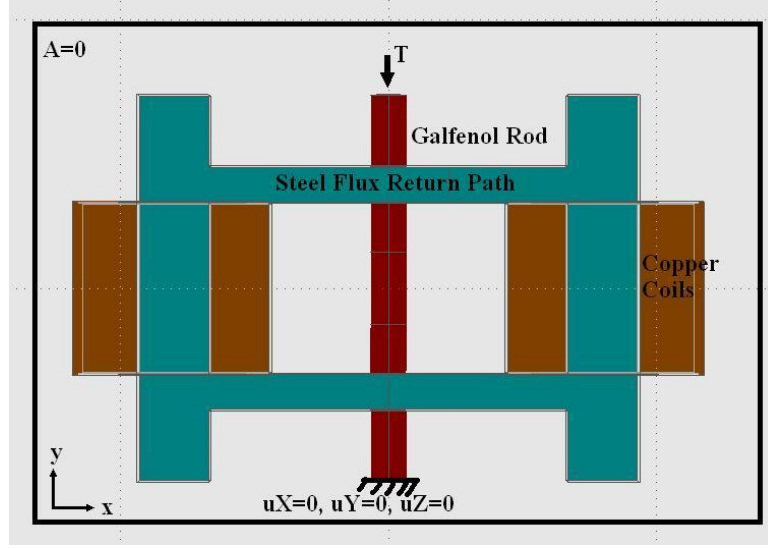


Figure 3.11: COMSOL model mechanical boundary conditions.

Figure 3.16 shows the modulated applied field. The same demodulation scheme discussed in the previous section was used to demodulate the flux density and applied field to obtain the susceptibility. The demodulated susceptibility is shown in Figure 3.17. The stress cyclic was limited to ± 10 MPa. We obtain a linear relation of the susceptibility change as a function of stress, this is because we used a linear relation to model the permeability change as a function of stress. If a non-linear material model is used for the Galfenol sample to model the stress-dependent susceptibility we can obtain the susceptibility change as a function stress that can be compared to the experimental demodulated plot (Figure 3.10). A fundamental idea of governing equations and material behavior is learned by theoretically simulating the sensor in COMSOL. The linear model is very helpful in studying the principle of using the weak forms to solve the boundary value problems. Future work would be to use a nonlinear material model derived from energy principles.

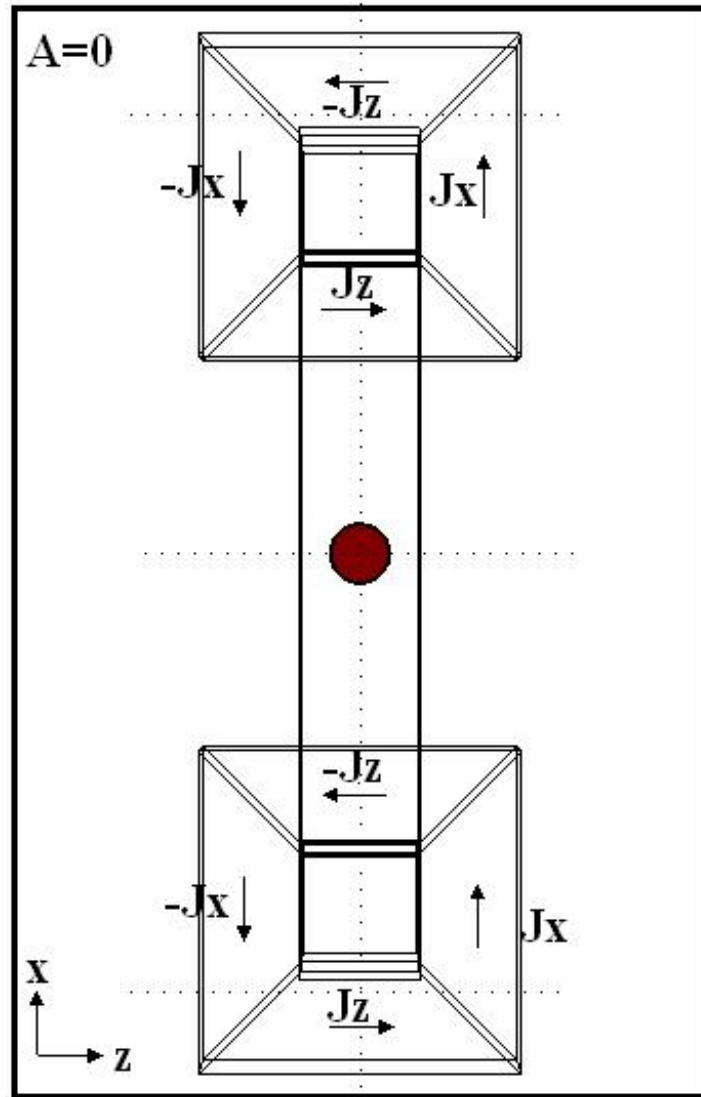


Figure 3.12: COMSOL model boundary conditions and direction current density in the coils.

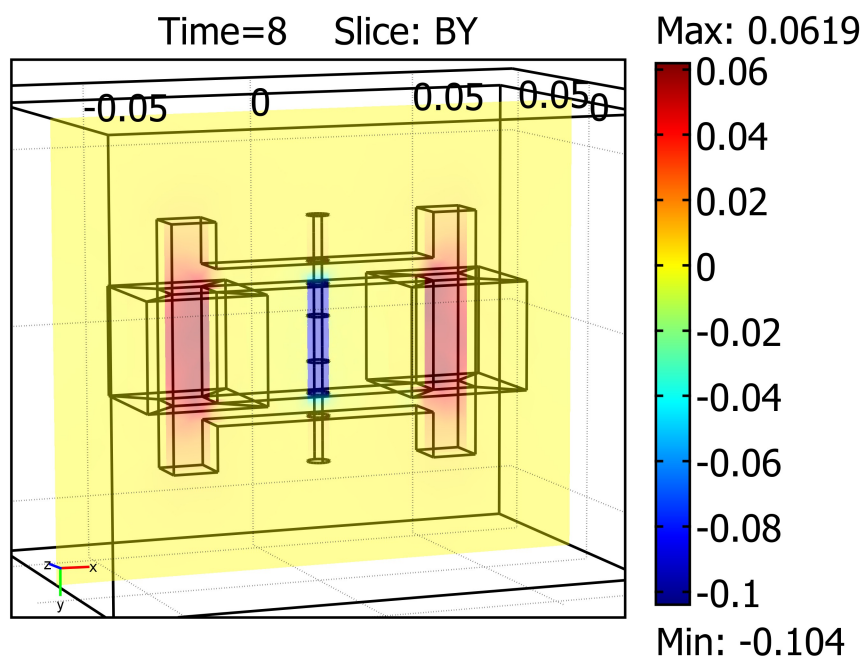


Figure 3.13: COMSOL Model - Slice plot of flux density B_Y (Tesla).

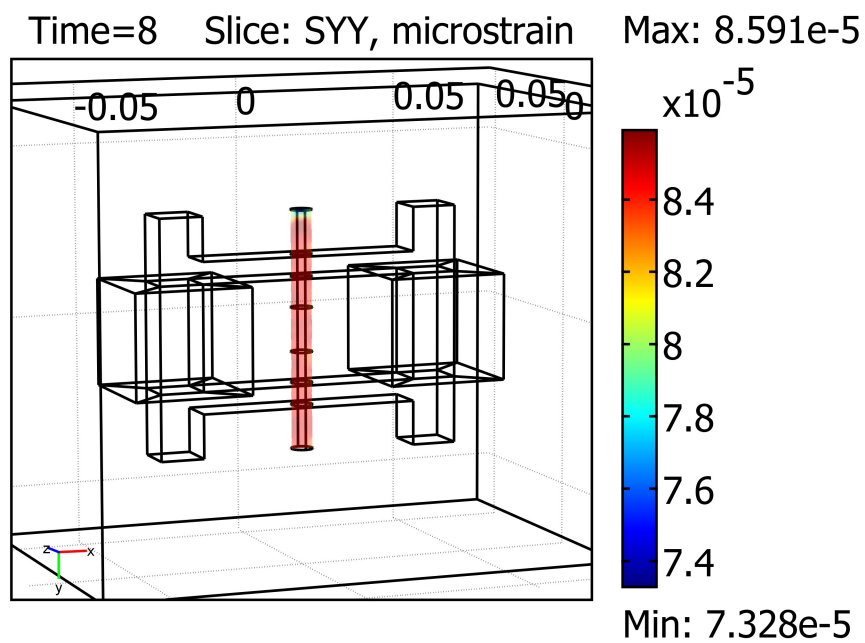


Figure 3.14: COMSOL Model - Slice plot of Strain S_{YY} (microstrain).

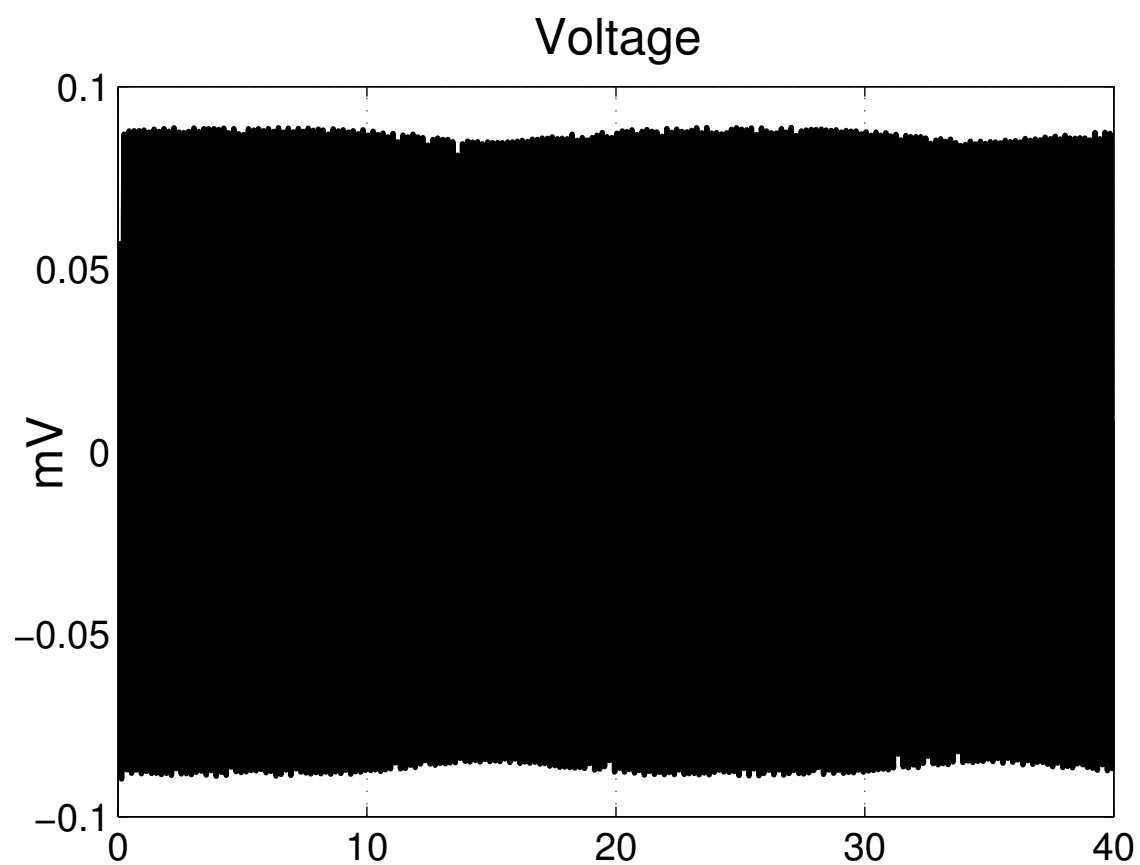


Figure 3.15: Modulated change in flux density measured as voltage across pick up coil for a cyclic stress of -10 MPa to 10 MPa.

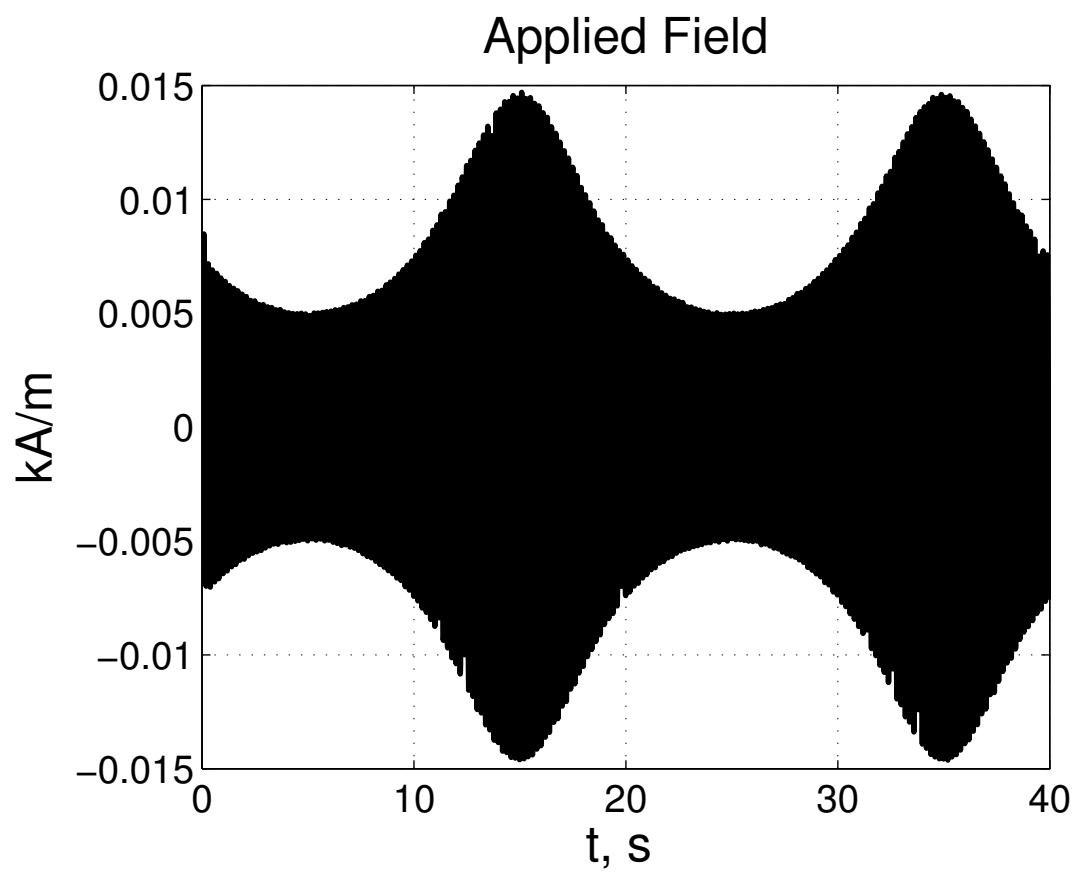


Figure 3.16: Modulated applied field for a cyclic stress -10 MPa to 10 MPa.

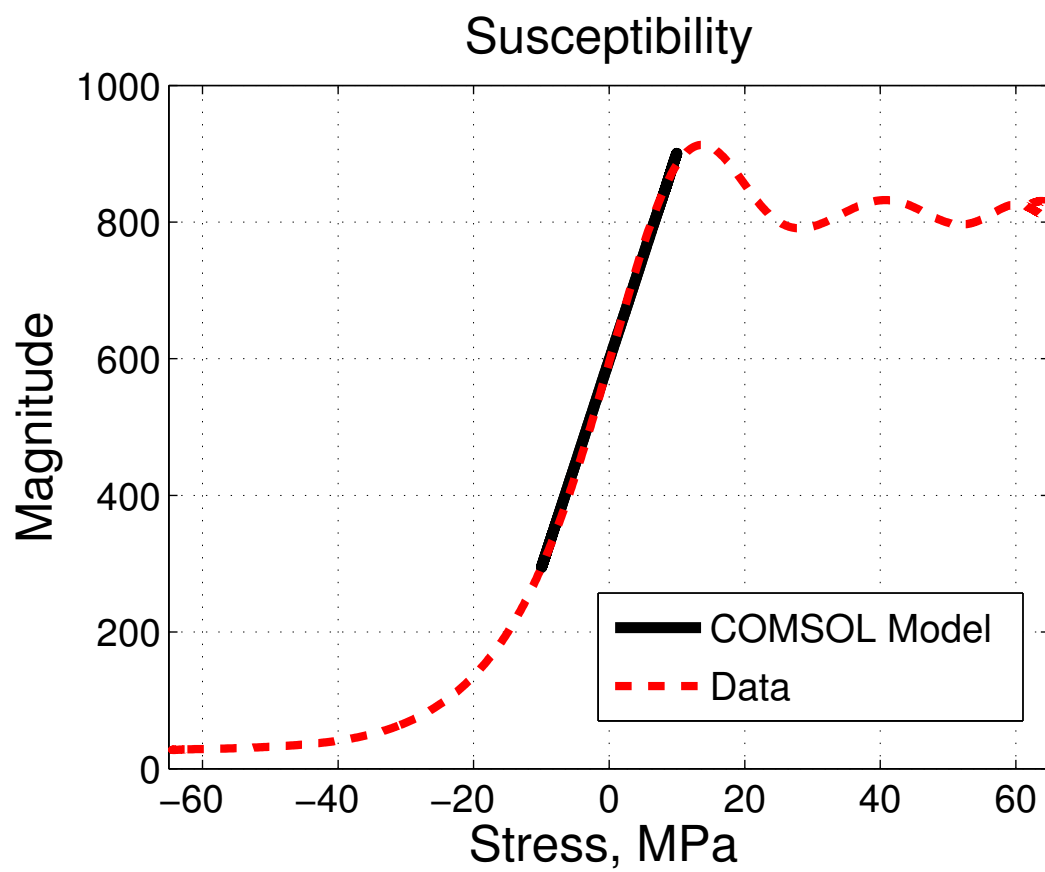


Figure 3.17: Demodulated susceptibility for a cyclic stress -10 MPa to 10 MPa.

CHAPTER 4

TORQUE SENSING USING TEXTURED POLYCRYSTALLINE ROLLED GALFENOL

Various magnetostrictive torque sensors have been proposed comprising a magnetoelastically active element and a magnetic sensor, such as a Hall effect sensor or fluxgate magnetometer [12] [5]. Torque sensors based on the permeability change of magnetostrictive materials have also been proposed [18]. In the current work the formability and the stress dependent susceptibility of Galfenol alloys is used to develop a contactless torque sensor.

4.1 Contactless Sensing Principle

A contactless sensing principle is established utilizing the stress dependent permeability of Galfenol alloys. An AC excitation and demodulation scheme is used to detect the permeability change of rolled Galfenol steel. A schematic of the magnetic circuit used is shown in Figure 4.1. A rolled Galfenol steel patch is a part of the closed magnetic circuit; the flux path in the circuit is shown. When the patch bonded to the substrate is stressed, the permeability change in the circuit is detected by the change in the voltage in a pickup coil. An AC excitation is used and the permeability change is sensed as a modulated voltage in the pick-up coil. The demodulated voltage can in

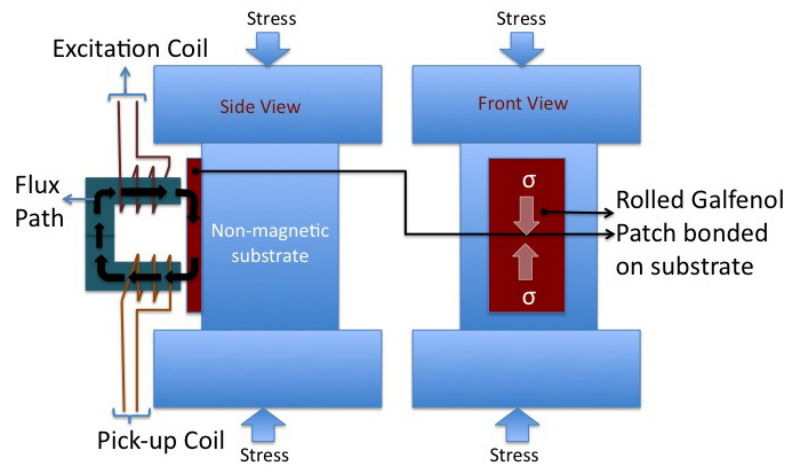


Figure 4.1: Magnetic circuit schematic.



Figure 4.2: Schematic of Galfenol patch bonded at 45° on the shaft.

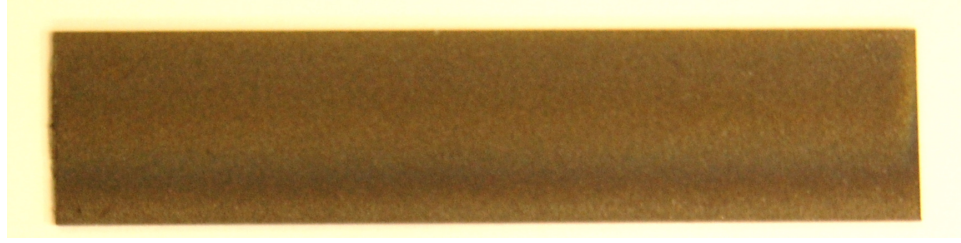


Figure 4.3: Highly textured polycrystalline Fe_{81.6}Ga_{18.4} rolled Galfenol patch with $\langle 100 \rangle$ orientation along the length.

turn be related to the stress. For torque sensing the rolled Galfenol patches can be hot formed to the shape of the shaft. The patches are then bonded to the shaft with the $\langle 100 \rangle$ orientation along the 45° shear direction (Figure 4.2). When torque is applied to the shaft the shear stress causes the permeability of the Galfenol to change along the 45° . This change in the permeability is detected by a suitable magnetic circuit with a flux return path. In the next section the hot forming of Galfenol to the shape of the shaft is discussed. Followed by the hot forming, contactless measurements were acquired from a rolled Galfenol patch bonded to an aluminum substrate as shown in Figure 4.1. Future tests will involve contactless torque test using hot formed rolled Galfenol ring with preferred $\langle 100 \rangle$ alignment along the 45° shear axis.

4.2 Hot Forming of Rolled Galfenol Steel

Galfenol combines good magnetostriction and excellent strength. It can be rolled as sheets and used as unimorph or bimorph beams for sensors and actuators [15] [7] [8]. Alloy additions like Boron and Sulphur can improve its ductility and can control the surface energy and formation of the selective growth of $\{100\}$ grains during annealing [16]. Rolled Galfenol steel is 18.4 at%Ga Galfenol alloy with carbon steel alloy

additions to improve its strength. It can be used as patches or strips for torque sensing applications. Bridgman Galfenol steel was obtained from Etrema. The Bridgman Galfenol steel has a typical composition of 18.4 at.% Ga + 1002 low carbon steel components. The magnetostriction of this material at 7 ksi preload, 500 Oe magnetic field, is typically 180 to 200 ppm [21]. This is slightly less than the binary, 18.4 at.% Ga Bridgman values of 200 to 220 ppm. This is most likely attributed to the presence of tramp elements from the low carbon steel and a possible decrease in the desired orientation [21]. The rolled Galfenol steel patch is shown in Figure 4.3, it has $\langle 100 \rangle$ orientation along the rolling direction which is along the length. The measured magnetostriction of rolled Galfenol steel patch at zero load is shown in Figure 4.4. The rolled material is not ductile at room temperature. In order to use the material for torque sensing applications the material need to be hot formed to the shape of the shaft to facilitate bonding and strain transfer. This section will discuss the hot forming and bonding procedure. Strain matching between the substrate shaft and bonded Galfenol steel is done to validate the bonding process.

4.2.1 Hot Forming and Bonding of Rolled Galfenol Steel

For torque sensing applications the magnetostrictive material needs to be coated on the substrate shaft by deposition or the shaft needs to be preferentially magnetized. Galfenol is suitable for torque sensing applications because it can be used as the shaft and preferentially magnetized or it can be deposited with preferential domain alignment. The advent of rolled Galfenol steel makes it possible to bond Galfenol strips or patches with preferential domain alignment on the shaft for torque sensing. The rolled Galfenol steel is shown in Figure 4.3. It cannot be directly bonded on the

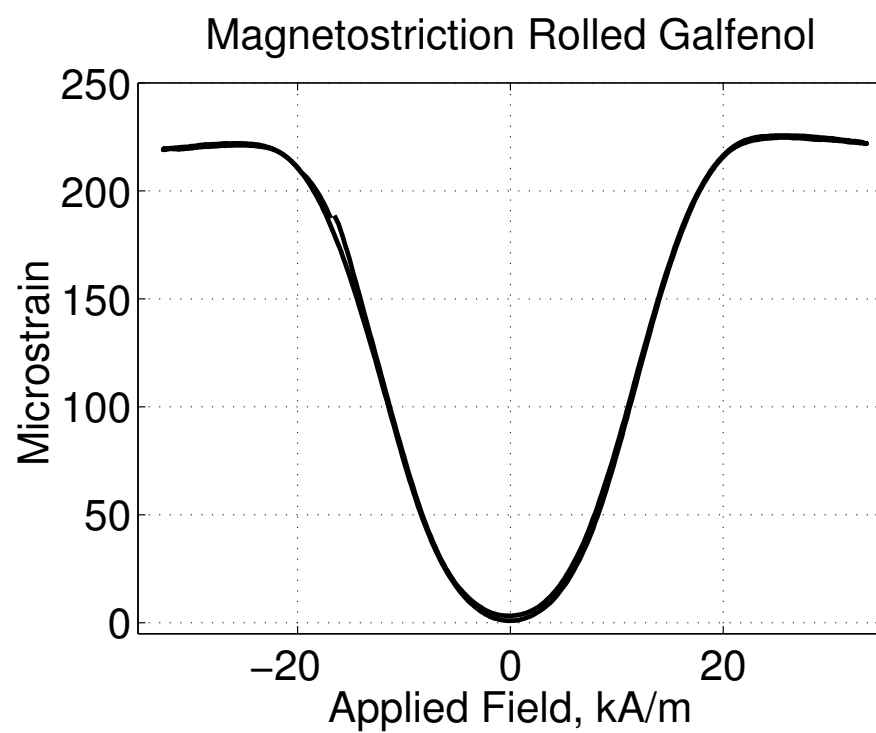


Figure 4.4: Magnetostriction of highly textured polycrystalline rolled Galfenol steel (18.4 at.% Ga + 1002 low carbon steel).

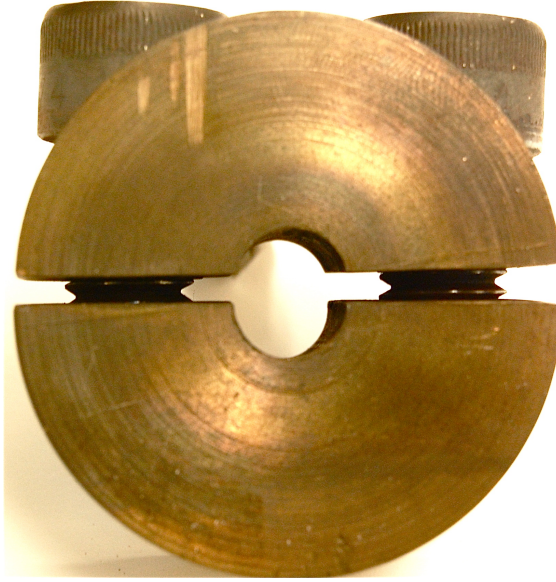


Figure 4.5: Hot forming dies.

shaft due to its brittle nature. It needs to be formed to the shape of the shaft. When it is hot formed to the shape of the shaft, it can be easily bonded for maximum strain transfer from the shaft to the magnetostrictive material. The hot forming process involves heating the sample to 900°C in two hours. The sample is maintained at that temperature and shaped to the shaft diameter using the dies shown in Figure 4.5. The actual shaft can be used as the male part of the die or a shaft having the same diameter as shown in Figure 4.6 can be used. The shaping is done by holding the shaft and dies in a vice and tightening the screws with the Galfenol strip in between the dies. The sample becomes brittle when cooled below $\sim 250^{\circ}\text{C}$, so the temperature of the strip is maintained at $\sim 900^{\circ}\text{C}$ using a flame torch. When using a flame torch care is taken to keep the temperature of the patch below 1100°C . The preferential $\langle 100 \rangle$ alignment along the length of the strip will be lost if heated above 1100°C [21].

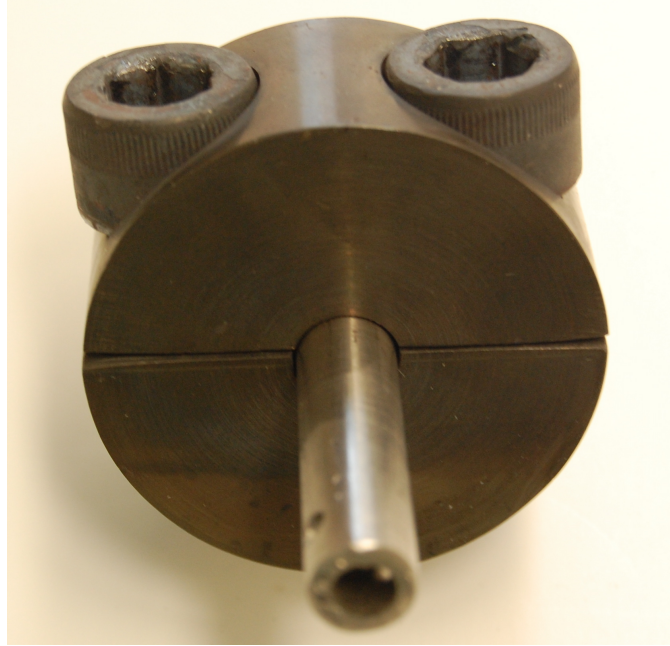


Figure 4.6: Hot forming dies with the polycrystalline rolled Galfenol sandwiched between the dies.

Once the strip is hot formed to the shape of the shaft, an annealing process is done to relieve the stress in the material.

During the annealing process the hot formed ring clamped between the die set and heated in a heating chamber to 900°C in two hours. The strip sandwiched between the die set is shown in Figure 4.6. The set-up is maintained in the heating chamber for one hour after which it is quenched in air. Once the hot formed ring has cooled, it is removed from the die set. The surface of the ring becomes oxidised during the hotforming process. The surface oxides can be cleaned using abrasive paper. Once the inner surface of the ring is cleaned of the oxides, the surface is prepared for bonding to the shaft. Figure 4.7 shows a hot formed ring to suit a 0.375 inch diameter shaft after annealing and surface cleaning.



Figure 4.7: Hot formed polycrystalline $\text{Fe}_{81.6}\text{Ga}_{18.4}$ split ring.

In order to bond a Galfenol steel ring (Figure 4.8) to the surface of the shaft several adhesives were tried out. M-bond 200 adhesive is a commercially available adhesive used to bond strain gages, the same was found to give good results. The surfaces of the ring and the shaft are removed of all grease and oil. The standard strain gage bonding procedure is used to bond the hot-formed ring to the shaft. Figure 4.9 shows a hot formed Galfenol steel ring bonded to a 2 inch diameter shaft using M-bond 200 adhesive.

4.2.2 Strain Matching

The efficiency of the bond is studied by measuring the strain transfer between the steel shaft and the bonded Galfenol steel ring. The hot formed Galfenol steel ring is bonded to the steel shaft as shown in Figure 4.9. The spline shaft is torqued using



Figure 4.8: Polycrystalline rolled Fe_{81.6}Ga_{18.4} hot formed to suit a 2 in diameter shaft.

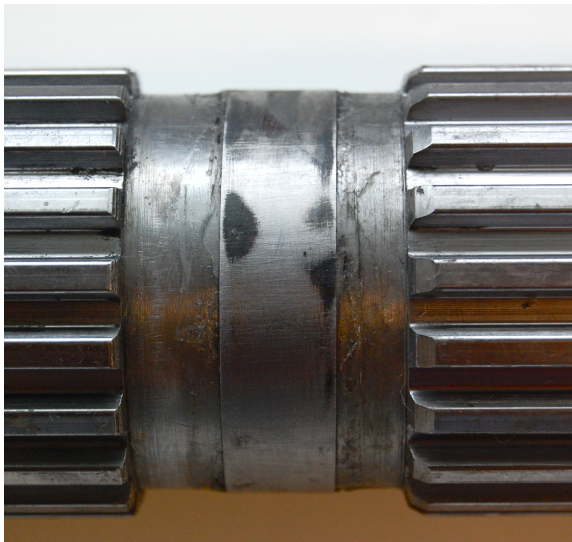


Figure 4.9: Polycrystalline rolled Fe_{81.6}Ga_{18.4} hot formed and bonded on a 2 in diameter shaft.

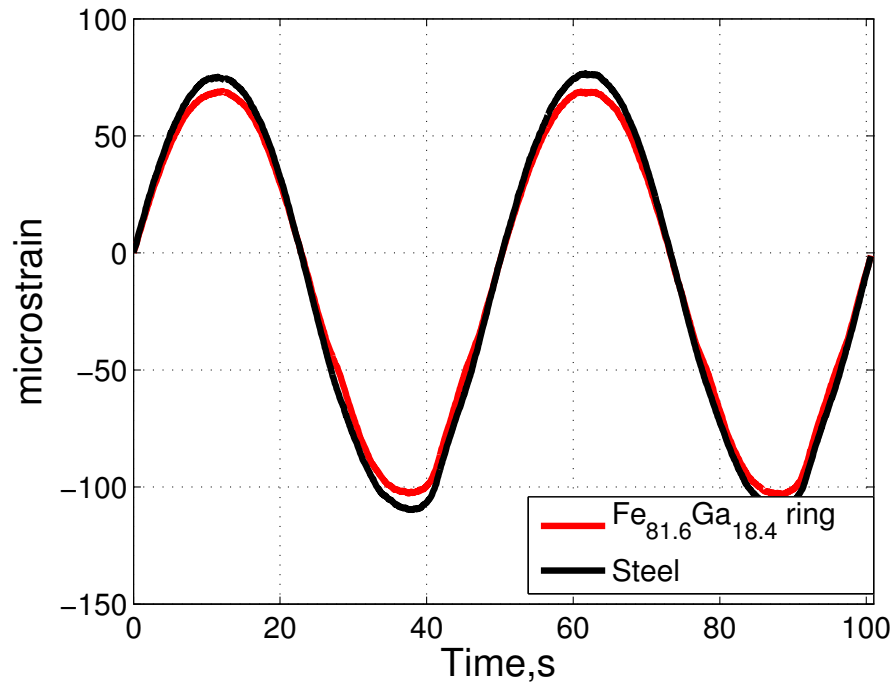


Figure 4.10: Strain matching between the bonded Galfenol ring and steel shaft.

a lever arm on an Interlaken M5651B frame (Figure A.8). Strain gages are bonded along the 45° shear direction on the steel shaft and the Galfenol patch in a quarter bridge configuration. The strain gage along with the Vishay 2310 B conditioner are used to measure the shear strain on the steel shaft and Galfenol steel ring. Figure 4.10 shows the strain measured on the steel shaft and the Galfenol steel ring. The strain measured is in response to a sinusoidal torque applied to the lever arm starting with a bias torque. The hot-forming and bonding process results in good strain transfer between the steel shaft and Galfenol ring.

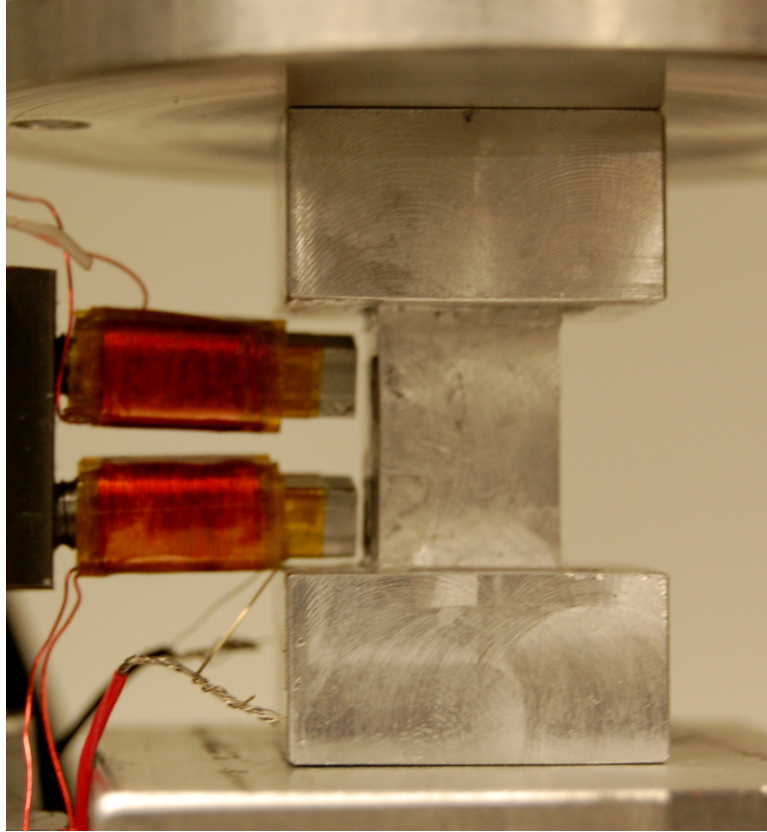


Figure 4.11: Measurement system with polycrystalline rolled $\text{Fe}_{81.6}\text{Ga}_{18.4}$ bonded to aluminum substrate.

4.3 Contactless Measurements

The principle of the contactless torque sensor using the stress dependent susceptibility change of Galfenol is verified by a simple measurement setup. A laboratory setup as shown in Figure 4.11 was built. The polycrystalline Galfenol steel patch was surface prepared and bonded on one of the faces of a aluminum sample with a square gage section. The gage section of the aluminum sample was 0.5 inch square and 1.0 inch length. The patch bonded on one of the face of the gage section was 0.75×0.4 inch and 0.016 inch in thickness.

The sensor shown in Figure 4.11 was made of a magnetic steel core in the shape of a horse shoe. An excitation coil of 100 turns was wound on one of the legs and a pick-up coil of 100 turns was wound on the second leg of the horse shoe core. An AC excitation current of 600mA at 5 Hz frequency was supplied to the excitation coil. The legs of the sensor were positioned at a distance of 0.25 mm from the surface of the Galfenol patch. The flux path in the magnetic circuit is as shown in Figure 4.1. A compressive preload of 40 MPa was applied to the aluminum sample and a cyclic stress as shown in Figure 4.12 was applied at a frequency of 40 mHz using the Interlaken frame. The prestress was applied to always load the sample in compression. The feedback voltage in the circuit was measured from the pick-up coil. An axial strain gage was bonded on the Galfenol patch. The strain gage along with the Vishay conditioner is used to measure the strain on the Galfenol steel patch. A Dynamic Signal Analyzer and Signal Calc data acquisition system was used to collect the data. The data was sampled at a frequency of 81.92 Hz for a time span of 50 seconds. Figure 4.13 shows the modulated voltage output from the pick-up coil. The same demodulation scheme discussed in Chapter 3 was used to perform the demodulation. Figure 4.14 shows the demodulated voltage as a function of the strain measured on the Galfenol steel patch.

4.4 Discussion and Future Work

We note that the demodulated output relates well to the measured strain. The contactless measurement of the stress-dependent susceptibility of the Galfenol patch can be used to construct a torque sensor. The output depends on the distance of the sensor from the surface of the Galfenol patch. It also depends on the orientation of

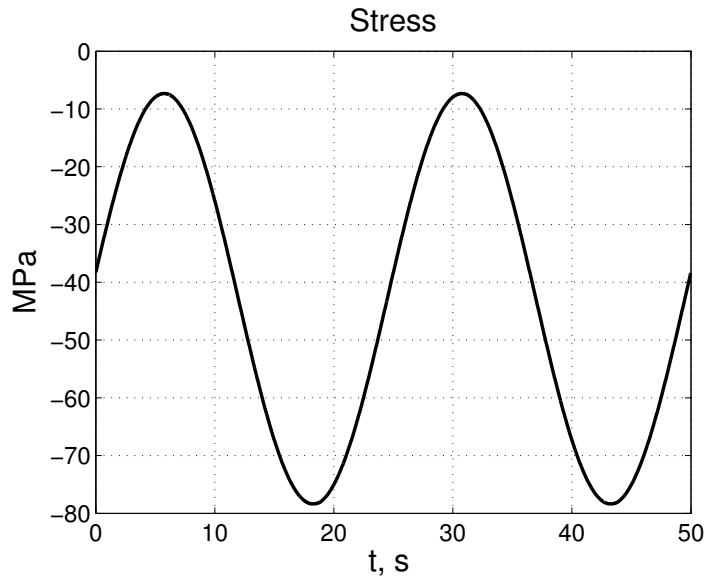


Figure 4.12: Stress input to the aluminum sample with the bonded Galfenol steel patch.

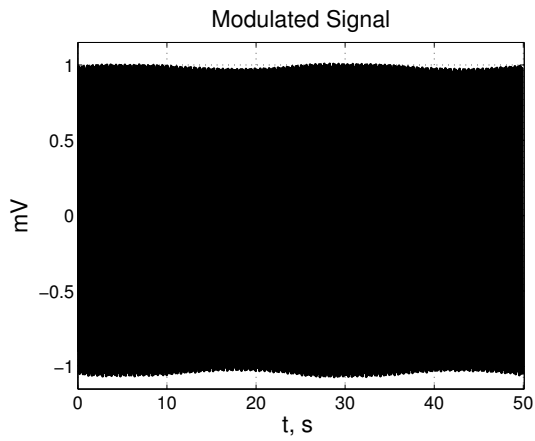


Figure 4.13: Modulated voltage measurement from pick-up coil for a sinusoidal compressive stress input to the Galfenol Steel patch bonded on aluminum substrate.

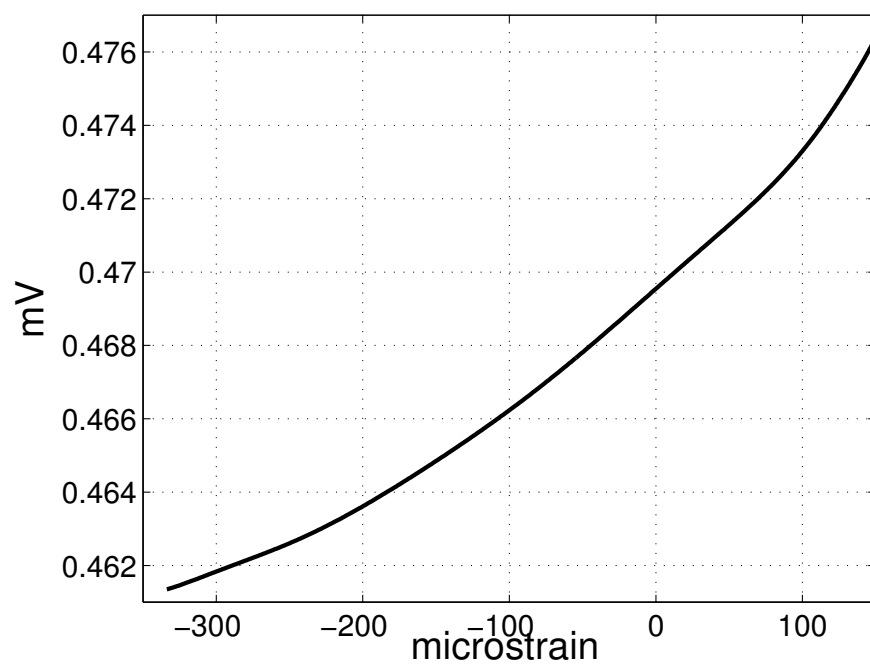


Figure 4.14: Demodulated voltage measurement from pick-up coil as function of strain measured on the Galfenol steel patch.

the domains in the bonded Galfenol patch and the substrate material. The next step would be to test the principle on the hot-formed Galfenol ring bonded on the shaft that is subjected to torque with different substrate materials. Future work would also involve testing the influence of the orientation of the domains and the most optimum flux path that would result in the maximum sensitivity. It would also be interesting to study the domain orientation and texture of the hot formed Galfenol steel ring.

CHAPTER 5

SUMMARY AND CONCLUSIONS

The actuation characteristics M-H and λ -H have been studied for the 18.4 at.% Ga and 20.9 at.% Ga Galfenol alloys in the -63.71 MPa to 63.71 MPa stress range. The M-H curves show a steep rise in magnetization under constant tensile stress and a distinct kinking behavior under constant compressive stress for the 18.4 at.% Ga alloy. The saturation magnetostriction λ_s , decreases with increasing tensile stress and drops to zero at 21.23 MPa and higher tensile stress levels. The saturation magnetostriction increases with increasing compressive stress up to -49.56 MPa and there is a slight drop in the saturation magnetostriction at -56.63 MPa and -63.71 MPa for the 18.4 at.% Ga. The behavior of 20.9 at.% Ga alloy is similar to lower Ga content alloy under tensile loading but under compressive loading the magnetization curves are different. The distinct kinking observed in the lower Ga content alloy is absent and the magnetization curves are smoother and more rounded. The saturation magnetostriction λ_s decreases with increasing tensile stress and drops to zero at 35.4 MPa and higher tensile stress levels. The saturation magnetostriction λ_s increases with increasing compressive stress up to -49.56 MPa and there is a slight drop in the

saturation magnetostriction at -56.63 MPa and -63.71 MPa. The saturation magnetostriction is less for the 20.9 at.% Ga alloy ($\lambda_s=200\text{ppm}$ at -49.56 MPa prestress) compared to the 18.4 at.% Ga alloy ($\lambda_s=265\text{ppm}$ at -49.56 MPa prestress).

The sensing characteristics magnetization versus stress ($M-\sigma$) and magnetostriction versus stress ($\epsilon-\sigma$) have been studied for 18.4 at.% Ga and 20.9 at.% Ga Galfenol in the -63.71 MPa to 63.71 MPa stress range at applied fields ranging from 0 Oe to 180 Oe. The magnetization change is more sensitive to changes in stress when the magnetic field is constant which make the $M-\sigma$ curves look steeper when compared to the constant drive current measurements. The former measurements require a relatively simple close loop control system based on PI control. In comparison to the sensing characteristics of the 18.4 at.% Ga alloy the 20.9 at.% Ga alloy has smoother and more rounded curves. The change in magnetization as a function of stress is more gradual in the 20.9 at.% Ga alloy. The operating stress range of the 20.9 at.% Ga alloy is larger than it is for the 18.4 at.% Ga alloy. The magnetization change of the 20.9 at.% Ga alloy is dominated by stress anisotropy rather than crystal anisotropy, and the low crystal anisotropy is responsible for the larger stress bandwidth.

The stress-dependent susceptibility of 18.4 at.% Ga and 20.9 at.% Ga Galfenol alloys calculated from magnetization measurements has been studied. The susceptibility change as a function of stress is maximum at zero applied field for both the alloys. The susceptibility of the lower Ga content alloy has greater sensitivity to stress in the domain rotation region at stresses ranging from -20MPa to 20MPa, but starts to decay below -20 MPa. The susceptibility of the higher Ga content alloy is sensitive to a larger stress range from -56.63 MPa to 20 MPa in the domain rotation region and the stress-dependent susceptibility change is more gradual than it is for the lower Ga

content alloy. This stress-dependent susceptibility change decays below -56.63 MPa and there is little change in the susceptibility with further increase in stress. The 20.9 at.% Ga alloy has not been characterized before and has the potential of being used in sensors, working on the principle of stress-dependent susceptibility change. Scope for future work can be to conduct dynamic characterization of these alloys to study, hysteresis, and thermal effects.

A force sensor principle based on demodulated stress-dependent susceptibility and proof-of-concept experiments and finite element calculations are presented. The sensor is shown to perform well under low excitation current (338 mA at 5 Hz); higher operating frequencies will require higher excitation frequencies. The $\text{Fe}_{81.6}\text{Ga}_{18.4}$ sample can be used in the low stress region with high sensitivity whereas the $\text{Fe}_{79.1}\text{Ga}_{20.9}$ alloy has two linear regions of susceptibility change, one between -20 MPa and 10 MPa and another between -63.71 MPa and -30 MPa. Both alloys can be used for a force sensor working on the principle of stress-dependent susceptibility, the low Ga content alloy can be used in the low stress regime with large sensitivity and the higher Ga content alloy can be used over a larger range of stress. Future work would involve dynamic characterization of the sensor to determine the performance envelop and fatigue properties of the sensor.

The contactless measurement of the stress dependent susceptibility of the bonded rolled Galfenol steel patch can be used to construct a torque sensor. The contactless sensing principle has been verified. Ongoing work focusses on characterizing rolled Galfenol steel and testing the contactless sensing principle on the hot-formed Galfenol ring with preferential alignment along the 45° shear direction . Future work can also include study of the influence of substrate material and distance between sensor and

bonded Galfenol patch. The performance of 20.9 at.% Ga rolled Galfenol alloy can also be studied as it has good sensing characteristics.

APPENDIX A

TORQUE SENSING USING POLYCRYSTALLINE ROLLED Galfenol STEEL AND AN INTEGRATING FLUXGATE MAGNETOMETER

A magnetostrictive material in the form of a solid shaft or a coating deposited on the shaft or a ring bonded to a rotating shaft is subjected to torque. The shear stress due to the applied torque causes the domains in the magnetostrictive material to align itself to an external field causing an increase in the magnetic field intensity. A fluxgate magnetometer is used to detect the change in the magnetic field intensity when the magnetostrictive material is subjected to torque. In the current study polycrystalline rolled Galfenol steel that is hot formed to the shape of the shaft is used as the magnetostrictive material. The hotformed Galfenol ring in the form of a split ring as discussed in the previous chapter is bonded to the shaft. A laboratory fluxgate magnetometer as shown in Figure A.1 is used to detect the change in the magnetic field intensity in response to the applied torque.

A.1 Integrating Fluxgate Magnetometer

Two ferromagnetic cores are joined on either side by two integrating rings. The magnetic cores and the integrating rings are made of high permeability materials like metglas. The two cores are wound by primary excitation coil in series to each



Figure A.1: Laboratory fluxgate magnetometer for a 1 inch diameter shaft

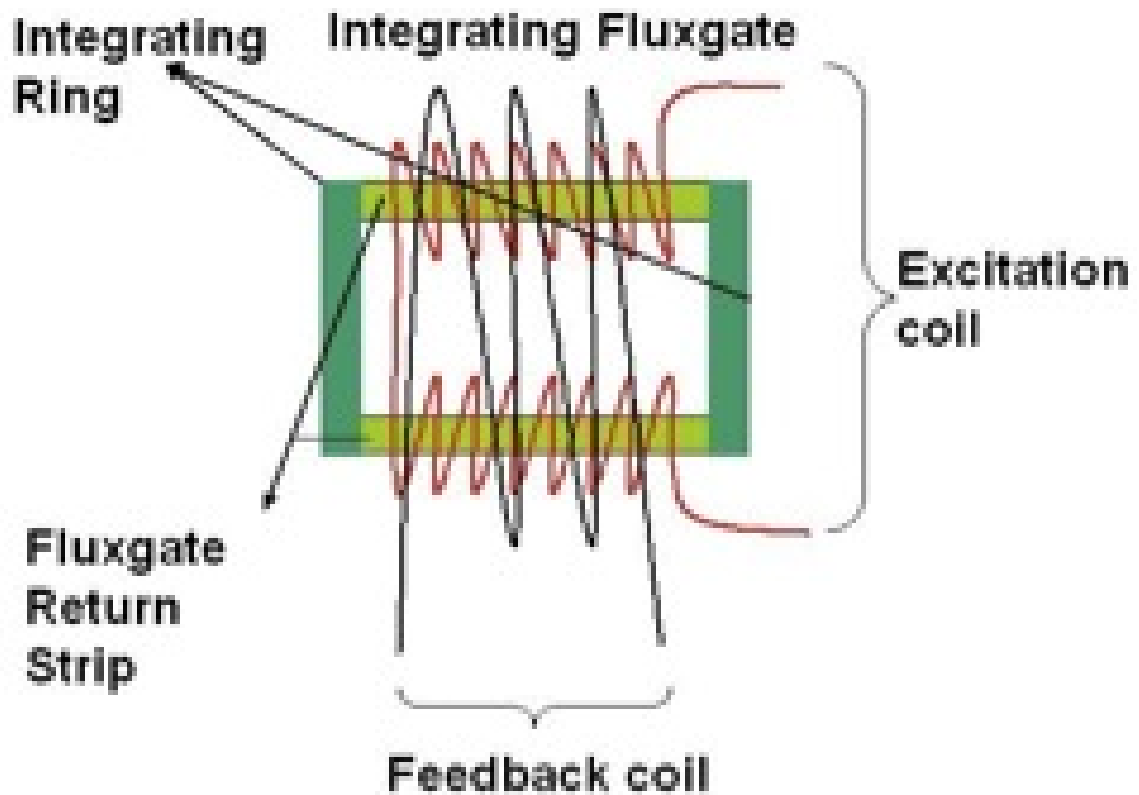


Figure A.2: Integrating fluxgate magnetometer schematic.

other, i.e, the direction in which the coil is wound on one of the cores is opposite in direction to the other. Enclosing both the core materials and the primary coils is a secondary feedback coil. This entire setup forms a closed loop magnetic circuit; the magnetic field due to excitation circulates between the integrating rings and the feedback coil[17]. The schematic of the integrating fluxgate magnetometer is shown in Figure A.2 The primary coils are excited by an AC voltage The excitation voltage and the frequency are adjusted such that the two cores and the integrating rings are below magnetic saturation in the absence of applied torque. The two integrating rings

are designed to pick up the flux generated due to the magnetostrictive material when subjected to torque. The flux picked up by the integrating rings pass through the two core materials. In the absence of an applied torque there is no distinct waveform observed in the feedback coil, but in the presence of an external torque the two magnetic cores become saturated at different times and a voltage waveform in the 2nd harmonic can be observed in the feedback coil. The measure of the voltage could be directly calibrated to give the torque or a null detection scheme could be used to measure the current that is used to bring the two core materials out of saturation[17].

A.1.1 An Analytical Model for an Integrating Fluxgate Magnetometer

The soft magnetic material is periodically saturated in both polarities by the AC excitation field, which is produced by the excitation current I_{ex} through the excitation coil. The sinusoidal excitation of the coil causes the core permeability to change, and the measured DC flux associated measured DC magnetic field B_0 is modulated. In this section an analytical model for the fluxgate by Marshall[14] is discussed. Followed by the model the influence of excitation voltage and number of turns in the secondary coil are studied. For the fluxgate shown in Figure A.3, the voltage induced in the secondary in the presense of an external field H_x and due to a periodic excitation voltage E_p of odd symmetry which drives the core well into saturation, twice each excitation period, is

$$E_s = NA \frac{dB}{dH} \cdot \frac{dH}{dt}. \quad (A.1)$$

By Taylor Series expansion of $\frac{dB}{dH}$ we get,

$$E_s = NA \frac{dH}{dt} \left[\left(\frac{dB}{dH} \right)_0 + \delta H \cdot \left(\frac{d^2 B}{dH^2} \right)_0 + \dots \right] \quad (A.2)$$

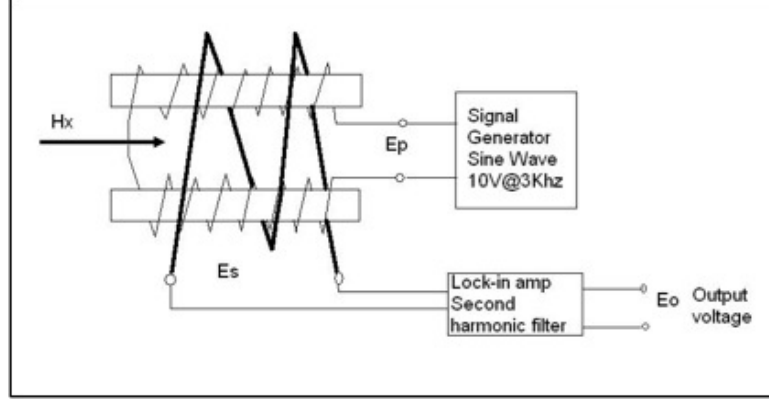


Figure A.3: Schematic of fluxgate magnetometer

for $0 < t < \frac{T}{2}$, and

$$E_s = -NA \frac{dH}{dt} \left[\left(\frac{dB}{dH} \right)_0 - \delta H \cdot \left(\frac{d^2B}{dH^2} \right)_0 + \dots \right] \quad (\text{A.3})$$

for $\frac{T}{2} < t < T$, where

N is the number of turns in the feedback coil, A is the area of the core, $\frac{dH}{dt}$ is the excitation field, $\mu_d = \frac{dB}{dH}$, δH is the perturbation in H within the core due to the presence of the ambient field, $(\mu)_0 = \frac{dB}{dH}$ for $\delta H = 0$ and $(\mu')_0 = \frac{d^2B}{dH^2}$ for $\delta H = 0$.

A perturbation in B is substituted for the perturbation in H giving

$$E_s = NA \frac{dH}{dt} \left[(\mu_d) + \frac{\delta B}{\mu_d} \cdot \mu_d' + \dots \right] \quad (\text{A.4})$$

for $0 < t < \frac{T}{2}$, and

$$E_s = -NA \frac{dH}{dt} \left[(\mu_d) - \frac{\delta B}{\mu_d} \cdot \mu_d' + \dots \right] \quad (\text{A.5})$$

for $\frac{T}{2} < t < T$. The lock-in-amplifier filters the second harmonic component of E_s .

The filtered second harmonic function is approximated by the first two terms for small ambient fields giving,

$$E_0 = NA \frac{dH}{dt} \frac{\delta B}{\mu_d} \cdot \mu_d' \quad (\text{A.6})$$

for $0 < t < T$. The $\frac{dH}{dt}$ term is related to the excitation voltage by

$$\frac{dH}{dt} = \frac{E_p}{AN_p \cdot \mu_d} \quad (\text{A.7})$$

where N_p is the number of turns in the excitation coil, and the perturbation in δB may be expressed as $\delta B = \mu_a H_x$, where μ_a is the apparent permeability or effective permeability of the fluxgate core to the field H_x . Substituting Equation A.7 and δB in Equation A.6 we get

$$E_0 = E_p \cdot \frac{N}{N_p} \cdot \mu_a \frac{\mu_d'}{\mu_d^2} H_x \quad (\text{A.8})$$

$$E_0 = E_p \cdot \frac{N}{N_p} \cdot F_H \cdot H_x \quad (\text{A.9})$$

where $F_H = \mu_a \frac{\mu_d'}{\mu_d^2}$.

A.1.2 Characterization and Testing of an Integrating Fluxgate Magnetometer

The fluxgate shown in Figure A.1 was characterized to study the influence of excitation voltage, number of turns in the pick-up coil and the excitation waveform. Figure A.4, A.5 and A.6 show the results.

A.2 Contactless Torque Sensing

As discussed in Chapter 4 several applications would benefit from a non-contact torque sensor. A non-contact magnetostrictive torque sensor has been proposed by Naidu et al[17]. In the current work polycrystalline rolled Galfenol steel is hot formed to the shape of the shaft and bonded to the shaft. The bonded material is the active magnetostrictive material. Applying torque to the shaft stresses the bonded material and the magnetoelastic anisotropy of the material changes. The applied torque gives rise to stress induced easy axis in the direction of the principle stress which is along

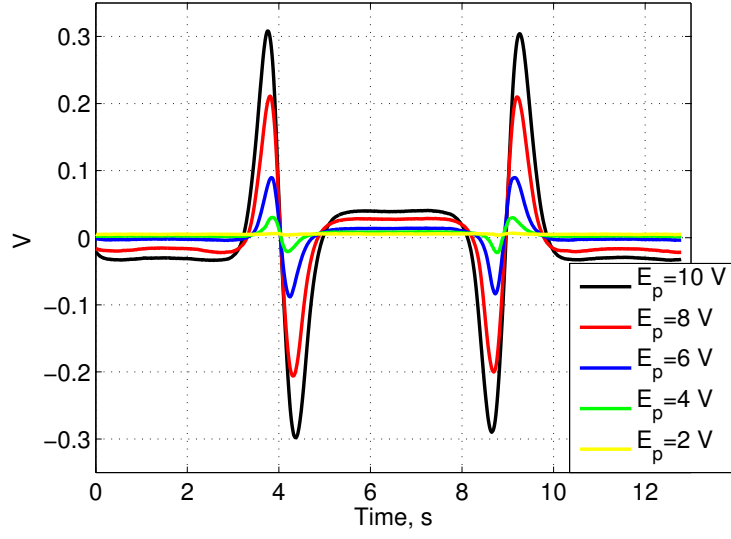


Figure A.4: Second harmonic output voltage from the feedback coil at increasing sinusoidal excitation voltage at a frequency of 3 KHz, for a sinusoidal external field (H_x) of ± 30 kA/m at 0.04 Hz.

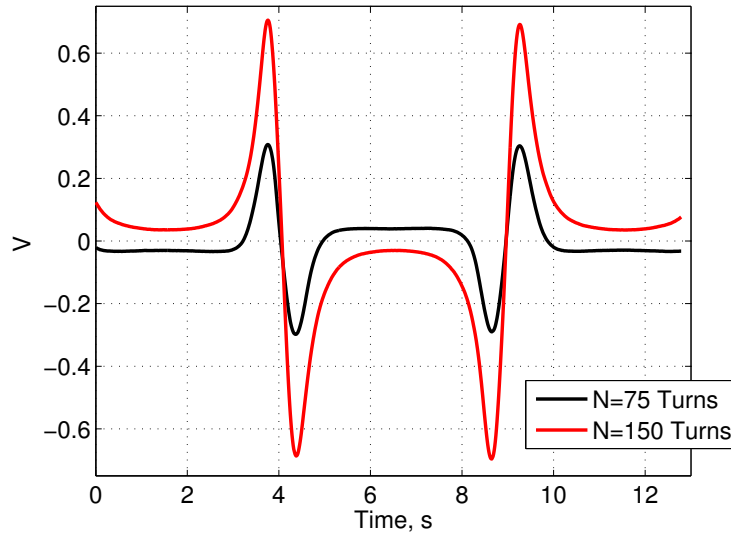


Figure A.5: Second harmonic output voltage from the feedback coil at increasing number of turns in the feedback coil, 10 V sinusoidal excitation voltage at a frequency of 3 KHz, for a sinusoidal external field (H_x) of ± 30 kA/m at 0.04 Hz.

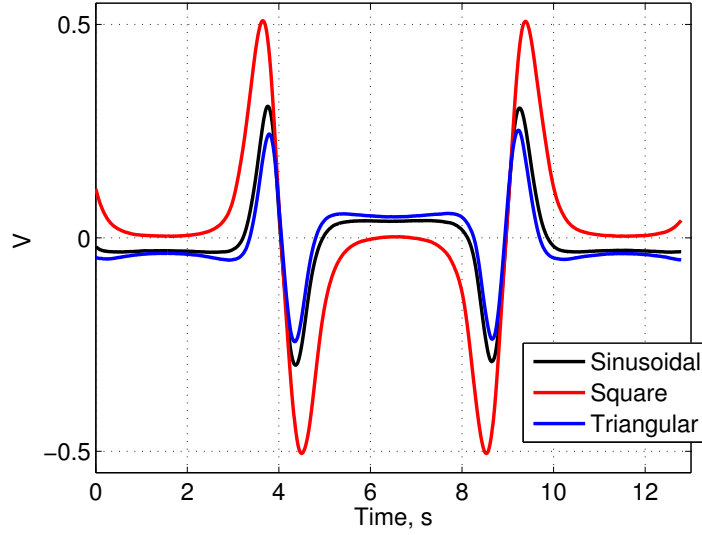


Figure A.6: Second harmonic output voltage from the feedback coil at different excitation waveform, 10 V_{pp} voltage at a frequency of 3 KHz, for a sinusoidal external field (H_x) of ± 30 kA/m at 0.04 Hz.

the 45° helix[20]. Consequently the overall magnetization vector changes giving rise to surface poles which produce a magnetic field. An integrating fluxgate magnetometer is used to detect the field. An analytical model for a non contact torque sensor is discussed by Andreescu et al[20]. Torque tests were conducted on a 2 inch diameter shaft with a split ring of hotformed Galfenol steel bonded onto the shaft, the measurement setup and results are discussed in the following subsections.

A.2.1 Contactless Torque Sensing Measurement Setup

A polycrystalline rolled Galfenol steel strip with no preferred moment orientation was hotformed to suit a 2 inch diameter shaft. The hotforming and bonding procedures are discussed in Chapter 4. A torque moment arm as shown in Figure A.8

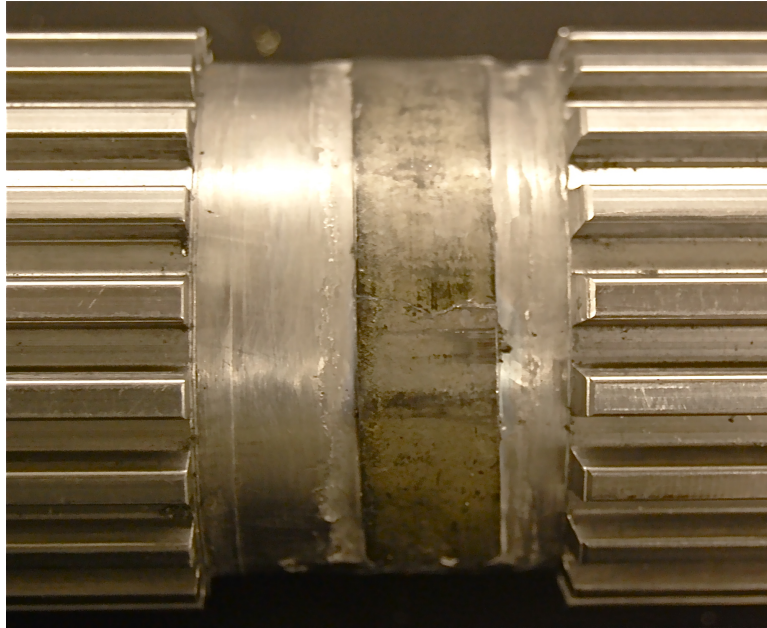


Figure A.7: Spline shaft with the hot formed polycrystalline rolled Galfenol ring bonded to the shaft using M bond 200.

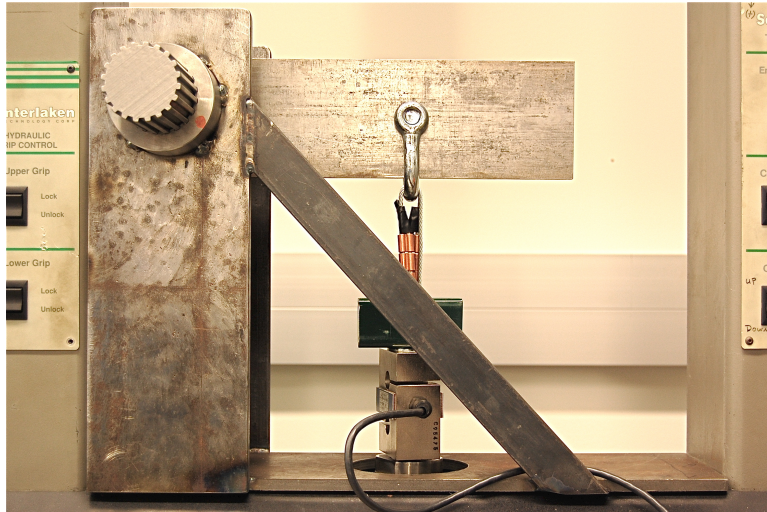


Figure A.8: Torque arm used to torque the spline shaft with the bonded Galfenol.

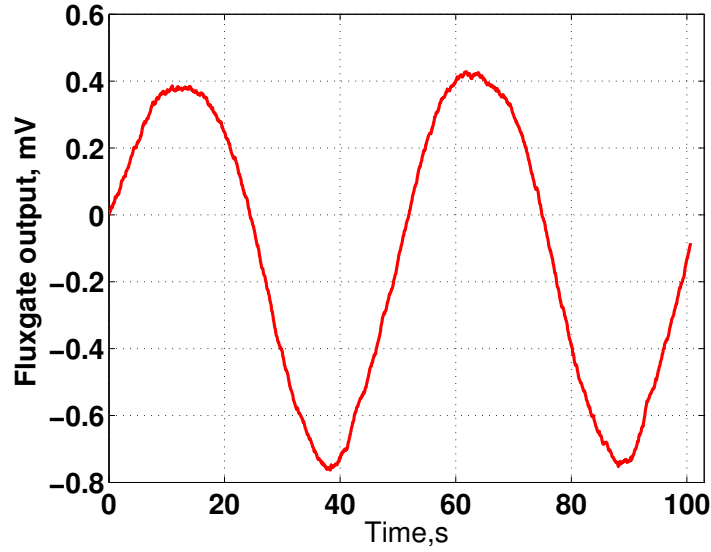


Figure A.9: Second harmonic output of the integrating fluxgate magnetometer.

was used to torque the spline shaft. A strain gage bonded along the 45° shear direction in the quarter bridge configuration along with the 2310 B Vishay Conditioner Amplifier was used to measure the shear strain on the shaft. An integrating fluxgate magnetometer concentric to the shaft was used to measure the change in the field(Figure A.7). A schematic of the circuit is shown in Figure A.3. The primary coils of the integrating fluxgate was excited by a 10V sinusoidal signal at 700Hz frequency. An SR 510 Lock-in-amplifier was used to extract the second harmonic component of the feedback voltage. The reference to the lock-in amplifier was given from the signal generator. An initial bias torque of 3300 lbs-in was given to the torque arm and a sinusoidal torque of ± 3000 lbs-in at frequency of 40 mHz was given to the lever arm.

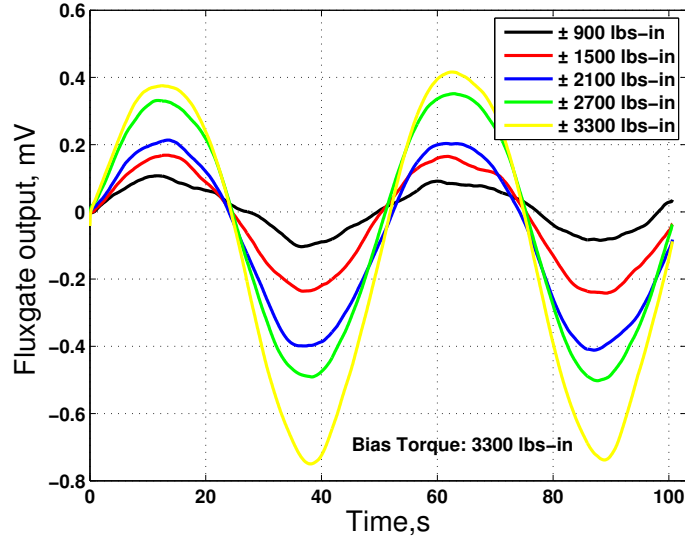


Figure A.10: Fluxgate output at different magnitudes of torque starting from a bias torque of 3300 lbs-in.

A.2.2 Results and Discussion

Figure A.9 shows the second harmonic output from the feedback coil of the integrating fluxgate magnetometer in response to a sinusoidal input torque to the spline shaft. Figure A.10 shows the output measured from the fluxgate starting from a bias torque of 3300 lbs-in and cycling the torque between different magnitudes. Figure A.11 shows the fluxgate output as a function of input torque and Figure A.12 shows the fluxgate output as function of strain measured on the bonded Galfenol.

The second harmonic fluxgate output corresponds well to the torque input. The sensitivity is $\sim 6.25 \mu\text{V}/\mu\text{-strain}$. Hysteresis is observed in the measurement which is due to the fluxgate magnetometer. The contactless system works well but with low sensitivity and certain amount of hysteresis. The tests were done at different torque cycle frequency, the results are shown in Figure A.13 and Figure A.14. The

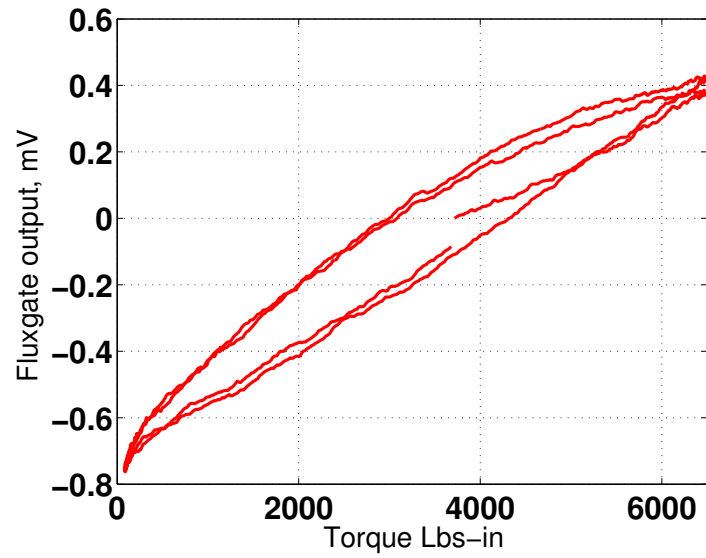


Figure A.11: Fluxgate output as a function of input torque.

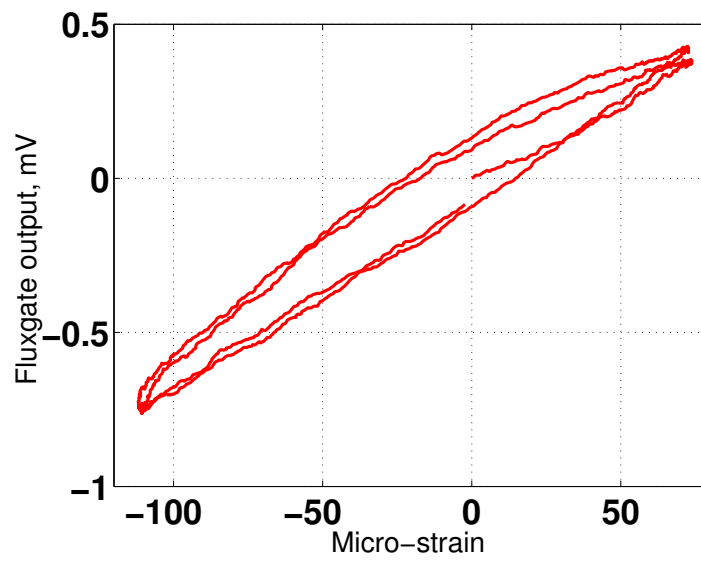


Figure A.12: Fluxgate output as a function of shear strain on the rolled Galfenol ring.

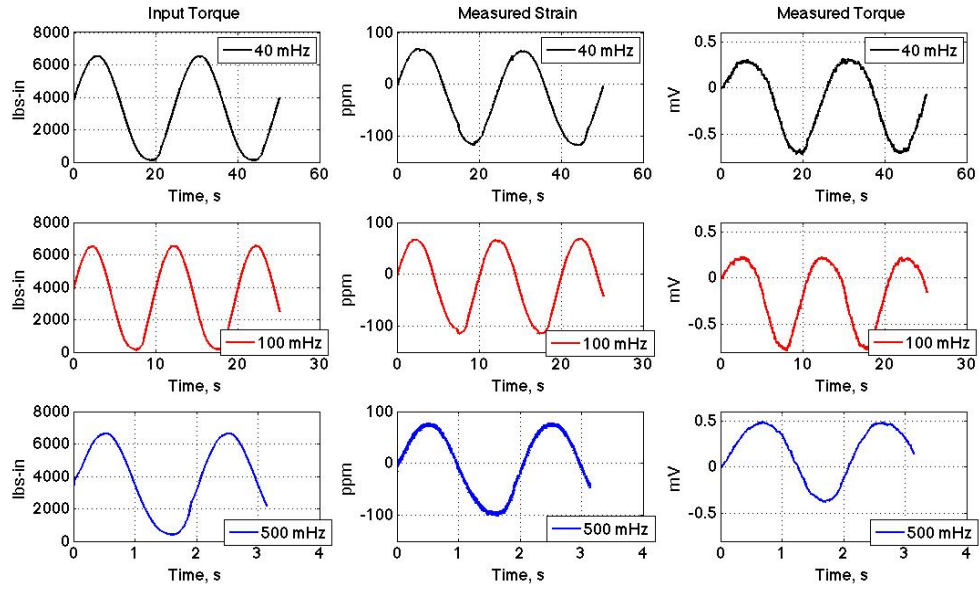


Figure A.13: Fluxgate output as at different torque cycle frequency.

fluxgate measures the torque response at all the frequencies studied. With increasing frequency of torque cycle the sensitivity reduces slightly and the hysteresis becomes larger.

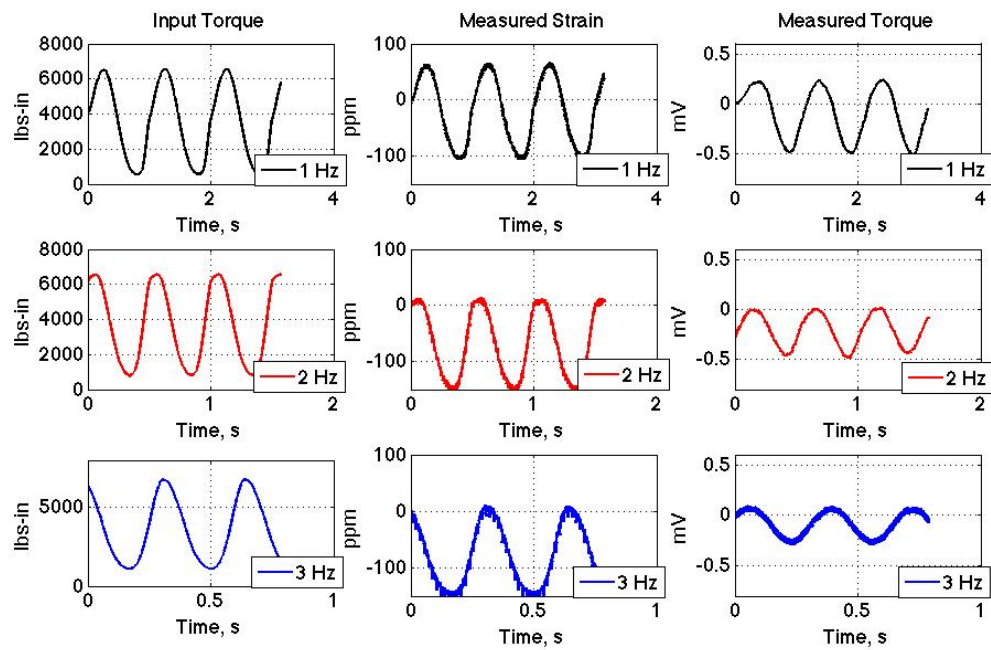


Figure A.14: Fluxgate output as at different torque cycle frequency.

BIBLIOGRAPHY

- [1] J. Atulasimha, A. B. Flatau, and J. R. Cullen. Analysis of the effect of gallium content on the magnetomechanical behavior of single crystal fega alloys using an energy based model. *Smart Mater. Struct.*, 17(025027), 2008.
- [2] J. Atulasimha, A. B. Flatau, and E. Summers. Characterization and energy-based model of the magnetomechanical behavior of polycrystalline iron–gallium alloys. *Smart Materials and Structures*, 16:1265–1276, 2007.
- [3] A. E. Clark, K. B. Hathaway, M. Wun-Fogle, J. B. Restorff, T. A. Lograsso, J. M. Keppins, G. Petculescu, and R. A. Taylor. Extraordinary magnetoelasticity and lattice softening in bcc fe-ga alloys. *Journal of Applied Physics*, 93(10):8621–8624, 2003.
- [4] A. E. Clark, J. E. Yoo, J. R. Cullen, M. Wun-Fogle, G. Petculescu, and A. Flatau. Stress dependent magnetostriction in highly magnetostrictive $\text{fe}_{100-x}\text{ga}_x$, $20 < x < 30$. *Journal of Applied Physics*, 105(07A913), 2009.
- [5] David W. Cripe. Magnetoelastic torque sensor using fluxgate magnetometer to measure magnetic field. *United States Patent Application*, US2002/0162403, 2002.
- [6] M. J. Dapino. On magnetostrictive materials and their use in adaptive structures. *Structural Engineering and Mechanics*, 17(3-4):303–329, 2004.
- [7] S. Datta, J. Atulasimha, and A. B. Flatau. Modeling of magnetostrictive galferol sensor and validation using four point bending test. *Journal of Applied Physics*, 101:09–521, 2007.
- [8] P. R. Downey and A. B. Flatau. Magnetoelastic bending of galferol for sensor applications. *J. App. Phys.*, 97:10–505, 2005.
- [9] P. G. Evans and M. J. Dapino. Stress dependent susceptibility of galferol for sensing force. *Journal of Applied Physics*, in review.
- [10] Phillip G. Evans. Comsol modeling for magnetostrictive materials. Technical report, Smart Materials and Structures Lab, The Ohio State University, 2009.

- [11] I. J. Garshelis. Circulatory magnetized non-contact torque sensor and method for measuring torque using the same. *United States Patent Application*, US 2001/0029792 A1, 2001.
- [12] I. J. Garshelis. Collarless circumferentially magnetized torque sensor and method of measuring torque using the same. *United States Patent Application*, US 2001/0035056 A1, 2001.
- [13] D. K. Kleinke and H. M. Uras. A magnetostrictive force sensor. *Rev. Sci. Instrum.*, 65(5):1699–1710, 1994.
- [14] Stanley V Marshall. An analytical model for the fluxgate magnetometer. *IEEE Transaction of Magnetism*, 3(3), 1967.
- [15] C. Mudivarthi, S. Datta, J. Atulasimha, and A. B. Flatau. A bidirectionally coupled magnetoelastic model and its validation using a galphenol unimorph sensor. *Smart Materials and Structures*, 17, 2008.
- [16] Suok-Min Na and A. B Flatau. Magnetostriction and crystallographic texture in rolled and annealed fe-ga based alloys. In *Materials Research Society Symposium Proceedings*, volume 0888-V06-10.1, 2006.
- [17] Malakondaiah Naidu, Joseph Pierre Hermans, Thomas Wolfgang Nehl, John R. Smith, and Brian K. Fuller. Integrating fluxgate for magnetostrictive torque sensors. *United States Patent Application*, 2005/6871553 B2, 2005.
- [18] Song Ouyang and Ryoichi Menju. Magnetostrictive torque sensor. *United States Patent Application*, 2006/0179959 A1, 2006.
- [19] S. Rafique, J. R. Cullen, M. Wuttig, and J. Cui. Magnetic anisotropy of fe-ga alloys. *J. Appl. Phys.*, 95(11):6939–6941, 2004.
- [20] R.Andreescu, B.Spellman, and E.P.Furlani. Analysis of a noncontact magnetoelastic torque transducer. *Journal of Magnetism and Magnetic Materials*, 320, 2008.
- [21] Eric Summers. Personal communications. *Etrema Products Inc.*, May, 2009.
- [22] M. Wun-Fogle, J. B. Restorff, and A. E. Clark. Magnetomechanical coupling in stress-annealed fe-ga (galphenol) alloys. *IEEE Transactions on Magnetism*, 42(10):3120–3122, October 2006.